Synaptic vesicle recycling investigated by high-resolution

microscopy in a conventional and a sensory synapse

Dissertation

for the award of the degree

Dr. rerum naturalium (Dr. rer. nat.)

Division of Mathematics and Natural Sciences

of the Georg-August-Universität Göttingen

submitted by

Dirk Kamin

from Meppen, Germany

Göttingen, March 2011

Members of the Thesis Committee:

Dr. Silvio O. Rizzoli (Reviewer)

      STED Microscopy of Synaptic Function, European Neuroscience Institute Göttingen

Prof. Dr. Tobias Moser (Reviewer)

      InnerEarLab, Department of Otolaryngology, UMG

Dr. Stefan Eimer

      Molecular Neurogentics, European Neuroscience Institute Göttingen

Date of the oral examination: to be determined

I hereby declare that this dissertation has been written independently and with no other sources and aids than quoted.

Dirk Kamin

Publications

Parts of the work presented in this thesis are based on the following publications. I want to thank all co-authors and all acknowledged people therein for the successful collaboration.

Kamin D, Lauterbach MA, Westphal V, Keller J, Schönle A, Hell SW, Rizzoli SO.
High- and low-mobility stages in the synaptic vesicle cycle.
Biophys J, 2010 July 21; 99 (2): 675-684.

Lauterbach MA, Keller J, Schönle A, **Kamin D**, Westphal V, Rizzoli SO, Hell SW.
Comparing video-rate STED nanoscopy and confocal microscopy of living neurons.
J Biophotonics, 2010 July; 3 (7): 417-424.

Kamin D, & Rizzoli SO.
Die Mobilität der synaptischen Vesikel.
Neuroforum – Perspektiven der Hirnforschung, 2009 September; 15 (3): 84-92.

Westphal V, Rizzoli SO, Lauterbach MA, **Kamin D**, Jahn R, Hell SW.
Video-rate far-field optical nanoscopy dissects synaptic vesicle movement.
Science, 2008 April 11; 320 (5873): 246-249.

Contents

Abstract

Synaptic neurotransmission depends on the action of highly specialized small secretory organelles – synaptic vesicles. At all chemical synapses the synaptic vesicles release in a strictly regulated fashion their neurotransmitter into the synaptic cleft, by fusing with the plasma membrane (exocytosis) at structurally and functionally well organized sites (active zones). The fused vesicles get retrieved (endocytosis), refilled with neurotransmitter and returned to the vesicle cluster near the active zone in order to supply fusion-competent vesicles for further rounds of neurotransmission, thus completing a process termed vesicle recycling. While the molecular key players in the synaptic vesicle cycle have been characterized in detail for conventional synapses, the general mobility of synaptic vesicles is still poorly understood, with only averaged behaviors (over populations of vesicles) known. How could vesicle behavior actually be described when single vesicles are analyzed? The small size of synaptic vesicles (~ 40 nm in diameter) and the dense clustering at the active zone makes it difficult to study their behavior, since conventional imaging techniques are restricted to a resolution of ~200-300 nm by the diffraction limit of light. I investigated here synaptic vesicle mobility throughout the synaptic vesicle cycle, using both conventional and sub-diffraction high-resolution stimulated emission depletion (STED) fluorescence microscopy. I obtained a thorough description of vesicle recycling in hippocampal synapses. Single vesicle tracking revealed that a large resting pool of vesicles has a low mobility, while active, recently endocytosed vesicles exhibit a high-mobility state for a substantial amount of time. They eventually become resting vesicles by integrating into the vesicle cluster ("maturation"). After exocytosis the fused vesicles appear to remain and move as multi-molecular protein patches in the plasma membrane, which afterwards recycle back into the synapse. All these mobility characteristics are in good agreement with the well-known pathway of vesicle recycling. FM photo-oxidation, in combination with high-resolution electron microscopy revealed that endosomes are involved in this recycling process, in good agreement with previous literature. Having thus obtained a thorough understanding of vesicle behaviour and recycling in conventional synapses, I proceeded to compare this with a non-conventional sensory synapse, the mammalian cochlear inner hair cell (IHC). I used various membrane labeling techniques, and chose FM photo-oxidation as the optimal tool to analyze

vesicle recycling in IHCs. I observed that a variety of recycling organelles are present, and I suggest that several organelle classes are involved in vesicle recycling, largely in contrast to conventional synapses. I conclude that the basic mechanisms of vesicle recycling in conventional and sensory synapses are related, but that sensory synapses contain particularities which may reflect the much stronger membrane recycling in IHCs compared to conventional synapses.

List of Figures

List of Tables

List of Abbrevations

AZ	active zone
AAA$^+$	ATPase associated with cellular activities
AP2	adaptor protein 2 complex or assembly protein
ATP	adenosine triphosphate
AU	arbitrary units
BWSV	black widow spider venom
CME	clathrin-mediated endocytosis
CNS	central nervous system
CP	cuticular plate
DAB	3,3'-diaminobenzidine
DCF	dodecanoyl fluorescein
DMEM	Dulbecco's modified Eagle's medium
DMSO	dimethyl sulfoxide
EGTA	ethylene glycol tetraacetic acid
ES	efferent synapse
EXC	excitation
FP	focal plane
FRAP	fluorescence recovery after photobleaching
FWHM	full width at half maximum
GFP	green fluorescent protein
GTP	guanosine triphosphate
HBSS	Hanks´ balanced salt solution
HCN	hippocampal cultureed neurons
HEPES	4-(2-Hydroxyethyl)piperazine-1-ethanesulfonic acid
HRP	horseradish peroxidase
Hz	hertz
IHC	inner hair cell
kDa	kilo-dalton
MDCK	Madin-Darby canine kidney cells
MTG	MitoTracker Green FM
N	nucleus
NA	numerical aperture
NH$_4$Cl	ammoniumchloride
NMJ	neuromuscular junction
NSF	N-ethylmaleimide-sensitive factor
PBS	phosphate buffered saline
PC12	pheochromocytoma 12 cells
PDF	probability density function
PFA	paraformaldehyde
PMT	photomultiplier tube
PO	propylene oxide
PSF	point spread function

ROS	reactive oxygen species
RRP	readily releasable pool
RT	room temperature
SC	stereocilia
SE	standard error
SNAP	soluble NSF attachment factor
SNAP-25	synaptosome-associated protein of 25 kDa
SNARE	soluble NSF attachment protein receptor
STED	stimulated emission depletion
SV	synaptic vesicle
Syph	synaptophysin
Syt	synaptotagmin
TTX	tetrodotoxin
VAMP2	vesicle associated membrane protein

1 Introduction

1.1 Synaptic Function

The nervous system is composed of functional independent units – termed nerve cells or "neurons" (Wilhelm Waldeyer, 1891, see Golgi, 1906). The human brain contains around 10^{11} neurons (with around 1000 subtypes) and 10-50 times as many supporting cells. More than a century ago the first light microscopic studies on nerve cell morphology were performed by Santiago Ramón y Cajal. In his "Neuron Doctrine" he postulated that the nervous system is formed by anatomically and functionally discrete cells (Cajal, 1894). Furthermore, he also postulated that nerve cells are the basic units of signal processing in the brain by propagating the nervous impulse along their processes to finally transmit the information from one nerve cell to another at specialized contacts – eventually termed "synapses" (Forster and Sherrington, 1897). Accordingly, the synaptic connections of nerve cells are the fundamental basis of sensory processing, behavior and general brain function.

Despite the enormous diversity of neuronal cell types, each nerve cell is specialized for the propagation and transmission of electrical signals. All nerve cells exhibit the same general morphological features: a nucleus-containing cell body from which various processes arise. These can be separated into numerous branched dendrites and a single axon. A signal usually reaches the cell at a dendrite or the cell body, is processed at the cell body and then forwarded along the axon. In the final step the information is transmitted to other nerve cells or non-neuronal cells (e.g. muscle cells) at the above mentioned specialized synapses.

Two types of synapses are known, chemical and electrical neuronal junctions. Electrical synapses are less numerous than chemical synapses, but are found in all nervous systems where fast neuro-transmission is of importance (see review of Bennett and Zukin, 2004). The characteristical feature of an electrical synapse is a specialized intercellular structure that links both communicating nerve cells together which is called "gap junction". Gap junctions are composed of several superimposed channels in both cells. Ions and other molecules (e.g ATP) can passively diffuse between the neurons through the large pores of these channels

(Purves et al., 2001). The synaptical part of the neuron from which the current flows is called presynapse; the synaptical part in the receiving neuron in turn is called postsynapse. The current flow directly triggers the change in the postsynaptic membrane potential. The electrical synapse features two important properties: first, the signal transmission can in principle occur bidirectional, and second, the transmission speed is very high.

The pre- and postsynaptic site of chemical synapses in turn are separated through a 20-40 nm "synaptic cleft" (Kandel et al., 2000) (see Figure 1.1). Thus, the signal cannot be transmitted electrically via current flow. The crucial role for the signal transmission is played by small, membrane-enclosed organelles – termed synaptic vesicles (Sudhof, 2004; Takamori et al., 2006). The synaptic vesicles store chemical substances (neurotransmitters) that are used for the signal transduction process – hence the name chemical synapse. Neuronal transmission starts with the action potential-triggered release of the neurotransmitter into the synaptic cleft (Katz, 1969). The chemical messenger diffuses across the cleft and binds to their appropriate receptors on the postsynaptic plasma membrane, leading thereupon to the opening or closing of ion channels. Finally, an inward flow of ions changes the membrane potential of the postsynaptic cell. Consequently, Cajal was only partially right with his statement of nerve cells being the basic unit of signal transduction – perhaps this title would fit better the neurotransmitter-containing synaptic vesicles (see above).

It is obvious that the entire transmission process at a chemical synapse is substantially slower when compared to electrical synapses, where the presynaptic neuron is directly linked with the postsynaptic membrane potential, and where signal transmission is not dependent on vesicle release, or neurotransmitter diffusion and binding to receptors.

1.1.1 Vesicles: Small Organelles with Great Responsibility

Vesicles are the smallest membrane-enclosed organelles that store or transport substances between different compartments within a cell. Therefore, they fuse with the membrane of target organelles to load or unload their cargo. Due to their appearance and features, vesicles are subdivided into various types (e.g. secretory vesicles (synaptic vesicles), transport vesicles, dense core vesicles).

One important vesicle type are the secretory synaptic vesicles of nerve cells (see above). Their sole function is neurotransmitter release. An ordinary, mature synaptic vesicle is spherical in shape and has on average an outer diameter of approximately 42 nm (Takamori et al., 2006). The vesicles of a synapse are grouped in vesicle clusters (Figure 1.1). The synaptic vesicle has an unique lipid composition (Benfenati et al., 1989) and high quantities of membrane-associated and trans-membrane proteins (130×10^3 trans-membrane regions/μm^2) that are for the most part accountable for the accurate vesicle function in the release process (Takamori et al., 2006). Important trans-membrane proteins are for example the neurotransmitter transporters, which actively transport in co-operation with a vesicular ATPase (proton exchange) small neurotransmitters into the vesicle lumen (e.g. glutamate, GABA (γ-aminobutyric acid), acetylcholine or glycine).

A second type of synaptic-related vesicles is accountable for the release of hormones and neuroactive-peptides – termed "dense core vesicles". They are named after their dark/ black appearance on electron micrographs, caused by proteins and nucleotides which are incorporated as a binding matrix for the real signal molecules (Artalejo et al., 1998). In contrast to dense core vesicles, the small neurotransmitter-containing synaptic vesicles appear translucent on electron micrographs and are thus called clear core vesicles. The second disparity between the two vesicle types is the size. The dense core vesicles are substantially larger, ranging between ~80-120 nm in diameter (Sorra et al., 2006). It is believed that the smaller dense core vesicles are used as transport organelles for the delivery of important synaptic components from the cell body to the synapse, e.g. the active zone proteins bassoon/ piccolo (see below) (Shapira et al., 2003; Sorra et al., 2006; Santos et al., 2009). Thus, only the larger ones (~100-120 nm) may be responsible for the secretion of neuroactive-peptides (e.g. neuropeptide Y, growth hormones) (Sorra et al., 2006). Furthermore, the secretion of synaptic vesicles and dense core vesicles varies, with a slow release of the contents from dense core vesicle versus the fast release of neurotransmitter from small vesicles (1.3 ms for 80000 molecules and 260 µs for 4700 neurotransmitter, respectively) (Bruns and Jahn, 1995). However, the initiation for release appears to be equally fast for both vesicle types (Bruns and Jahn, 1995).

An important role can also be assigned to the general transport vesicles within the cell. All cells are to some extent compartmentalized, containing various organelles that accomplish different tasks within the cell. In this respect the transport vesicles are used for the specific intracellular protein and lipid trafficking between the organelles (e.g. protein transport from the endoplasmic reticulum to the Golgi complex and to the plasma membrane). In particular, theses vesicles are outstanding actors in the secretory and endocytic pathways (Palade, 1975). Since the axon and the synapses lack the machinery for the protein biosynthesis and assembling (e.g. endoplasmic reticulum and Golgi complex) a role in supplying the presynaptic nerve terminal is assigned to transport vesicles (for example realized by small dense core vesicles, see above). Thus, packages of axonal plasma membranes, synaptic vesicle membrane proteins, and synaptic plasma membranes are transported down the axon after their synthesis in the neuronal cell body, by microtubule-associated motor-proteins (e.g. kinesin). Evidence for the biosynthesis of synaptic vesicle proteins in the cell body came from immunostaining experiments, showing the colocalization of synaptic vesicle proteins with the Golgi complex (e.g. synaptophysin (Fletcher et al., 1991; Mundigl et al., 1993), synaptotagmin, synaptobrevin, p29 and SV2 (Mundigl et al., 1993)). Upon arrival at the presynaptic nerve terminal, the synaptic vesicle membrane proteins undergo cycles of constitutive exo- and endocytosis prior to their final separation into mature synaptic vesicles (reviewed in Santos et al., 2009).

1.1.2 Key Players of Vesicle Release in Conventional Synapses

Synaptic vesicles are directly and indirectly (for example by storing neurotransmitter) involved in the function of the synapse. Neurotransmitter release is a complex process that involves a strictly regulated cascade of protein interactions. Prior to neurotransmitter release, important steps of the synaptic vesicles need to be conducted. The essential stages before fusion are vesicle docking (or tethering) and priming at the membrane. Docking, priming and release is conducted at specialized presynaptic plasma membrane sites – termed "active zones" (AZs) (reviewed in Dresbach et al., 2001). AZs are composed of an electron-dense, biochemical insoluble material connected to the plasma membrane, and contain various linked proteins, forming the cytomatrix assembled at the active zone. These include the two large scaffolding proteins piccolo and bassoon (tom Dieck et al., 1998), the multi-domain

proteins of the RIM family (Rab3-interacting molecules), and CAST/ERC proteins as well as alpha-liprins and Munc13 (Brose et al., 1995). The synaptic vesicle protein Rab3 guides and docks the synaptic vesicle to the AZ and interacts with the cytomatrix protein RIM (Gracheva et al., 2008). The synaptic vesicle becomes primed through the further interaction of RIM with the AZ protein Munc13, resulting in the formation of a tripartite complex (Betz et al., 2001; Dulubova et al., 2005). The primed vesicle is thus fusion competent for calcium triggered vesicle release.

The arrival of an action potential in the synapse opens voltage-gated calcium channels at the AZ which leads to a local increase in the calcium concentration. Calcium ions can then bind to the synaptic vesicle protein synaptotagmin, the vesicle calcium sensor, and trigger neurotransmitter release of the primed vesicles. Synaptotagmins are trans-membrane proteins with a short intra-vesicular (N-terminal) domain, a single trans-membrane domain and two cytoplasmic C_2-domains – C_2A and C_2B (Geppert et al., 1991). These domains bind three and two calcium ions, respectively (Ubach et al., 1998; Fernandez et al., 2001). As a result of the calcium binding, the C_2-domains become attached to the plasma membrane (Brose et al., 1992). Additional binding spots are thereupon allocated for the calcium ions through the negatively charged head groups of the phospholipids and consequently more calcium ions are able to bind to the C_2-domains (Fernández-Chacón et al., 2001). The further connections of synaptotagmin with the membrane protein neurexin (Hata et al., 1993) and the calcium channels (Leveque et al., 1992) possibly locates the vesicle in an optimal position to respond to the local calcium increase at the active zone. Besides the calcium-dependent complex formation with phospholipids, synaptotagmin binds as well to syntaxin 1 of the SNARE complex (Bennett et al., 1992b; Chapman et al., 1995; Li et al., 1995).

The SNARE proteins (soluble N-ethylmaleimide-sensitive factor attachment protein receptor) are the key actors for the actual fusion process. They are diverse in structure and size but all have a small homologous sequence (60-70 amino acids) – named "SNARE motif". This motif is the important structure of the SNARE proteins (Fasshauer et al., 1998). Besides the many SNAREs used for intracellular fusion events (reviewed in Bonifacino and Glick, 2004), a specific set of SNAREs mediates synaptic function (synaptobrevin, syntaxin, SNAP-25). SNAREs are needed on both opposing membranes. The ones on the vesicle are called v-SNAREs and the ones on the target plasma membranes are called t-SNAREs (Söllner et al., 1993b). The synaptic vesicle protein synaptobrevin-2 is the synapse specific v-SNARE (also

known as VAMP2: vesicle associated membrane protein (Baumert et al., 1989)). The neuronal t-SNAREs on the plasma membrane are syntaxin 1 (Bennett et al., 1992a)(also known as p35) and SNAP-25 (synaptosome-associated protein of 25 kDa; (Oyler et al., 1989). For vesicle fusion the three SNARE proteins come into close proximity, resulting in the assembly of the SNARE domains in a ternary parallel helical bundle between the synaptic vesicle and the plasma membrane (Sutton et al., 1998). Ultrastructural analysis of this twisted bundle revealed the presence of four helices, as SNAP-25 contributes two alpha-helical domains that are connected by an unstructured loop (Sutton et al., 1998). The opposing vesicle membrane and the plasma membrane connect and fuse using the free energy that is released during the "zipper-like" assembly of the four-helix SNARE complex (Hanson et al., 1997). Although SNAREs are sufficient for vesicle fusion in vitro (Pobbati et al., 2006), other partners are mandatory to fulfill membrane fusion at the AZ, for example Munc13 may bind to the t-SNARE syntaxin 1, and RIM may interact with SNAP-25 (Betz et al., 1997; Coppola et al., 2001). For a more detailed view of the function of SNARE proteins and the protein-protein interplay in membrane fusion see Jahn et al., 2003 and Rizo and Rosenmund, 2008. After membrane fusion and neurotransmitter release the individual SNARE proteins get "recycled" by the dissociation of the twisted bundle. The re-assembling of the ternary SNARE complex is mediated by the enzymatic ATPase activity of the AAA$^+$ (ATPase associated with cellular activities) protein NSF (N-ethylmaleimide-sensitive factor) (Block et al., 1988) and its co-factor alpha-SNAP (Söllner et al., 1993a).

1.2 Synaptic Vesicle Pools

Although clear core synaptic vesicles all look identical in electron micrographs, and appear to have identical molecular compositions (Takamori et al., 2006), they are functionally different, as some vesicles are more "releasable" than others. Therefore, the vesicles of each synapse have been categorized into vesicle pools according to their position relative to the active zone and their release probability (reviewed in Rizzoli and Betz, 2005). Two major vesicle pools have been described so far: the recycling pool and the resting pool. The former includes a small third pool of almost negligible size, but of high importance – the "readily releasyble pool" (RRP). The RRP are the synaptic vesicles that are docked and primed at the AZ and released first upon the arrival of an action potential (Schikorski and Stevens, 2001).

Non-docked recycling pool vesicles replenish the RRP after its depletion. Thus, the recycling pool vesicles (~10-20% of all synaptic vesicle in a synapse) are the vesicles that undergo rounds of exo- and endocytosis (the synaptic vesicle cycle, see below) (Schikorski and Stevens, 2001; Sudhof, 2004). The other 80-90% of the vesicles belong to the resting pool and do not directly participate in vesicle release at physiological activity. However, they are recruited to release upon high frequency stimulation (non-physiological) after the depletion of the recycling pool (Sudhof, 2004; Rizzoli and Betz, 2005).

Most recently, other vesicle pools were proposed, like the pool of stranded vesicle proteins on the plasma membrane (Gandhi and Stevens, 2003; Wienisch and Klingauf, 2006), the pool for spontaneous vesicle release (Sara et al., 2005), and a "superpool" of vesicles that are shared by multiple neighboring release sites (Darcy et al., 2006; Westphal et al., 2008; Staras et al., 2010) reviewed in (Staras, 2010)), although these "pools" are typically easy to reconcile with the vesicle types described above (see Denker and Rizzoli, 2010).

1.3   Synaptic Vesicle Recycling in Conventional Synapses

In a conventional central nervous system (CNS) synapse the synaptic vesicles are accumulated in front of the AZ at rest (in what is termed the synaptic vesicle cluster) (Figure 1.1). Upon the arrival of an action potential the synaptic vesicle fuses with the plasma membrane (exocytosis). By a specific and rather complex mechanism − called endocytosis − the vesicle material gets retrieved form the membrane next to the AZ to form new vesicles, that are moved back to the vesicle cluster for subsequent rounds of release (De Robertis and Bennett, 1954; Birks et al., 1960; Ceccarelli et al., 1973; Heuser and Reese, 1973; Holtzman et al., 1973; reviewed in Sudhof, 2004; Doherty and McMahon, 2009). Two principles explain the importance of the compensatory retrieval (vesicle recycling) of the vesicle membrane from the synaptic surface. On the one hand constantly fusing vesicles would heavily increase the surface area of the synaptic plasma membrane. On the other hand at some point the synapse would run out of vesicles and the energy input for the biosynthesis of new synaptic vesicle membranes and proteins in the neuronal cell body would be much too expensive. In addition, the newly synthesized vesicle components need to be transported towards the release sites, and a segregation mechanism would be necessary to dispose of the old fused vesicle material from the plasma membrane (which again would result in high

cellular expenses). Thus, local vesicle recycling is the most effective way for the nerve cell, and to guarantee reliable neurotransmission.

This cycle of synaptic vesicles between intra-synaptic and synaptic surface localization is termed the "synaptic vesicle cycle" (Sudhof, 2004). After half a century of synaptic research, vesicle (re-) cycling is not completely understood. Up to now various models of vesicle retrieval and their reuse are controversially discussed (Sudhof, 2004; Doherty and McMahon, 2009) (see Figure 1.1 for a schematic representation of the different vesicle recycling models (Kamin and Rizzoli, 2009)). Three hypothesized recycling models are discussed below: kiss-and-run, clathrin-mediated endocytosis, and bulk retrieval.

1.3.1 Kiss-and-Run

Synaptic vesicle recycling is directly linked to the mode of vesicle fusion. Synaptic vesicles could connect briefly with the plasma membrane through the formation of a transient fusion pore to release their contents (Alvarez De Toledo et al., 1993; Fesce et al., 1994; Klingauf et al., 1998; Pyle et al., 2000; Aravanis et al., 2003). After neurotransmitter release, the pore closes and the synaptic vesicles could be reused immediately (Harata et al., 2006). The empty synaptic vesicles could then remain at the active zone and refill with neurotransmitter, what is termed "kiss-and-stay", or they detach from the active zone and get refilled elsewhere, what is termed "kiss-and-run" (Figure 1.1, black arrow) (Fesce et al., 1994; Aravanis et al., 2003; Gandhi and Stevens, 2003; Harata et al., 2006).

1.3.2 Clathrin-Mediated Endocytosis

Another fusion mode is described by a full-collapse of the synaptic vesicle with the plasma membrane (Heuser and Reese, 1973). The synaptic vesicle needs then to be recycled via an endocytic retrieval pathway (Ceccarelli et al., 1973; Heuser and Reese, 1973). Before synaptic vesicle retrieval, the vesicle moves laterally across the plasma membrane, possibly in a protein cluster (Willig et al., 2006; Opazo et al., 2010), to get then recycled at the periactive zone via clathrin-mediated endocytosis (CME) (Figure 1.1, red arrows) (Takei et al., 1996). In 1973, Heuser and Reese were the first who described the clatrhin-dependent

mode of synaptic vesicle recycling and generated a schematical model, which is since then taken as the "classical" model of the synaptic vesicle cycle (Heuser and Reese, 1973). CME is characterized by its major protein clathrin, named to indicate the lattice-like structure (the "coat") it forms around the endocytosed vesicle (Heuser and Reese, 1973; Pearse, 1976). The clathrin protein is composed of three 192 kDa heavy chains each linked to a 30 kDa light chain, which co-assemble to form a three-legged structure ("triskelion" (Kirchhausen et al., 1986)). Clathrin proteins are capable of their self-assembly into a lattice of hexagons and pentagons. These form a coated structure on the vesicle material at the plasma membrane – termed clathrin-coated pit. Clathrin works with various endocytic proteins through a cascade of protein interactions to build the cage around the fused material. One of the most important clathrin interaction partners is the adaptor protein 2 complex (or assembly protein, AP2 (Boucrot et al., 2010)), which is recruited to the membrane prior to the clathrin triskelions. It regulates the clathrin lattice-formation by interacting with both clathrin and the fused membrane to finally form a clathrin-coated pit (Miller and Heuser, 1984; Boucrot et al., 2010). After the pit formation the invaginated coated vesicle pinches off the membrane with the help of the GTPase activity of dynamin (Koenig and Ikeda, 1989; Takei et al., 1995; Takei et al., 1996; Ferguson et al., 2007). Dynamin, recruited by the protein amphiphysin to the clathrin-coated structure (David et al., 1996; McMahon et al., 1997), wraps in helical rings around the neck of the invaginated clathrin-coated pit. GTP hydrolysis then changes the dynamin conformation which regulates the tightening of the helical rings and finally scissors the clathrin-coated vesicle off the plasma membrane (Takei et al., 1995). In the end, the clathrin-coat recycles by the disassembly of the triskelion structures through the work of the uncoating ATPase hsc70 (Höning et al., 1994). After coat-disassembly the vesicles either move directly back to the vesicle cluster (Figure 1.1, red arrows), or they fuse with an endosome, from which then new fusion-competent vesicles bud (Figure 1.1, green arrows) (Heuser and Reese, 1973; Miller and Heuser, 1984; Takei et al., 1996; Sudhof, 2004; Rizzoli et al., 2006; Hoopmann et al., 2010).

1.3.3 Bulk Endocytosis

A third model of the synaptic vesicle cycle is believed to be activated only during/ after high frequency stimulations, which is termed bulk endocytosis (Figure 1.1, blue arrowheads; for a review see Clayton and Cousin, 2009). Under sustained levels of strong stimulation bulk membrane infoldings appear, because large amounts of vesicle material are added to the plasma membrane, which overstrain the normal CME pathway. In order to compensate for the sudden membrane overload the synapse invaginates the excessive membrane, from which coated vesicles bud via CME (Gennaro et al., 1978; Takei et al., 1996; Richards et al., 2000; Meunier et al., 2010). Likewise, the entire infolding could get retrieved to form a cisternal compartment, from which vesicles are regenerated (not shown in Figure 1.1, (Teng and Wilkinson, 2000)).
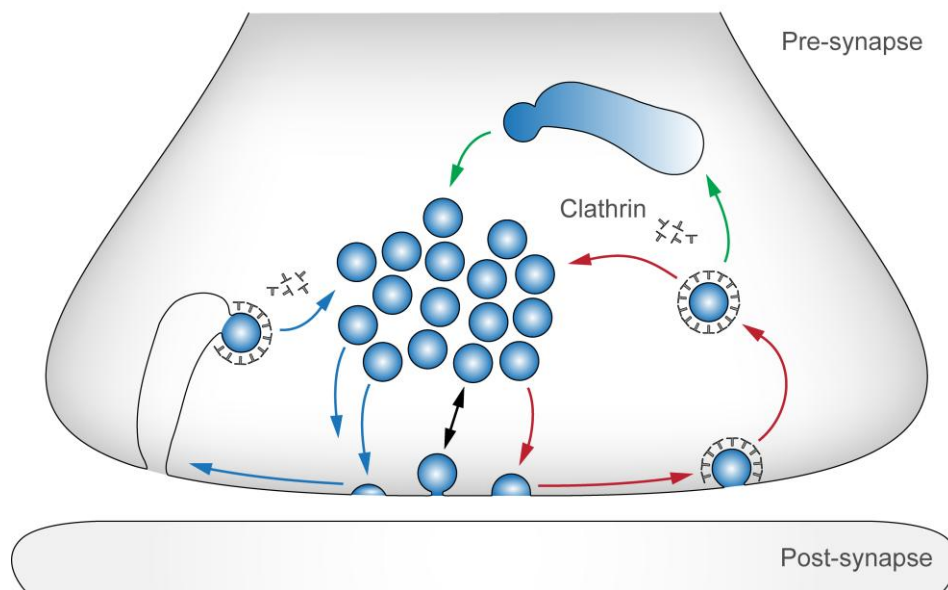
Figure 1.1: Schematic representation of a conventional synapse with the various suggested models of the synaptic vesicle cycle. The presynaptic nerve terminal lies opposing the postsynaptic compartment. Small, neurotransmitter-filled synaptic vesicles (~40-50 nm in diameter) are housed in the presynapse and are grouped together in a vesicle cluster. After action potential triggered neurotransmitter release (exocytosis), the synaptic vesicles are retrieved via different routes of endocytosis. Vesicle recycling can occur via "kiss and run" (black arrows, or "kiss and stay"), the clatrhin-mediated endocytosis pathway (red arrows) with the possibility of a recycling step through a sorting endosome, or via bulk endocytosis (blue arrows) in co-operation with CME.

1.4 Sensory Synapses

Most of what is known about the synaptic vesicle cycle was studied on conventional CNS synapses and neuromuscular junctions (NMJ). In contrast less is known about the vesicle cycle in non-conventional sensory synapses. How does the vesicle cycle of conventional synapses compare with the one of a sensory synapse?

Mammalian sensory synapses are present in the photoreceptors (e.g. rods and cones) of the visual system, the mechano-, thermo- and chemoreceptors (e.g. muscle receptors) of the somatosensory system, the chemoreceptors (e.g. taste buds) of the olfactory and gustatory systems, and the mechanoreceptors (e.g. hair cells) of the vestibular and auditory systems (Purves et al., 2001). While the various receptor types are usually completely different, all sensory systems share three common properties: first, a physical stimulus at the sensory receptor cell (the first cell in the sensory pathway), second, the transformation of the stimulus into an electrical nerve impulse (receptor signal), and third, the reaction to the signal (perception) (Kandel et al., 2000).

Since in this work the vesicle recycling in sensory cochlear hair cells will be investigated, the following part will exclusively deal with the sensory synapses of the mammalian ear.

1.4.1 The Auditory System

The mammalian ear is composed of three functional parts: the external ear, the middle ear, and the inner ear. The external ear conducts the sound wave onto the eardrum (*membrana tympani*) of the middle ear. From the eardrum the sound is transferred onto the three inter-connected middle ear bones (or ossicles; *malleus* (hammer), *incus* (anvil), *stapes* (stirrup)). Eardrum and ossicles represent the sound conduction apparatus – they are responsible for the transduction of the acoustic sound wave into fluid displacements in the cochlea (from Greek cochlos: snail (Kandel et al., 2000)) (Kahle and Frotscher, 2005). The cochlea is composed of three fluid-filled tubes that run helically around the conical bony core of the cochlea (*modiolus cochleae*). The upper tube is the *scala vestibuli*, which is characterized by the basal oval window (closed by the footplate of the stapes). The lowest tube is the *scala tympani* with the basal, diaphragm-closed, round window. Interjacent of these tubes lies the cochlear duct or *scala media*. Its upper boundary (to the *scala vestibuli*) is represented by the Reissner´s

membrane, and the lower boundary is formed by the basilar membrane (Purves et al., 2001). The basilar membrane supports the important auditory transduction apparatus – the organ of Corti (Figure 1.2). The organ of Corti is composed of various types of supporting cells (e.g. inner and outer pillar and phalangeal cells) and neuroepithelial cells, as well as of the essential sensory receptor cells of the auditory system – the inner and outer hair cells (Figure 1.2).
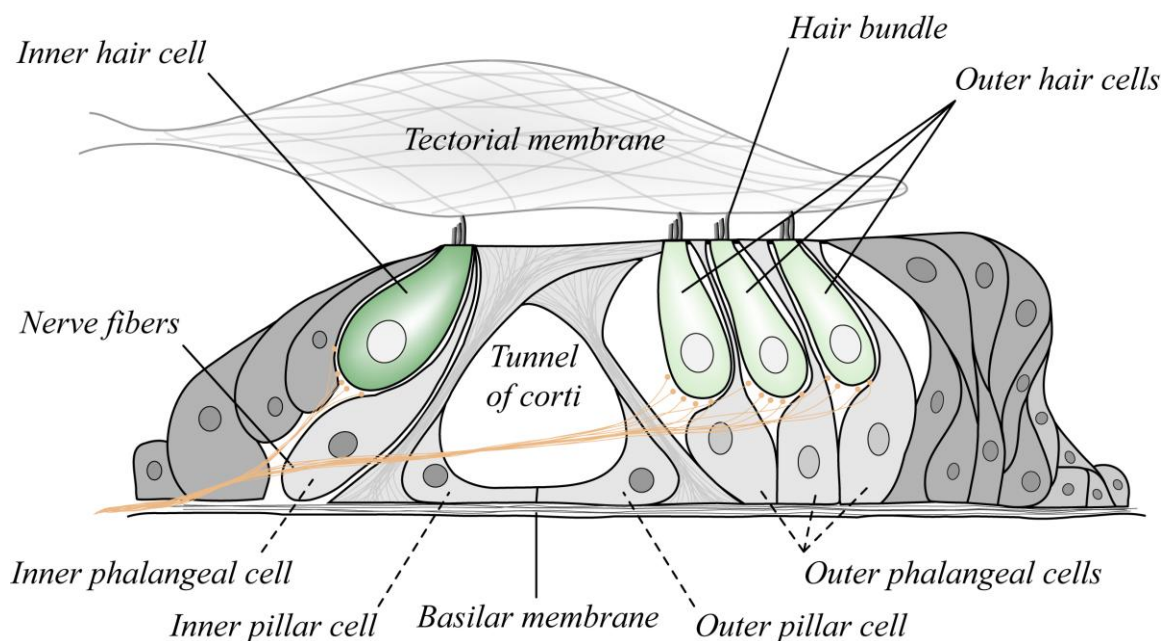
Figure 1.2: Cross-section schematic of the organ of Corti. The auditory organ is located on the basilar membrane in the cochlear duct. It is composed of different types of supporting and epithelial cells with various fluid-filled tunnels in between (e.g. tunnel of Corti). Embedded among these cells are the sound encoding inner hair cells (IHCs, dark green) and the sensitivity controlling outer hair cells (OHCs, light green) located. The IHCs are arranged in one row, the OHCs in three rows. Both stretch their sensory hair bundles (stereocilia) at the apical pole out into the endolymph-filled cochlear duct. The tallest tips of the cilia touch the overlying tectorial membrane, a gelatinous layer. At the basal parts (the locations of the active zones) synaptic contacts are formed with afferent nerve fibers that project to higher brain regions (the spiral ganglion neurons; orange).

1.4.2 Sensory Inner Hair Cells

The sensory hair cells are non-neuronal epithelial-derived cells with apical hair bundles (stereocilia, hence its name) (Figure 1.2, Figure 1.3). The organ of Corti is characterized by three rows of outer hair cells (OHCs) and only one row of inner hair cells (IHCs, Figure 1.2). However, IHCs are the actual sensory receptors, while the OHCs are possibly unrelated to sound encoding and are thought to control the cochlear sensitivity. Thus, in this work only vesicle recycling in the sound-encoding cochlear IHCs was investigated.

Each IHC contains around 30 to a few hundred stereocilia that are bathed in the potassium-rich endolymph (contrary to the sodium-rich environment of conventional synapses). The tallest one of the hair bundle is a microtubule-containing kinocilium; the smaller stereocilia are only filled with actin. They are ordered in a bilateral-symmetric shape and vary gradually in height. Fluid motion in the *scala vestibuli* and *scala tympani* in the cochlea leads to the movement of the basilar membrane and thus to the deflection of the hair bundles (through the connection of the stereocilia with the tectorial membrane located above the hair bundle (Kahle and Frotscher, 2005)). Each stereocilia is connected with its neighboring stereocilia by filamentous processes – the tip links. They are linked at one end with an ion channel, which transmits potassium and calcium (Purves et al., 2001). As a result of the deflection of the stereocilia the tip links elongate and mechanically open selective transduction channels (hence they are named mechanotransduction channels). Potassium flows in and depolarizes the hair cell (graded receptor potential) (Corey and Hudspeth, 1979), which in turn opens baso-lateral located voltage-gated calcium channels in the plasma membrane (functioning in a similar fashion to conventional synapses) and as a consequence triggers neurotransmitter release at their specialized synapses (see below) (Figure 1.3).

1.4.3 Key Players of Vesicle Release in Sensory Synapses

The basal part of the mouse IHCs exhibits numerous presynaptic active zones (~10-20 (Francis et al., 2004; Khimich et al., 2005). Their active zones have a specialized feature, a structure called synaptic ribbon or body – hence these synapses are termed ribbon synapses. Ribbon-type active zones are also found in sensory photoreceptors and bipolar cells of the retina, as well as in vestibular hair cells (for review, see Lenzi and Von Gersdorff, 2001). The

molecular composition of the ribbon remains unclear. However, it is known that the ribbon specific protein RIBEYE (Schmitz et al., 2000; Khimich et al., 2005), and the large cytomatrix scaffolding proteins bassoon and piccolo are present (common to the AZ of conventional synapses; (tom Dieck et al., 2005)). Bassoon anchors the synaptic ribbon to the plasma membrane (Dick et al., 2003; Khimich et al., 2005), which is thought to act as a "conveyor belt" that actively guides the vesicles toward the AZ (it may also have other properties (Parsons and Sterling, 2003)).

Vesicle fusion is likely similar regulated as in conventional synapses, because the t-SNAREs syntaxin 1 and SNAP-25, as well as the v-SNARE synaptobrevin-1 are expressed (but not synaptobrevin-2 like in CNS synapses; (Safieddine and Wenthold, 1999)). Interestingly, some of the major synaptic proteins are absent from the IHCs. The general synaptic vesicle protein synaptophysin (Jahn et al., 1985) (which is present in 32 copies per synaptic vesicle in CNS synapses (Takamori et al., 2006)) is not expressed in cochlear hair cells; the same for the synaptic vesicle-associated phosphoprotein synapsin (8 copies per vesicle in CNS synapses (Takamori et al., 2006)) (Safieddine and Wenthold, 1999). Moreover, the calcium sensor of conventional synaptic vesicles (synaptotagmin 1/2) is not present in cochlear hair cells (Safieddine and Wenthold, 1999). In conclusion, the lack of highly important conventional vesicle proteins in hair cell ribbon synapses raises the question of how synaptic vesicle cycling functions here. It was recently shown that synaptotagmin IV and VI-IX are expressed in the mammalian cochlea (Safieddine and Wenthold, 1999). Synaptotagmin IV knockout-mice were used to investigate its role in vesicle release (Johnson et al., 2010), with the result of decreased calcium-dependent transmitter release. Thus, synaptotagmin IV seems to be directly connected to synaptic vesicle fusion in IHCs.

However, others have shown that the IHC-specific vesicle protein otoferlin may be the major calcium sensor of synaptic vesicle fusion. It binds calcium via C2-domains like the conventional synaptotagmin protein, and shows calcium-dependent interactions with the SNARE proteins syntaxin 1 and SNAP-25 (Roux et al., 2006). Its role in exocytosis is in addition supported by results of otoferlin knockout mice, where exocytosis events in IHCs were virtually abolished (Roux et al., 2006).
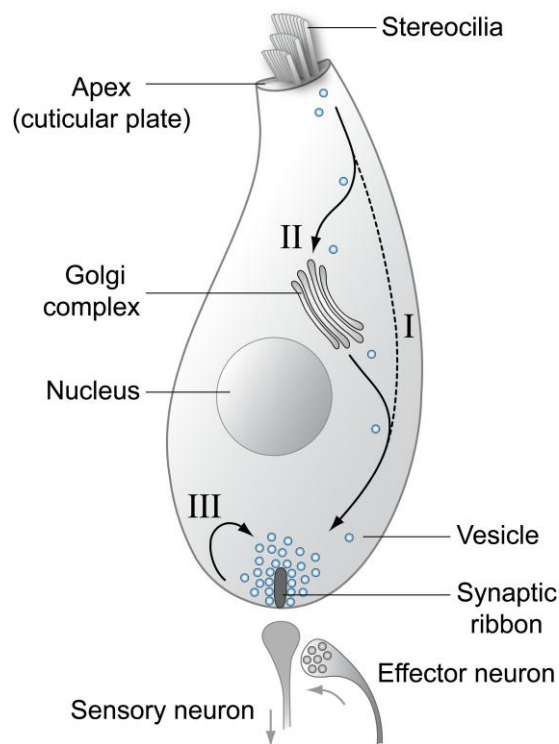
Figure 1.3: Inner hair cell representation with the debated vesicle recycling routes. The apical pole of the hair cell is characterized by the sensory hair bundle (stereocilia), which is connected with the apical electron dense structure (cuticular plate). The glutamatergic ribbon-type active zones (~10-20) are located at the basal pole and host large amounts of synaptic vesicles (blue). Afferent synapses of the sensory ganglion neurons are located adjacent to the ribbon to propagate the electric impulse into higher brain regions. They are selectively controlled by efferent neurons from the brain and OHCs. Different models of vesicle/ membrane recycling are hypothesized: Membrane recycling occurs at the apical pole with the downwards transit of the vesicle to the release sites (I). Possibly the vesicles fuse with the Golgi complex from which new vesicles are transported down to replenish the vesicles at the ribbons (II), or a local vesicle recycling pathway exists near the ribbon synapses (comparable to conventional synapses; III).

1.4.4 Vesicle Recycling in Sensory Synapses

Importantly, the ribbon docks a highly packed monolayer of vesicles and supplies large amounts of vesicles at the release site (Lenzi et al., 1999; Khimich et al., 2005) (Figure 1.3)). The amount of vesicles in the cytoplasm close to ribbon-type active zones of hair cells and bipolar terminals is at least 30-fold higher than in non-synaptic regions (Rizzoli and Betz, 2005), with a size of 10000 – 30000 cytoplasmic vesicles per saccular hair cell synapse of the frog (Lenzi et al., 1999). Thus, in response to the graded receptor potential the sensory cells can sustain neurotransmitter release with hundreds of vesicles fusing per second over long

periods (retinal bipolar cells (Lagnado et al., 1996) cochlear inner hair cell (Beutner et al., 2001; Nouvian et al., 2006)). According to the concept of the graded receptor potential IHC ribbon synapses have substantially more numerous fusion events compared to conventional synapses and neuromuscular junctions. Consequently, IHCs request an efficient machinery for vesicle recycling to replenish the vesicles at the ribbon-synapse. Unfortunately, the pathway of vesicle recycling in IHCs remains in contrast to conventional synapses almost unknown. It was shown that endocytosis in cochlear IHCs can occur in less than half a second (maximal rate ~0.3 seconds) in parallel with a slower compensatory endocytic rate ($\tau \approx 15$ seconds) (Beutner et al., 2001). Since clathrin-coated pits and coated vesicles were found close to the ribbon-type AZs of saccular hair cells of the goldfish and the frog and of cochlear hair cells of chinchillas and gerbils, the retrieval mechanism could be clathrin-dependent (Hama and Saito, 1977; Siegel and Brownell, 1986; Lenzi et al., 1999). The localization of the clathrin-coated organelles predict a local endocytosis mechanism, comparable to conventional synapses. The recycled vesicles in gerbil cochlear hair cells intermix with the large common vesicle pool and presumably refill the ribbon-attached vesicles (Siegel and Brownell, 1986). In addition, large plasma membrane infoldings were observed near the ribbon synapses after high stimulation, comparable with bulk endocytosis at conventional synapses (Lenzi et al., 1999; Lenzi et al., 2002).

Besides a local CME mechanism at the basal part it was suggested that membrane retrieval takes place at the apical pole. The endocytosed vesicles move down to fuse with the Golgi complex, from which newly formed vesicles are transported to the basal release sites to refill the vesicles at the ribbon-synapses (Figure 1.3) (Griesinger et al., 2002; Griesinger et al., 2004; Griesinger et al., 2005). These studies used the fluorescent styryl dye FM1-43 to specifically label recycled membranes. FM dyes are amphiphilic molecules (see Figure 2.2 in Methods) that are able to incorporate into the plasma membranes of cells and most important of synaptic vesicles and can therefore be internalized in vesicles upon their retrieval (Gaffield and Betz, 2006). Importantly, styryl dyes can only enter a cell through endocytosis, because their amphiphilic structure prevents penetration or flipping across the plasma membrane. Fluorescent dye uptake has been used since decades in conventional synapses and neuromuscular junctions to label recycling vesicles in an activity-dependent fashion (frog NMJs (Betz and Bewick, 1992; Betz et al., 1992) hippocampal cultured neurons (Ryan et al., 1993). The advantage of FM dyes is that the release/ wash out of the dye from labeled

synaptic vesicles could be imaged when they fuse again with the plasma membrane. This makes FM dyes a reliable reporter of synaptic vesicle cycling (Cochilla et al., 1999; Gaffield and Betz, 2006).

Interestingly, when FM dyes are used to monitor vesicle recycling in cochlear hair cells, their fluorescence is readily observable at the apical pole and was interpreted as apical endocytosis (Griesinger et al., 2002; Griesinger et al., 2004; Griesinger et al., 2005)).

Nevertheless, the existence of an apical endocytosis pathway for vesicle recycling is controversially debated. Another view on apical FM dye entry is based on the fact that FM dyes work as an acute blocker of the mechanotransduction channels (Gale et al., 2001). Moreover, breaking the tip-links of the stereocilia blocks FM loading (Gale et al., 2001; Crumling et al., 2009). These results suggested that FM dyes enter the cells through the non-selective mechanotransduction channels, and not via apical endocytosis (Nishikawa and Sasaki, 1996; Gale et al., 2001; Meyers et al., 2003). Consequently, the apical penetration would label all membranes inside the cell, starting at the apical pole.

Taken together, with FM dyes being general membrane markers, it cannot be assumed that FM dye uptake is solely due to vesicle recycling. In particular one has to keep in mind that the cell also has to deal with other major cellular functions, which possibly require exo- and endocytosis (constitutive recycling, transferrin uptake) and would thus take up the dye.

1.4.5 Morphology of the Vesicle Cycle in Sensory Synapses

Referring to the differing molecular compositions of sensory ribbon synapses and conventional synapses, the chance of success for live-investigations of vesicle cycling in IHCs seems to be rather limited at the moment. A more promising way to map the vesicle recycling steps is related to ultrastructural investigations of sensory hair cells. In the mid-'80s Siegel and Brownell (Siegel and Brownell, 1986) performed laborious *in vivo* HRP labeling experiments on gerbils and chinchilla cochlear hair cells to investigate recycling by high-resolution electron microscopy (similar to the "classical" vesicle recycling studies of (Ceccarelli et al., 1973) and (Heuser and Reese, 1973) on neuromuscular junctions). They anaesthetized the animals and perfused HRP through the cochlear turns for up to 30 minutes while stimulating acoustically. After fixation the preparations were treated with diaminobenzidine as the enzymatic HRP reaction substrate to finally uncover the organelles

that took up the marker during incubation. Siegel and Brownell observed various labeled organelles, e.g. small synaptic vesicle-like organelles at the ribbon synapse, endosome-like organelles of diverse sizes, coated organelles (clathrin), labeled cisternae of the Golgi complex as well as labeled and unlabeled tubules (Siegel and Brownell, 1986). The scientists were rather cautious about the interpretation of the vesicle recycling pathway and did not relate the Golgi complex labeling to synaptic vesicle recycling, as later stated by Griesinger and colleagues who used fluorescence imaging of FM labeled hair cells to conclude that the Golgi complex is involved in the vesicle recycling pathway (see above (Griesinger et al., 2002; Griesinger et al., 2004; Griesinger et al., 2005)).

Ten years later, another study investigated the recycling organelles of the lateral line organs of Xenopus larvae by the use of FM1-43 in combination with its photo-oxidation and electron microscopy (see 1.6 for the principle behind the photo-oxidation method (Nishikawa and Sasaki, 1996)). They reported immense labeling of mitochondria and tubular structures like Siegel and Brownell, as well as small synaptic vesicle-like organelles at the afferent ribbon type active zones.

A further ultrastructural study on cochlear IHCs that did not use any kind of uptake marker also reported the presence of cisternae and tubular structures close to the ribbon synapse, likewise indicating the existence of a specialized retrieval mechanism in IHCs (Spicer et al., 1999).

In summary, ultrastrutural investigations have the potential to uncover the vesicle recycling pathway in IHCs in terms of its morphology.

1.5 Synaptic Vesicle Mobility

On the one hand the individual steps of the synaptic vesicle cycle have been described in molecular detail, at least for the conventional synapses as shown above, although on the other hand only few aspects are known about the general mobility of the synaptic vesicles. Since the vesicle recycling mechanism in sensory IHCs is less well known, a brief overview of the current knowledge of vesicle mobility in conventional synapses and neuromuscular junctions will be presented.

The first part of the introduction made clear that synaptic vesicles need to be mobile in order to undergo the vesicle cycle in both conventional and sensory synapses. Vesicles have to reach the AZ for fusion and release of their contents (exocytosis). Furthermore, the synaptic vesicles move across the plasma membrane after exocytosis, and need to move back to the vesicle cluster after endocytosis. The issue of vesicle mobility is controversially discussed, with a number of studies indicating that vesicle movement is very limited, although substantial displacements within and between synapses have also been observed.

In the absence of synaptic activity the resting synaptic vesicles are clustered at the AZ and are thought to be immobile. The first confirmations of a low-mobility state were revealed by labeling vesicle clusters with the already mentioned membrane marker FM1-43 (frog NMJ (Betz and Bewick, 1992), hippocampal cultured neurons (Ryan et al., 1993)). These findings were supported by electron microscopy studies showing that the synaptic vesicles in the cluster are tightly packed, cross-linked to each other, and connected to cytoskeletal filaments like actin (Hirokawa et al., 1989; Siksou et al., 2007; Fernández-Busnadiego et al., 2010). Moreover, fluorescence recovery after photobleaching (FRAP) studies, where a small spot in the fluorescently-labeled vesicle cluster was bleached, reported no vesicle movements at rest into the bleached area (vesicle cluster labeled with FM1-43 (Henkel et al., 1996a; Henkel et al., 1996b), or with CY3-tagged antibodies (Kraszewski et al., 1995)). However, with antibody-labeled vesicles, which are not lost upon vesicle fusion, the fluorescence recovery was much higher after stimulation, indicating the entry of recycling vesicles into the vesicle cluster (Kraszewski et al., 1996). Interestingly, FRAP experiments in ribbon-type cone photoreceptors revealed high recovery values (Rea et al., 2004), showing that in these cells a highly mobile vesicle fraction exists, which contradicts the findings presented above.

In conventional synapses high movements of the vesicle cluster were only detected after treating the preparations with the phosphatase inhibitor okadaic acid (Betz and Bewick, 1992; Kraszewski et al., 1996). Okadaic acid treatment results in the phosphorylation of various proteins, one of which is synapsin, (De Camilli et al., 1983a; De Camilli et al., 1983b; Huttner et al., 1983; Torri Tarelli et al., 1992; Hilfiker et al., 1999; Fernández-Busnadiego et al., 2010)). Dephosphorylated synapsin presumably immobilizes the synaptic vesicles at rest by cross-linking them to each other and connecting them to the actin cytoskeleton as it was observed with electron microscopy (Hirokawa et al., 1989; Siksou et al., 2007). During synaptic activity this protein gets phosphorylated and releases the vesicles from their bonds, and thus regulates their motion.

Further studies confirmed the findings of a highly organized vesicle cluster in conventional synapses by using fluorescence correlation spectroscopy. Thus, different mechanisms were suggested that constrain vesicle movements. One proposal is "stick-and-diffuse", in which the synaptic vesicles bind to and detach from cellular components like the cytoskeleton (Shtrahman et al., 2005; Yeung et al., 2007). Another proposal is "caged diffusion", which describes a random synaptic vesicle motion in a virtual circular cage inside the synapse (cage size of 50-100 nm, (Jordan et al., 2005)). Vesicle movements were also very low at rest and during stimulation when single vesicles were labeled and analysed by single-particle-tracking methods (of diffraction limited spots (Lemke and Klingauf, 2005)). The vesicles remained virtually at their origin and could be described as completely immobile; hence the proposed caged diffusion model may in general not be relevant for all synaptic vesicles.

As mentioned above the vesicle cluster of a synapse has been roughly divided in two pools of different properties, the active recycling pool, to which the readily releasable pool belongs, and the resting or reserve pool (see above Rizzoli and Betz, 2005). The so far mentioned studies investigated all synaptic vesicles randomly. However, Gaffield and his colleagues labeled specifically both pools and performed FRAP experiments. They could show that the resting synaptic vesicles were entirely immobile while the recycling synaptic vesicles were rather mobile (Gaffield et al., 2006). Interestingly, an ultrastructural study in combination with the FM photo-oxidation method showed that the recently endocytosed vesicles were randomly distributed throughout the synaptic vesicle cluster and not separated from this pool, indicating that the vesicles need to be mobile in order to reach the AZ for release (see 1.6 for the principle behind the photo-oxidation method (Rizzoli and Betz, 2004)).

The current literature suggests that overall the movement of synaptic vesicles is relatively low, both at rest and during stimulation. Recently endocytosed vesicles may behave differently, but no direct investigations on their mobility were performed. Kraszewski and colleagues only found that antibody-labeled vesicles move back to the vesicle cluster after high potassium stimulation and intermix with the resting vesicles (Kraszewski et al., 1996).

In contrast to the movement within synapses (intra-synaptic), the vesicle movements between synapses (inter-synaptic) are less well described. In a recent FRAP study on hippocampal cultured neurons, FM-labeled single boutons were photobleached and the fluorescence recovery indicated that vesicles move continuously from synapse to synapse (Darcy et al., 2006; Fernandez-Alfonso and Ryan, 2008; Staras et al., 2010). Moreover, FM photo-oxidation in combination with high-resolution electron microscopy revealed that the newly arrived vesicles intermix with the pre-existing vesicle cluster similar to recycling vesicles of the same synapse (Rizzoli and Betz, 2004; Darcy et al., 2006). However, live-imaging showed that most of the vesicles passed through the boutons, without their incorporation into any vesicle cluster (Darcy et al., 2006).

Finally, the mobility of fused vesicle in the plasma membrane is almost unknown as (i) FM dyes are rapidly lost from the fused vesicles after exocytosis (Zenisek et al., 2002) and (ii) antibody-labeled synaptic vesicles cannot be separated according to their intra-synaptical or surface exposed location (Kraszewski et al., 1995). Sankaranarayanan and Ryan found that GFP-tagged synaptic vesicle proteins (pHluorins: pH-sensitive variant of GFP, see Miesenböck et al., 1998) spread into the axons under tetanic stimulation (Sankaranarayanan et al., 2000). However, it is not obvious whether the fused vesicle material would behave similar under physiological or resting conditions.

1.6 The Importance of High-Resolution Microscopy

As reviewed above, synaptic vesicle movements in conventional synapses are not so clear. The characterization of the vesicular behavior was achieved only by averaged analysis over populations of vesicles with sparse vesicle labeling (Gandhi and Stevens, 2003; Lemke and Klingauf, 2005; Zhang et al., 2009) or indirect behavior measurements using FRAP (Kraszewski et al., 1995; Henkel et al., 1996b; Kraszewski et al., 1996; Gaffield et al., 2006) or correlation spectroscopy (Jordan et al., 2005; Shtrahman et al., 2005; Yeung et al., 2007). Consequently, the question arises how synaptic vesicle behavior could be described when single vesicles are analyzed?

The best resolution one can achieve for single organelle investigations is provided by high-resolution electron microscopy. However, their drawback is a very low labeling efficiency. Additionally, this technique is labor-intensive and does not allow any *in vivo* investigations.

The most excellent labeling efficiency is achieved by fluorescence immunolabeling. However, conventional far-field fluorescence microscopes are restricted in resolution by the spatial resolution limit of the microscope, which is the result of the wave nature of light (diffraction limit of light). This natural law was first identified by Ernst Abbé in the late 19th century (Abbe, 1873). He found that the resolution of a standard microscope is limited by the diffraction of light to $\lambda/(2NA)$, with λ representing the wavelength of light and NA symbolizing the numerical aperture of the objective lens.

Related to this, single synaptic vesicles (or proteins of interest) that are closer together than about half of the wavelength of light (visible spectra: $\lambda \sim 390\text{-}750$ nm, hence $\lambda/2$ is at the lowest ~ 200 nm) appear as one blurred object, which impedes resolving their individual positions. As synaptic vesicles are small (~ 40 nm in diameter) and densely clustered in the synapse, their individual positions cannot be resolved with conventional optics.

In the last years the diffraction barrier of far-field fluorescence microscopes has been broken by several sub-diffraction high-resolution microscopy techniques (Hell, 2007, 2009), with stimulated emission depletion (STED) microscopy as being the first one (Hell and Wichmann, 1994). The diffraction-unlimited resolution of a STED microscope is typically achieved by the implementation of an additional laser line (the STED beam) to the excitation laser of a standard confocal laser-scanning microscope (see Figure 2.1). The excitation laser is overlapped in the focal area by this second, usually doughnut-shaped beam. The STED

laser brings the fluorescent molecules in the periphery of the excitation spot down to the ground state (depletion) by the effect of stimulated emission. Finally, fluorescence is only detected from the central area of the excitation spot – where the intensity of the STED beam is close to zero. As a result, the effective fluorescent spot is much narrower than the diffraction-limited excitation spot of a conventional fluorescence microscope, and leads to significantly higher resolution.

It was already shown that the specific high-resolution features of a STED microscope allow the separation of single synaptic vesicles in the confined space of the synapse (Willig et al., 2006). I will use in this work STED microscopy to image the vesicle movement in living hippocampal cultured neurons, which will allow me to track multiple synaptic vesicles simultaneously and describe their motion behavior.

Similar to standard confocal microscopy techniques STED microscopy has the drawback of a low penetration depth into living tissue (several micrometer). This makes its use for deep tissue imaging, as for the tissue embedded inner hair cells, impossible. To circumvent these difficulties I will attempt a morphological characterization of the recycling organelles using the specific method of FM dye photo-oxidation in combination with unsurpassed high-resolution electron microscopy.

The principle of the photo-oxidation method is the conversion of a fluorescent signal into an electron dense product that is visible with electron microscopy. The amphiphilic structure of a FM dye consists of a lipophilic tail group (which allows the dye to incorporate into membranes) and a positively charged head group that prevents the dye from flipping across the membrane (see Figure 2.2). Two aromatic rings in the middle part represent the fluorophore. In an aqueous environment the quantum yield of the dye is close to zero but increases by two orders of magnitude when it inserts via the lipophilic tail into membranes (Gaffield and Betz, 2006).

The illumination of the FM dye leads to the emition of photons (fluorescence) while in the same time it produces reactive oxygen species (ROS, Figure 2.2). The ROS can oxidize 3,3'-diaminobenzidine (DAB) in the close proximity of the dye, which results in the precipitation of DAB to an electron dense product. Endocytic organelles that took up the dye during incubation can therefore be photoconverted (I employ here this classically-used term,

although the correct term is photo-oxidation) from a fluorescent signal (coming from the FM dye itself) to an electron dense signal for electron microscopy (coming from the DAB oxidation), allowing their distinction from unlabeled organelles.

This technique will essentially allow me to perform a morphological description of the involved recycling organelles in IHCs on the single organelle level.

1.7 Aims of This Work

As presented above the mobility of synaptic vesicles in conventional synapses is still poorly understood, with the general vesicle mobility usually investigated over populations of vesicles (averaged behavior) using diffraction-limited imaging techniques. The current literature left the question unanswered on how mobile are actually the synaptic vesicles in the small space of the synapse when observed separately?

The first goal of this work was to describe in detail the properties of synaptic vesicle mobility using both conventional and sub-diffraction high-resolution stimulated emission depletion (STED) fluorescence microscopy. The well-known model system of primary hippocampal cultured neurons was used to investigate vesicle mobility in conventional synapses *in vivo*. Based on high-resolution STED imaging, I wanted to conduct a descriptive study of synaptic vesicle mobility and provide a thorough view of the vesicle behavior during the individual steps in the vesicle cycle. Finally, the analysis of vesicle recycling in morphological terms, by the FM photo-oxidation technique, should complete the vesicle recycling studies.

How can the vesicle recycling in conventional synapses be compared with that of non-conventional sensory synapses? Synaptic transmission in inner hair cells is an essential step for hearing. Unfortunately, the steps of the vesicle recycling and their molecular key players are less well known in cochlear IHCs. Thus, the second goal of this work was to compare the findings from the conventional synapse to sensory IHCs. In an attempt to elucidate vesicle recycling in IHCs I wanted to use live fluorescence imaging techniques to study vesicle recycling *in vivo*.

Moreover, the FM photo-oxidation technique followed by high-resolution electron microscopy was used as well to characterize the recycling organelles in IHCs in morphological terms. Based on this technique, I wanted to (i) identify the morphological nature of the organelles that are involved in the vesicle retrieval process in IHCs (large or small organelles, membrane infoldings, endosomes) and (ii) give the first morphological characterization of the vesicle recycling pathway in sensory IHCs. Finally, with the ultrastructural analysis I wanted to discover the location of the major membrane endocytosis site in IHCs (apical as proposed by FM dye studies, or baso-lateral near the AZs as in other ribbon synapses).

2 Materials and Methods

2.1 Materials

2.1.1 Animals

C57BL/6J and C57BL/6N mice were used for membrane recycling studies on sensory IHCs. Mice were used between postnatal day 14 to 18. All animal experiments meet the terms of the national animal care guidelines.

2.1.2 Antibodies

Antibodies used for live-cell imaging (STED and FRAP) and live-labeling of hippocampal cultured neurons were: monoclonal mouse antibodies 604.2 and 604.1 (ascites fluid; 1mg/ml) against the intravesicular (lumenal) domain of the synaptic vesicle protein synaptotagmin I (Synaptic Systems, Göttingen, Germany). The antibodies were used either directly fluorescence-labeled with Atto647N (in case of 604.2) or with a secondary labeling with Atto647N fluorescence-labeled anti-mouse Fab fragments from donkey or goat (AffiniPure Fab fragments from Jackson ImmunoResearch Laboratories, West Grove, PA, USA; organic fluorophore Atto647N from Atto-Tec, Siegen, Germany). Live-labeling of hippocampal neurons was also performed with directly fluorescence-labeled Oyster-550 monoclonal mouse anti-synaptotagmin I antibodies (604.2; 1mg/ml).

Primary antibodies for immunohistochemistry were as follows: anti-synaptophysin, anti-clathrin light chain and anti-SNAP-25 polyclonal rabbit antibodies (named G96 (Jahn et al., 1985), Clc (Takamori et al., 2006) and casanova (Aguado et al., 1996), respectively; kind gifts from R. Jahn, Max Planck Institute for Biophysical Chemistry, Göttingen, Germany). Anti-alpha-tubulin, anti-amphiphysin, anti-GluR1 (AMPA1), anti-Rab3, anti-synapsin 1/2, anti-Munc13-1, and anti-bassoon: all polyclonal rabbit antibodies (Synaptic Systems).

Secondary antibodies for immunohistochemistry were Cy2-, Cy3 and Cy5-conjugates to goat anti-rabbit IgGs and Cy5-conjugated goat anti-mouse IgGs (AffiniPure, Jackson ImmunoResearch Laboratories).

Antibodies used for live-labeling of sensory inner hair cells were: rabbit polyclonal otoferlin antibodies (0.6 mg/ml) against the intravesicular (lumenal) domain of the vesicle protein otoferlin (Synaptic Systems, Göttingen, Germany).

2.1.3 Buffers

The standard chemicals and other reagents were purchased from Sigma-Aldrich (Steinheim, Germany) or Merck (Darmstadt, Germany) unless otherwise specified.

Tyrode buffer (pH 7.4) with 124 mM NaCl, 5 mM KCl, 2 mM $CaCl_2$, 1 mM $MgCl_2$, 30 mM glucose, and 25 mM HEPES was used for experiments on hippocampal cultured neurons (Willig et al., 2006).

High potassium Tyrode buffer (pH 7.4) with 59 mM NaCl, 70 mM KCl, 2 mM $CaCl_2$, 1 mM $MgCl_2$, 30 mM glucose, and 25 mM HEPES.

For immune labeling the following buffers were required:

Ammoniumchloride (NH_4Cl, 100 mM) in phosphate buffered saline (PBS).

PBS (pH 7.4) with 150 mM NaCl and 20 mM Na_2HPO_4.

PBS-high salt (pH 7.4) with 500 mM NaCl and 20 mM Na_2HPO_4.

PBS supplemented with 0.1% Triton-X-100 (TX-100)

PBS supplemented with 1.5% bovine serum albumin (BSA) and 0.1% TX-100.

For inner hair cell experiments the following buffers were required:

For experiments in absence of calcium (zero calcium conditions) the standard HEPES-buffered Hanks´ balanced salt solution (HEPES-HBSS, pH 7.2) with 141.7 mM NaCl, 5.36 mM KCl, 1 mM $MgCl_2$, 0.5 mM $MgSO_4$, 10 mM HEPES, 1.25 mg/ml glucose, 0.5 mg/ml L-glutamine was used.

High potassium HEPES-HBSS had the following components: 65.36 mM KCl, 79,7 mM NaCl and 2 mM $CaCl_2$, the rest was identical to the standard HEPES-HBSS buffer.

For the HEPES-HBSS with calcium, 2 mM NaCl were replaced by 2 mM $CaCl_2$ in the standard HEPES-HBSS buffer.

For all HEPES-HBSS buffers glucose and L-glutamine were added fresh prior to use. The osmolarity of the buffers were around 290 mmol/kg.

2.2 Methods

2.2.1 Antibody Labeling

Monovalent Fab fragments of affinity-purified antibodies (AffiniPure donkey Fab fragments, Jackson ImmunoResearch Laboratories) for secondary fluorescence live-labeling of conventional synapses were tagged with the organic fluorophore Atto647N (Atto-Tec) via its succinimidyl ester. Instead of whole IgGs, Fab fragments were used, as they do not cross-link different monoclonal antibodies.

A secondary fluorescence labeling was used instead of directly fluorescence-labeled monoclonal antibodies, since both 604-variants (604.1 and 604.2, Synaptic Systems) lost their binding specificity after chemically fixing the Atto647N dye onto them (please see appendix for antibody specificity, Figure A 3). The organic dye probably modified the native conformation of the synaptotagmin antibodies. Nevertheless, directly fluorescence-labeled anti-synaptotagmin antibodies (labeled with Atto647N) were used in some experiments, because higher quality, fully functional antibodies became purchasable from Synaptic Systems (Göttingen) during this work and showed no difference in synaptic vesicle labeling efficiency compared to secondary fluorescence labeling.

2.2.2 Cell Culture

PC12 Cells (*Experiment in appendix*)

Neuroendocrine PC12 (pheochromocytoma) cells were cultured in Dulbecco's modified Eagle's medium (DMEM; Invitrogen, Darmstadt, Germany) with the following additions: 5% fetal calf serum, 10% horse serum, 4 mM glutamine and 100 units/ml each of penicillin and streptomycin. Cells were grown on culture dishes at 37°C in 10% CO_2 and 90% humidity and passaged when reached confluence. PC12 cells were passaged by detaching them from the dish using trypsin/EDTA (Lonza, Cologne, Germany).

Primary cultured hippocampal neurons

Primary cultures of hippocampal neurons were prepared from brains of newborn rats (postnatal day 1) using a standard protocol (Kaech and Banker, 2006). The preparation was

carried out by the technician Christina Schäfer. The cultures were overlayed onto a pre-plated monolayer of astrocytes (continental neuronal cell culture) or plated directly on poly-d-lysine coated 18 mm coverslips. The cultures were grown at 37°C in 10% CO_2 and 90% humidity and used between days 11 and 30 *in vitro*.

2.2.3 Live-Labeling Methods

Mitochondria live-labeling

MitoTracker Green FM (MTG; Invitrogen, Darmstadt, Germany) was used to label specifically the mitochondria in hippocampal cultured neurons by incubating them with 100 nM MTG in growth medium at 37°C for 15 minutes. Mitochondria labeled neurons were subsequently live-labeled against synaptotagmin (see below).

Synaptic Vesicle live-labeling

In vitro cultured hippocampal neurons were placed into Tyrode buffer (~ 2°C) on ice according to Willig et al., 2006. All following steps for synaptic vesicle live-labeling were performed on ice and with ice-cold buffers and antibody dilutions for a selective surface staining of the synaptic vesicle protein synaptotagmin.

Neurons were incubated with the primary antibody dilution (604.1 or 604.2 in Tyrode) for 5-6 minutes. After rapidly washing the cells 4-5 times with ice-cold Tyrode the secondary antibodies (fluorescence-labeled Fab fragments against mouse in Tyrode) were applied for 8 minutes. After washing with Tyrode buffer coverslips were transferred to room temperature for further treatments or imaging (No Incubation condition).

The procedure for live-labeling of synaptic vesicles with directly fluorescence-labeled anti-synaptotagmin antibodies (604.2 labeled with Atto 647N or Oyster-550) was identical, but without the secondary antibody labeling step.

For the investigation of the synaptic vesicle mobility after incubation (Incubation condition), the labeled neurons were placed back into their growth medium in the incubator at 37°C. After 120 minutes the neurons were washed once with Tyrode buffer at room temperature (RT), transferred to the microscope and imaged in Tyrode buffer at RT for up to 30-40 minutes.

To check whether the labeling technique itself harms the cultured neurons, a mock-labeling control was used. The neurons were treated exactly like for normal labeling, but without the addition of antibody dilutions during incubation. The cells were then placed back into the incubator exactly as the incubated neurons, and were finally labeled after 120 minutes with anti-synaptotagmin antibodies on ice.

For live STED imaging and FRAP imaging of fixed neurons, live-labeled cells were placed to room temperature for 3 minutes and then fixed for 60 minutes in PBS with 3% glutaraldehyde and 2% paraformaldehyde (PFA) at RT (in dark). Neurons were subsequently incubated in NH_4Cl (100 mM in PBS) for 20 minutes and washed with PBS. Imaging was performed in PBS.

2.2.4 Influence of Cytoskeleton-Perturbing Agents

To investigate whether active transport mechanisms are involved in synaptic vesicle movements the synaptotagmin live-labeled neurons were pre-treated for at least 5 minutes with Latrunculin A (20 μM in Tyrode buffer at RT) to disrupt the actin cytoskeleton by sequestering actin monomers (Sankaranarayanan et al., 2003), or the neurons were pre-treated for at least 20 minutes with nocodazole (20 μM in Tyrode buffer at RT) to disrupt microtubules (Kuromi and Kidokoro, 2005). STED movies were obtained within 10-45 minutes of incubation, or 20-60 minutes, respectively. Both drugs were dissolved in DMSO, hence the control samples were imaged in 0.5% DMSO without a pre-incubation step.

2.2.5 Investigation of Synaptic Vesicle Material on the Plasma Membrane

Black Widow Spider Venom

Preparation of the black widow spider venom (BWSV) was carried out according to Henkel and Betz, 1995. One pair of glands of the black widow spider were homogenized in 1 ml calcium-free Tyrode buffer supplemented with 1 mM EGTA. The solution was centrifuged for 20 minutes at 10 000g at RT. The venom containing supernatant was collected and used at a 1:4 dilution in the same buffer. Hippocampal neurons were incubated with BWSV for 15 minutes at 37°C prior to live-labeling with anti-synaptotagmin antibodies on ice (604.2 diluted in Tyrode buffer w/o calcium), which thus recognized specifically the synaptotagmin surface pool. Imaging was performed in the respective buffer.

Caffeine

Hippocampal cultured neurons were incubated in 1 mM caffeine in Tyrode buffer without divalents (no Mg^{2+} and Ca^{2+}, with additional 5 mM EGTA) for 5 minutes at RT prior to synaptotagmin live-labeling. Labeling and imaging were performed in the same buffer.

No Divalents (Control)

Hippocampal neurons were incubated in Tyrode buffer without divalents (supplemented with 5 mM EGTA) for 5 minutes at RT with subsequent synaptotagmin live-labeling and imaging in the respective buffer.

2.2.6   Stimulation Experiment

Electric field stimulation

Platinum plate electrodes with 8 mm distance between the plates were used to stimulate live-labeled hippocampal cultured neurons. An A310 Accupulser (World Precision Instruments, Berlin, Germany) delivered shocks of 100 mA with alternating currents at 20 Hz for 2 seconds. The accurate, time-controlled stimulation triggering was ensured using the microscope operating software Imspector (Imspector Image Acquisition & Analysis Software, Max Planck Innovation, Germany).

For FM experiments on hippocampal cultured neurons (Figure 3.16) the stimulation trains were generated using the A310 Accupulser that was triggered by an A385 Stimulus Isolator (both World Precision Instruments).

Blocking of synaptic activity

Tetrodotoxin (TTX) was used to inhibit synaptic activity. Live-labeled neurons were transferred to RT and incubated with TTX (1 μM in Tyrode buffer) for 10 minutes before STED imaging in presence of TTX.

2.2.7 Immunohistochemistry

Hippocampal neurons were either fixed with 4% PFA in PBS for 60 minutes at room temperature (in the dark, if cells were live-labeled before) or with ice-cold methanol (-20°C) for 20 minutes at RT with subsequent washing in PBS (for immunohistochemistry with anti-GluR1 (AMPA1) and anti-synapsin 1, 2 antibodies). Free aldehyde groups in PFA-fixed neurons were quenched by incubating them for 20 minutes in 100 mM NH_4Cl in PBS. Finally, neurons were washed two times and stored in PBS for further processing (immunostaining or embedding).

Fixed neurons were usually permeabilized with TX-100 (3 x 5 minutes in 0.1% in PBS at RT) prior to immunolabeling. Permeabilized neurons were incubated for 60 minutes with primary antibodies diluted in PBS supplemented with 1.5% BSA and 0.1% TX-100 in a humidified chamber. The coverslips were washed with PBS (+ 0.1% TX-100). To prevent bleaching of the secondary antibodies, the following incubation and washing steps were performed in dark. The fluorescence labeled secondary antibodies were applied in the same way as the primaries for 60 minutes. Unspecific bound antibodies were washed away using PBS-high salt (500 mM NaCl; 3 x 5minutes). After two washing steps with PBS the coverslips were embedded upside-down on a microscope slide with fluorescent mounting medium (Mowiöl: 6 g glycerol, 2.4 g Mowiöl 4-88 (Carl Roth, Karlsruhe, Germany), 6 ml H_2O, 12 ml 2 mM Tris buffer of pH 7.2) and dried at least 60 minutes at RT in dark prior to use.

Immunolabeling of fixed neurons without permeabilization was essentially performed using the same protocol, in which the buffers and antibody dilutions lack the TX-100 component.

2.2.8 Microscopy

Stimulated emission depletion (STED) microscopy

The principle of a STED microscope is illustrated in Figure 2.1 and has already been explained in the Introduction (see 1.6). STED microscopy was performed using a home-built setup as described in Westphal et al., 2008 (built by Dr. Volker Westphal and Dr. Marcel Lauterbach, Abteilung NanoBiophotonik, Max Planck Institute for Biophysical Chemistry, Göttingen). Excitation of the Atto647N dye was achieved using a pulsed LDH-P-635 picosecond laser diode at 635 nm (PicoQuant, Berlin, Germany). The pulsed depletion beam (STED beam) was generated by a MaiTai Ti:Sapphire-Laser at 750 nm wavelength (Newport, Irvine, CA, USA). The zero center in the STED focus was generated by a vortex phase plate in the parallel depletion beam path (VPP-A1, RPC Photonics, Rochester, NY, USA). A resonant mirror (SC-30, EOPC, Glendale, NY, USA) was used to pass both beams for one axis beam scanning and were focused by a 100x, 1.4 numerical aperture HCX PL APO oil objective (Leica). The focal peak intensities for the red excitation was 3.5-5 MW/cm², for the blue excitation 0.08 MW/cm², and for the STED beam 400 MW/cm². The second lateral axis and the axial scanning of the sample were provided by piezo stages (733-3DD and E-710, Physik Instrumente, Germany). Two avalanche photo diodes (SPCM-AQR13, Perkin Elmer, Waltham, MA, USA) recorded the emission light, which was filtered at 675±30 nm for the red channel, 530±40 nm for the blue channel (AHF, Tübingen, Germany). Movies were recorded with 28 frames per second (35 ms per frame). From each sample several movies were obtained. STED frames were filtered to increase signal-to-noise by a Gaussian algorithm with a convolution of 80 nm at full width at half maximum (no filtering was applied for Figure 3.4). High frame rates with a 30 nm pixel size were possible by using bidirectional image acquisition in the lateral axis, leading to a pixel dwell time of 3.8 µs in the horizontal center of the field of view with increasing dwell times to the edges to ~6 µs (as the speed of the resonant scanner is non-linear along the x-axis).
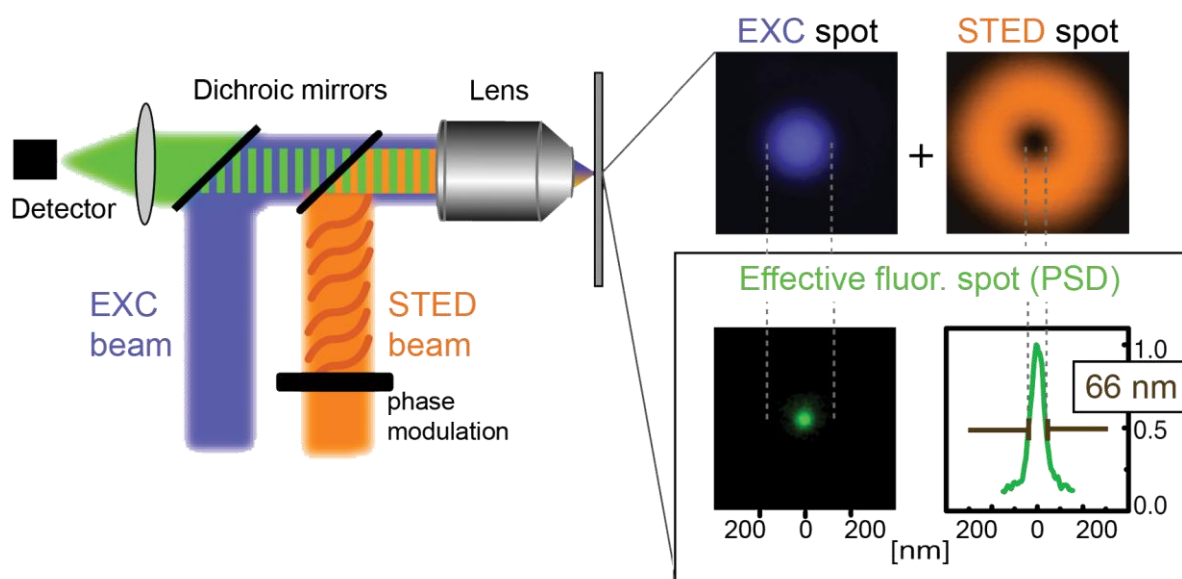
Figure 2.1: The principle of a STED Microscope. The excitation beam (EXC, blue) is focused to a diffraction-limited excitation spot (see right panel). The STED beam (orange) is phase modulated and usually doughnut-shaped (see right panel). The overlay of both beams allows the longer wavelength STED beam to de-excite (deplete) the fluorophores in the periphery of the excitation spot. The detected fluorescence originates only from the center, where the laser intensity of the STED beam is close to zero, which consequently results in a smaller effective fluorescent spot, and thus gives higher resolution (Figure from Willig et al., 2006).

Confocal microscopy

Confocal fluorescence microscopy and FRAP imaging were performed with a TCS SP5 STED confocal microscope (Leica Microsystems), using a 100x, 1.4 numerical aperture HCX PL APO CS oil STED objective (Leica Microsystems). Atto647N was excited at 633 nm with a Helium-Neon laser and fluorescence was detected with a photomultiplier tube (PMT) in the spectral range of 641-750 nm. The secondary cyanine dye Cy2 was excited with an Argon laser at 488 nm, fluorescence was detected in the spectral range of 500-580 nm with a PMT.

Epifluorescence microscopy

Epifluorescence microscopy was performed using an Olympus IX71 epifluorescence microscope. For more details see below.

Electron microscopy of hippocampal cultured neurons

Electron micrographs were captured using a Zeiss EM 902A electron microscope equipped with a 1024 × 1024 CCD detector (Proscan CCD HSS 512/1024; Proscan Electronic. The determination of the vesicle diameters was achieved by manually drawing line scans on the images using routines written in Matlab (experiments, imaging and analysis were performed by Dr. S.O. Rizzoli).

2.2.9   STED Microscopy Data Analysis

STED data analysis

Data analysis (single-particle-tracking) was carried out by Dr. Marcel A. Lauterbach and Dr. Volker Westphal as described in Westphal et al., 2008 and Kamin et al., 2010:

The vesicle positions were automatically determined in each frame of the recorded movies: First, the areas containing vesicles were extracted in all frames by deconvoluting each frame with a Gaussian function (full width at half maximum (FWHM) of 60-100 nm and a reasonable quadratic potential regularization (Vicidomini et al., 2009) to get smooth images with failure-free structures. Afterwards, the background was eliminated with a low threshold to receive the areas where the vesicles were localized. To quantify the vesicles in each area, the number of photons were divided by the average vesicle brightness (the average vesicle brightness is the mean number of emitted photons from single vesicles of various movies). Generally, ~2 vesicles were localized in each background subtracted area. The positions of the vesicles were fitted to model variable numbers of vesicles and shot noise in these areas (having their own position and brightness). Overfitting was prevented by introducing a penalty in the model to avoid that modeled vesicles differ highly from the average vesicle brightness. The intensity of the penalty was manually regulated by checking the position and the brightness of the fitted vesicles in various movies. Finally, the vesicle numbers and their positions were read-out in all areas of each movie frame and a map of the localized vesicles for each movie was acquired. A faster algorithm was used for some movies (with the same results of object localization), where all frames of the movie were deconvoluted with a Gaussian function (FWHM of 120 nm). Vesicle positions were localized by checking for

local intensity maxima. Intensities with less than 14% of the brightest vesicle in a movie were abolished.

All localized vesicle objects were tracked as performed according to (Westphal et al., 2008), with the algorithm of Crocker and Grier (Crocker and Grier, 1996).

The quantification of the vesicle mobility was expressed as the mean vesicle speed or the median vesicle speed. The median was used as it is less sensitive to incorrect vesicle localization connections from frame-to-frame, and single-particle-tracking in dense labeled parts of the cell is usually prone to errors.

The change in vesicle mobility (expressed as the median vesicle speed) was well determined in the distinct experiments with the used tracking method. Nevertheless, the computed values of the vesicle speed may not be perfectly in agreement with the actual mobility, as also tracking of glutaraldehyde fixed vesicles results in movement. However, this movement is caused by localization noise in the vesicle connection from one frame to the next.

Binning for the histograms was slightly randomized, as otherwise vesicle binning results in artifacts arising from the preferential assignment of vesicle positions to pixel centers

Particle influx analysis

Data analysis was carried out by Dr. Marcel A. Lauterbach and Dr. Volker Westphal.

The particle influx (vesicle entering per second) into the imaged area (Figure 3.2 C) was estimated by counting the traces of vesicles that started at the edge of the field of view. Vesicle counting started after 17.5 seconds to be aware of having bleached all initial vesicles in the imaged area. As four independent experiments showed variable densities of labeled vesicles, the particle influx was set in relation to the initial amount of labeled vesicles per frame, which was averaged from the vesicles found in the first ten frames of each movie.

Difference image analysis

Difference images (Figure 3.10) were generated by subtracting each frame of the movie from the next one and then the mean of the total pixel values in the difference image was calculated. The mean was expressed as percentage of the mean pixel value of the original movie frame and was carried out for all frames. The resulting plots were smoothed by a moving average with 15 frames.

"Hot spot" analysis

"Hot spot" analysis (Figure 3.6) was carried out by Dr. Marcel A. Lauterbach and Dr. Volker Westphal according to (Westphal et al., 2008).

A "hot spot" is an object that (i) had a clear maxima in a running average over 50 frames and (ii) had a minimal brightness that is higher than 10-25% of the brightest object in the averaged movie frames. Positions of "hot spots" were localized exactly as shown for vesicles (see above). To analyze how much time each vesicle spent in a "hot spot", a circle with a 7-pixel diameter was overlayed around the localized "hot spot" and the fluorescence intensity therein was measured and averaged over 7 frames. A vesicle was considered to be in a hot spot when the fluorescence intensity in the circular area increased more than 6.5 fold of the average background fluorescence intensity outside of the neuron. A vesicle was defined to be inside a hot spot, when its localization was inside a radius of 60 nm (2 pixels) of the hot spot localization.

2.2.10 Confocal Microscopy Data Analysis

Line profile correlation analysis

For the colocalization analysis (Figure 3.7) line scans of interest were drawn manually along the axon in the live-labeled synaptotagmin channel. The pixel intensity profiles along the line scan for both channels (synaptotagmin: red, protein of interest: green) were generated automatically. To compare the intensity profiles the Pearson's correlation coefficient was calculated and plotted for the different proteins of interest.

Colocalization analysis to clathrin machinery (Figure 3.15): a similar analysis was performed for getting the degree of colocalization between the membrane fused synaptic vesicle material and the clathrin machinery. First, the black widow spider venom (BWSV), caffeine, or control treated samples were fixed and immunostained against the surface exposed synaptotagmin protein without TX-100 permeabilization using Cy5-tagged secondary antibodies. Second, the samples were permeabilized with TX-100 and immunostained against the proteins of the clathrin-machinery (clathrin or amphiphysin) with Cy2-tagged secondary antibodies. Images were captured using an epifluorescence Olympus IX71 microscope

equipped with a 100x objective, 1.4 numerical aperture (Olympus), an F-View II CCD camera (Olympus), using standard FITC (excitation filter HQ 480/40, dichroic mirror LP Q 505, emission filter HQ 527/30) and Cy5 filters (excitation filter HQ 620/60, dichroic mirror LP Q 660, emission filter HQ 700/75).

FRAP data analysis

The alignment of the movie frames was carried out automatically by routines written in Matlab. The bleached region and various control areas were chosen manually and their average fluorescence intensity was calculated for each frame of the movie. As the sample bleaches during movie acquisition, the average decrease in fluorescence intensity in the control areas were calculated and used to normalize the FRAP curve to correct for the bleaching.

Surface pool of synaptotagmin

To analyze the fraction of the surface pool of synaptotagmin (Figure 3.12) that remains on the plasma membrane after BWSV, caffeine, or no divalents treatment the neurons were live-labeled with direct-labeled Oyster-550 anti-synaptotagmin antibodies on ice. The cultures were then either fixed directly on ice (no incubation), or left at RT for different time intervals in Tyrode before fixation on ice. After quenching with 100 mM NH_4Cl (in PBS) the neurons were immunostained without permeabilization with Cy5-tagged secondary anti-mouse antibodies that bind specifically to the synaptotagmin pool left on the plasma membrane.

Images were captured using an epifluorescence Olympus IX71 microscope equipped with a 60x oil Uplan SApo objective, 1.35 numerical aperture (Olympus), an F-View II CCD camera (Olympus), using TRITC filter cubes for the 604.2 Oyster 550 (excitation filter HQ 545/30, dichroic mirror LP Q 570, emission filter HQ 610/75), and Cy5 filter cubes for Cy5 fluorescence (excitation filter HQ 620/60, dichroic mirror LP Q 660, emission filter HQ 700/75). The relative fluorescence intensity of the surface pool of synaptotagmin labeled with Cy5 and the total pool of labeled synaptotagmin labeled with Oyster-550 was measured and expressed as percentage of the control condition (the samples fixed directly on ice after labeling).

2.2.11 Preparation of Organ of Corti

Mice were killed by decapitation and the skin was removed from the head. After cutting the head sagitally in two parts it was transferred to ice-cold standard HEPES-HBSS buffer. The brain was removed and the inner ear was softly removed from the cranium. The bony covering of the cochlea was gently opened and the apical turn of the organ of Corti was removed from the modiolus and placed into the proper buffer for further treatments.

2.2.12 Inner Hair Cell Labeling

Live imaging experiments

The organ of Corti was place into an imaging chamber with standard HEPES-HBSS buffer and positioned in place with fine nylon fibers. A high flow peristaltic pump and a suction pipette constantly exchanged the buffer. Dyes for labeling were added directly into the buffer in the chamber (bath application), which were then washed out by the pump and the suction pipette. Live-labeling of IHCs was imaged with a Leica SP2 upright confocal microscope (DMLFSA; Leica Microsystems) during dye application and its washout simultaneously in transmission and fluorescence mode using a 63x, 0.90 numerical aperture HCX APO L U-V-I water immersion objective (Leica Microsystems). Excitation of FM-dyes and dodecanoyl fluorescein was performed using an Argon laser at 488 nm; fluorescence was detected with a PMT in the spectral range of 500-700 nm. Dextran fluorescein and calcein are highly fluorescent in solution, which resulted in the absorption of the excitation light. Thus, imaging was performed using a multi-photon setup to restrict the focal spot to a smaller volume and thus reject out-of-focus excitation. Dextran fluorescein and calcein were excited at 800 nm (1.0 W output power) using a two-photon Ti:sapphire laser (Verdi-V8 femtosecond diode-pumped laser, pulsed by Mira Optima 900-F; Coherent, Santa Clara, USA). Fluorescence was detected at 500-660 nm. Sulforhodamin 101 was imaged using an Argon-Krypton laser at 561 nm, fluorescence was detected using a PMT in the spectral range of 600-750 nm.

FM photo-oxidation experiments

For FM photo-oxidation experiments the organ of Corti was pre-incubated in carbogen-charged standard HEPES-HBSS buffer at 37-40°C. After 5 minutes the organ was placed in 5

µM FM1-43 diluted in standard HEPES-HBSS (zero calcium condition) or in high potassium HEPES-HBSS (stimulated condition) for ~60 seconds at 37-40°C. The organ was either fixed immediately by dipping it in a large volume of ice-cold 2.5% glutaraldehyde in PBS (2°C) for 20 minutes on ice and additional 30 minutes at RT, or in case of stimulated organs they were rapidly washed and left in carbogen-charged HEPES-HBSS buffer (with calcium) at 37-40°C for different time intervals prior to fixation (5 and 30 minutes; with constant buffer exchange). Afterwards the preparations were fixed as described above.

2.2.13 FM Photo-Oxidation

Hippocampal cultured neurons

Photo-oxidation of hippocampal cultured neurons was performed by Dr. S.O. Rizzoli according to Rizzoli and Betz, 2004 (see details in Hoopmann et al., 2010).

Inner hair cells

Photo-oxidation of glutaraldehyde fixed IHCs was performed like the following (compare to Henkel et al., 1996a; Rizzoli and Betz, 2004; Denker et al., 2009: The organ of Corti was pre-incubated in fresh 100 mM NH_4Cl for 20 min at RT to quench free aldehyde groups. After 10 minutes washing in PBS the organ was pinned with fine needles (stainless steel, Minutiae, size class: 10) in a sylgard dish to prevent floating of the preparation and incubated with filtered DAB (1.5 mg/ml in PBS) for at least 35 minutes (4°C) in dark to allow its penetration into the tissue. After the addition of fresh DAB a focused spot was illuminated via an Olympus 20x, 0.5 numerical aperture UPlanFL N objective until the fluorescent signal disappeared and a crisp, brown precipitation product became visible (microscope: Axioskop 2 Fsplus (Zeiss, Göttingen, Germany) equipped with a 100 W mercury lamp (Zeiss), a 25% neutral density transmission filter, an excitation filter (HQ 470/40), a dichroic mirror (495 DCLP), and an emission filter (500 long pass; all from AHF, Tübingen, Germany). The sample was washed with filtered PBS and the photo-oxidized part was cut out and transferred into filtered PBS for further electron microscopy processing.
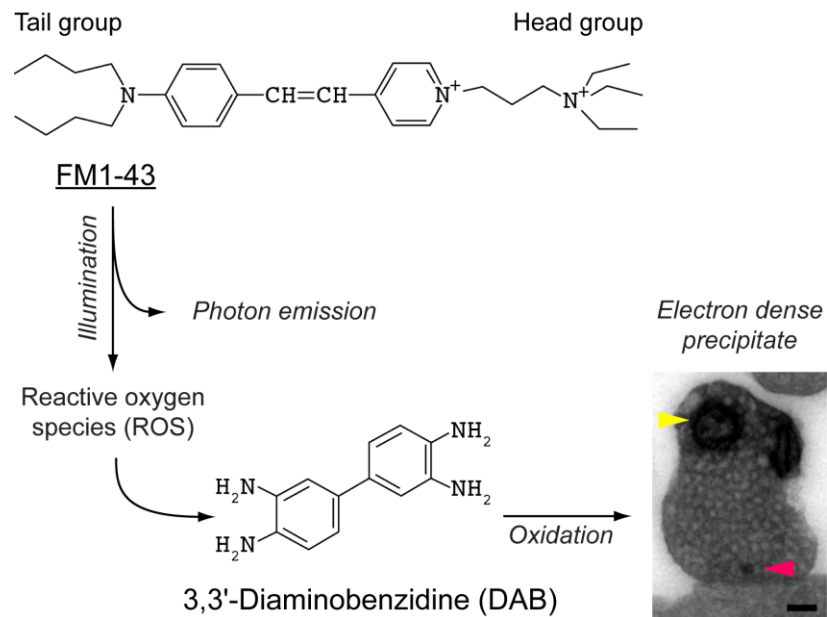
Figure 2.2: FM1-43 and the principle of photo-oxidation. FM1-43 is an amphiphilic molecule consisting of a lipophilic tail group, that allows the FM dye to partition into membranes, and a positively charged head group, which keeps it from flipping across the membrane. The fluorophore is composed of two aromatic rings, which are located between the head and the tail group. FM1-43 emits photons while illuminating with blue light, and simultaneously creates reactive oxygen species (ROS). In the presence of 3,3'-diaminobenzidine (DAB) during illumination, the ROS oxidize the DAB in the close proximity of the FM dye. Oxidation of DAB leads to its precipitation to an electron dense brown endproduct, which is visible in electron microscopy. The electron micrograph shows an efferent IHC nerve terminal with a single photo-oxidized synaptic vesicle (red arrowhead). Unlabeled clear core vesicles surround this labeled vesicle. The mitochondria (yellow arrowhead) show a darkening that is not related to vesicle recycling and is a known process of the photo-oxidation technique (Grabenbauer et al., 2005).

2.2.14 Sample Processing for Electron Microscopy

After photo-oxidation the samples were post-fixed for 60 minutes with 1% osmium tetroxide (OsO_4 in filtered PBS) and washed 3 times with filtered PBS. They were then dehydrated with an ethanol and propylene oxide (PO; Science Services, Munich, Germany) dilution series (series with 30%, 50%, 70% ethanol for 5 minutes each, 90% and 95% ethanol for 10 minutes each, 3 times 100% ethanol for 10 minutes each, 50% PO in ethanol for 10 minutes, 3 times 100% PO for 10 minutes each) and incubated under continuous rotation for 12-18 hours in 50% epon resin in PO (Science Services). The samples were incubated at RT in 100% epon resin in open vials to allow PO diffusion out of and epon diffusion into the tissue. After 6 hours the samples were embedded with fresh 100% epon resin and incubated at 60°C

for ~40 hours. Hardened resin samples were trimmed and consecutive sections of 100 nm were cut with a Leica microtome (Leica EM UC6, Leica) and placed on formvar (0.5%) covered copper grids (3.05mm, 2 mm x 1 mm; Plano GmbH, Wetzlar, Germany).

Electron micrographs were captured using a Zeiss EM 902A electron microscope equipped with a 1024×1024 CCD detector (Proscan CCD HSS 512/1024; Proscan Electronic Systems).
Each IHC section was scanned from the apical to the basal pole of the cell at a 20000x magnification (see Figure 2.3 A for examples of consecutive IHC sections).

2.2.15 Three-Dimensional Reconstruction of Inner Hair Cells

After scanning all serial IHC sections the individual electron micrographs of a section were assembled to get the full IHC image of this section (composed of 80-130 electron micrographs per section, depending on the imaged cell, see Figure 2.3 A). The serial sections were then aligned and warped with Photoshop (Adobe Photoshop CS3, version 10.0.1, Adobe Systems Incorporated). In all sections the plasma membrane, the nucleus, the cuticular plate, the active zone (ribbon) and the labeled, (photo-oxidized) organelles were manually redrawn in Photoshop, and saved as separate images (Figure 2.3 B). From these images three-dimensional reconstructions were generated using Matlab routines assuming a thickness of 100 nm for each section.
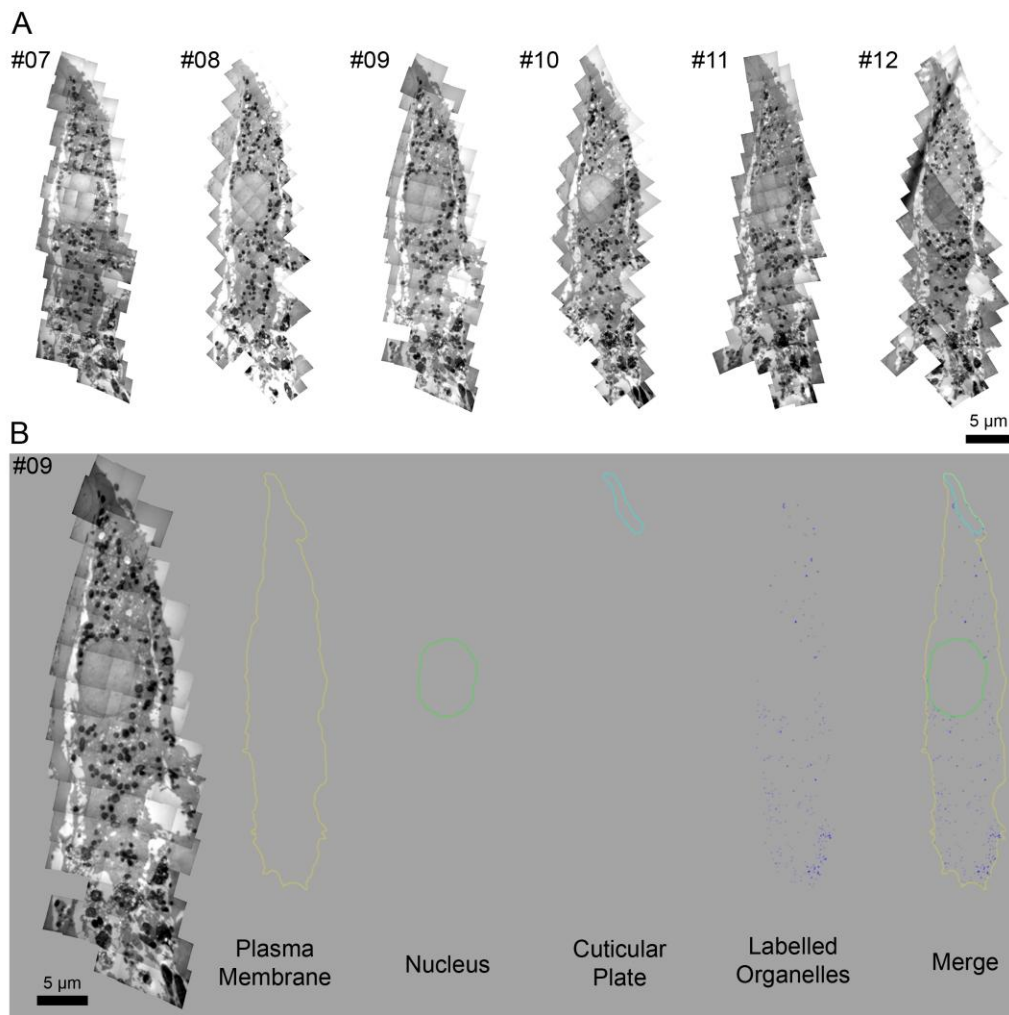
Figure 2.3: Three-dimensional reconstruction processing. (A) Serial sections of the 5-minute rest IHC are shown. Serial sections of 100 nm were cut and imaged with 20000x magnification by scanning the IHC (depending on the cell one IHC section is composed of 80-130 electron micrographs). (B) Example of three-dimensional reconstruction procedure. After assembling the individual IHC sections, all consecutive sections were aligned using Photoshop warp tools and the plasma membrane (yellow), the nucleus (green), the cuticular plate (cyan), and the labeled organelles (blue) were manually redrawn with Photoshop and saved as single images. If present the ribbon was also redrawn (not shown here). The IHCs were reconstructed from these images assuming a thickness of 100 nm for each section using Matlab routines.

2.2.16 Data Analysis of Sensory Inner Hair Cells

The localization of labeled organelles and their 3D-rendering were carried out using routines written in Matlab, described in Rizzoli and Betz, 2004 and Denker et al., 2009.

43

3 Results

3.1 Conventional Synapses

3.1.1 STED Microscopy Resolves Single Synaptic Vesicle Movements in Living Neurons

As outlined in the Introduction, synaptic vesicles are too small and densely packed in the confined space of a synapse to be resolved with standard microscopes. Willig and colleagues (Willig et al., 2006) showed recently that high-resolution STED microscopy (see Figure 2.1 in Methods) is able to resolve single synaptic vesicles in the boutons of fixed hippocampal cultured neurons. However, as this study used fixed cells the first aim of this work was to specifically investigate synaptic vesicle behavior with STED microscopy *in vivo*. Therefore, synaptic vesicles of hippocampal cultured neurons were live-labeled with monoclonal mouse anti-synaptotagmin antibodies and fluorescence-labeled (Atto647N) secondary Fab fragments on ice. The primary antibodies recognize the lumenal domain of the synaptic vesicle protein synaptotagmin (Matteoli et al., 1992; Mundigl et al., 1993; Kraszewski et al., 1995; Fernández-Alfonso et al., 2006). Thus, only synaptic vesicles that fused to the plasma membrane during antibody incubation became labeled (selective surface staining), i.e. only then the intravesicular domain of the protein is exposed to the extracellular environment (Willig et al., 2006). After transferring the cultures back to RT the synaptic vesicles actively recycled and incorporated the antibodies, thus labeling only the pool of recently endocytosed vesicles. The antibody uptake did not disturb the recycling process, as they were endocytosed relatively rapidly after switching the cultures back to room temperature (only ~18% of the antibodies were left on the plasma membrane after 2 minutes at RT, and ~8% after 10 minutes (Westphal et al., 2008)).

STED imaging was performed in Tyrode buffer for 2-30 minutes at RT. An area of 1.8 μm by 2.5 μm was imaged within 35 milliseconds, hence video-rate imaging with 28 frames per second was applicable. Standard confocal microscopy failed in detecting single synaptic vesicles (Figure 3.1 A, frame #1). However, high-resolution video-rate STED microscopy enabled the separation of well-resolved single vesicles in consecutive STED frames (Figure

3.1 A, frame #2 and #3) (For a comparison of video-rate STED nanoscopy and confocal microscopy of living neurons see (Lauterbach et al., 2010)). Filtering of the movie frames to increase the signal-to-noise ratio with a smoothing algorithm improved the localization of single vesicles in consecutive STED frames, but not in the confocal movie frame (Figure 3.1 B). The STED microscopy-based resolution enhancement is shown in Figure 3.1 C, demonstrating that STED microscopy resolved a single synaptic vesicle with a FWHM of 62 nm. Thus, a reduction by a factor of 18 was achieved when compared to standard confocal microscopy (with the here used video-rate imaging system, for details see Methods).
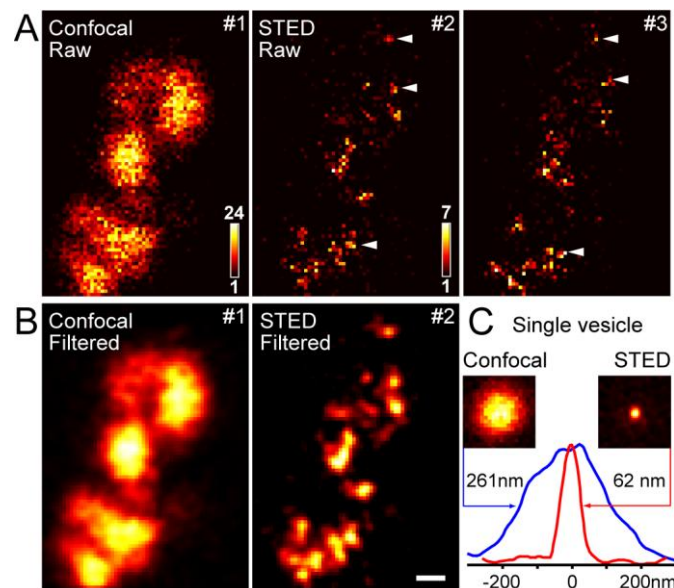
Figure 3.1: Video-rate STED microscopy. (A) First frames of a video-rate STED movie (imaging speed of 28 frames per second) showing a part of a neuron with live-labeled synaptic vesicles in confocal mode (frame #1) and STED mode (frame #2 and #3). The imaged area has a dimension of 1.8 μm by 2.5 μm. With confocal imaging single vesicles cannot be detected, however, live STED imaging allows for the detection of vesicles in consecutive frames, white arrowheads in frames #2 and #3 point to relatively stable single vesicles that reappear from one to the next frame. The inserts in frame #1 and #2 are the colormaps used in confocal an STED mode, respectively. (B) Filtering of the movie frames with a smoothing algorithm does not result in better object discrimination in confocal mode, but makes single-vesicle-tracking more comfortable in consecutive STED frames. Scale bar 250 nm. (C) The FWHM of a confocally resolved (diffraction limited, summed over 10 frames) and a STED resolved (summed over 50 frames) single vesicle demonstrates a reduction in the focal spot by a factor of 18. (Figure modified from (Westphal et al., 2008)).

Surprisingly, as visibly evident from the supporting Movie A1 (see attached CD and see Appendix A.1 for the movie legend) the recently endocytosed vesicles exhibited an unexpected high mobility. Filtering of the movie frames allowed automatic tracking of single vesicles (Figure 3.2 A) and revealed a vesicle mean trace speed of approximately 2 nm per ms (Figure 3.2 B; Movie A1).
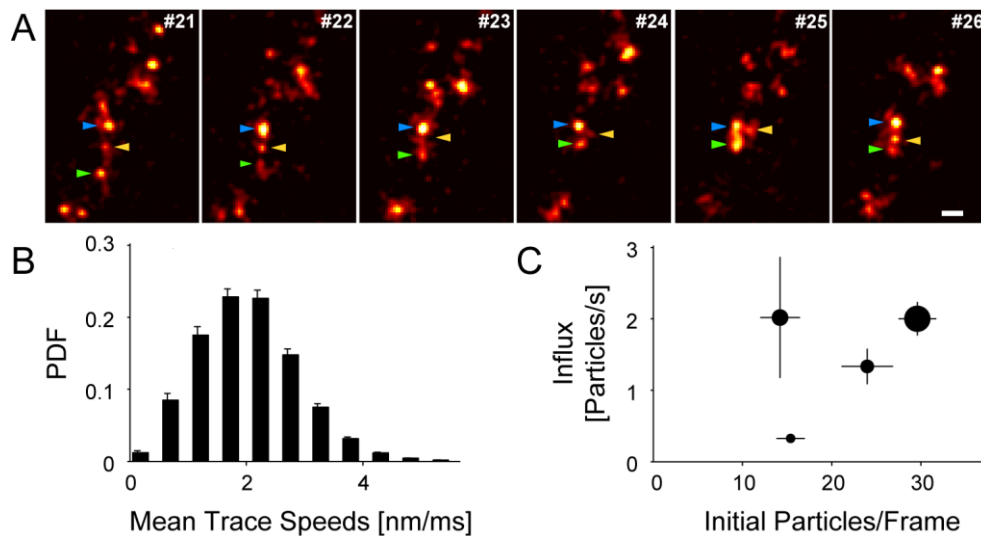
Figure 3.2: Synaptic vesicle speeds. (A) Consecutive STED frames (filtered, 35 milliseconds per frame) of moving synaptic vesicles in a hippocampal neuron (see also Movie A1). Single vesicles, which were tracked in the consecutive frames, are indicated by the colored arrowheads (relatively stable vesicles). Scale bar: 250 nm. (B) Automated tracking of vesicles allowed to calculate the average speed of the vesicles, shown as the mean trace speed. (PDF: probability density function) (C) Counting of synaptic vesicles entering the imaged area reveals high mobility of the recently endocytosed vesicles. Results are shown from 4 independent experiments with various movies for each sample. The diameter of the data points is proportional to the number of analyzed movies. (Figure modified from (Westphal et al., 2008)).

Moreover, the high level of vesicle mobility was more evident when the vesicle entry in the field of view was analyzed, since vesicles entered constantly from both directions (Figure 3.2 C). Counting of vesicle entry started after 17.5 seconds, to exclude the vesicles that were initially present at the beginning of the imaging. Around 0.5-3 particles (vesicles) entered the imaged area per second, indicating that most of the vesicles pass through the boutons. The substantial high-mobility state of the recently endocytosed vesicles was a completely unexpected result as the classical models of synaptic vesicle recycling propose that the

vesicles rapidly return to the original vesicle cluster after endocytosis, where they are immobile. However, the vesicles appear to be mobile after their retrieval for any length of time.

3.1.2   Active Transport is Partially Involved in Vesicle Motion

To test whether the movement of the recently endocytosed synaptic vesicles was diffusive or possibly motor-driven (active transport along the cytoskeleton) the vesicle mobility was investigated on neurons that were treated with cytoskeleton-perturbing agents. For the disruption of the actin cytoskeleton the live-labeled neurons (as shown above) were incubated for 10-45 minutes in Latrunculin A (20 μM) at RT and imaged in presence of the drug. Nocodazole was used to disrupt the microtubules (20μM) and was pre-incubated for 20-60 minutes before the start of the movie acquisition. Control conditions were directly imaged in 0.5% DMSO, which was used as the solvent for both drugs. Vesicle tracking and speed computation showed that the disruption of the cytoskeleton by one of the drugs decreased the vesicle speed when compared to control preparations, indicating the involvement of motor-driven vesicle transport (Figure 3.3; blue: Latranculin A, red: nocodazole). However, vesicle movement was not abolished, suggesting that vesicle motion is partially diffusive and not exclusively mediated by active transport mechanisms.
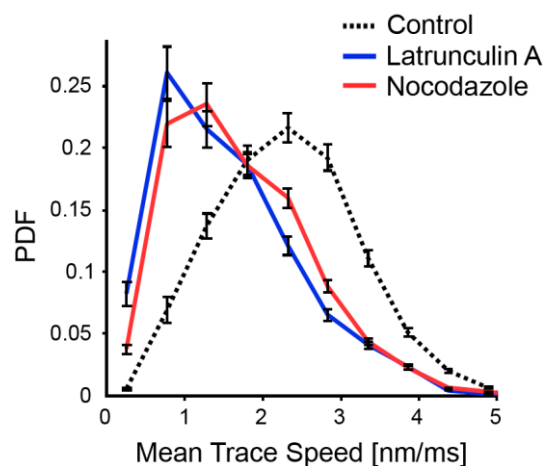
Figure 3.3: Influence of cytoskeleton-perturbing agents on synaptic vesicle motion. Hippocampal cultured neurons were live-labeled against synaptotgmin and treated either with Latrunculin A to disturb the actin cytoskeleton (blue) or with nocodazole to disturb microtubules (red). STED video-rate imaging was performed in presence of the drugs and started after 10-45 minutes of pre-incubation with Latrunculin A, or after 20-60 minutes with

nocodazole. Controls were imaged without a pre-incubation in DMSO. (Figure modified from (Westphal et al., 2008))

3.1.3 Mobility of Recently Endocytosed Vesicles

The above-presented results argue against the limited vesicle mobility described in the literature. The question raised whether the mobility of the recently endocytosed pool is equally high in every location of the neuron? To test for this, the vesicle motion was analyzed inside the axon and the bouton separately. Therefore, the neuronal morphology was visualized by selectively labeling the mitochondria with MitoTracker Green FM (MTG; 15 minutes at 37°C). The mitochondria staining allowed for the separation between the boutons and the axon (see Figure 3.4, A). Afterwards the synaptic vesicles were co-stained against the vesicle protein synaptotagmin (as described). STED imaging was performed only in the vesicle channel (red), whereas mitochondria were imaged in confocal mode (green). As the STED laser was highly bleaching the MTG fluorescence, imaging was performed for 18 frames in the vesicle channel in STED mode and was then switched to confocal scanning for 2 frames in the MTG channel (see Movie A2 and Appendix A.1).
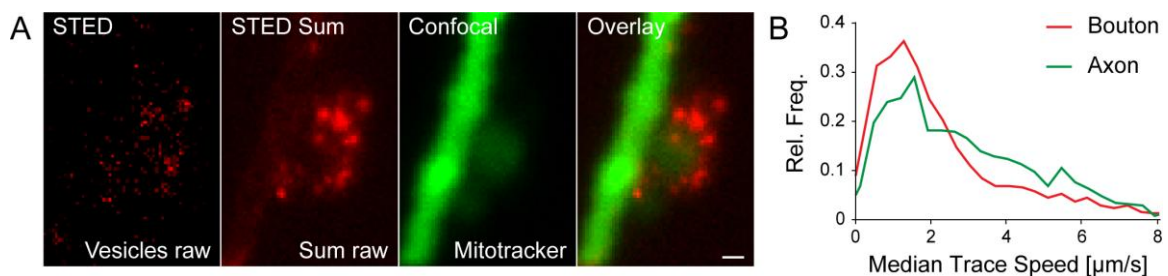
Figure 3.4: Mobility of synaptic vesicles. (A) A single, non-filtered raw frame of the STED movie (Movie A2) illustrates the temporary positions of the vesicles (left panel). A summation of all frames of the 22-second long movie shows the preferred locations of the vesicles (second panel from left). The selectively labeled mitochondria are shown in confocal mode and display the axon and the bouton (on the right side of the axonal shaft) (second panel from right). The overlay of the STED sum image and the confocal image of the MTG shows the accumulation of synaptic vesicles (bright spots) at the edge of the mitochondria-labeled bouton, giving evidence to be a functional release site (right panel). Scale bar: 250 nm. Voxel size: 30 nm^2; pixel dwell time: 3.7 µs at the center, increasing to the side. (B) Histograms of vesicle speeds separated for the axon and the bouton of the neuron shown in (A). Interestingly, the vesicles moved faster in the axon than within the bouton.

Tracking and calculation of the vesicle speeds in the axon and bouton separately revealed that the vesicles in the axon moved faster than within the presynaptic nerve terminal (Figure 3.4 B). This demonstrates that the mobility of the recently endocytosed vesicles depends on the vesicle location in the neuron, with lower movements in synaptic areas. These facts are in agreement with previous findings and correlate to the classical model of vesicle recycling (Sudhof, 2004). Nevertheless, the high overall vesicle mobility is in disagreement to the literature, as indicated above.

3.1.4 Resting Vesicles are Immobile

The discrepancy to most of the studies in the literature is that in this work the investigation was focused on the pool of the recently endocytosed vesicles and not on the total vesicle pool. To elucidate whether only the recently endocytosed vesicles are characterized by a high-mobility state, the vesicles were imaged at different time points after labeling. The cultured neurons were labeled against synaptotagmin, and either imaged directly (as above) or placed back into their growth medium at 37°C to be imaged after 2 hours. These 2 hours of incubation would allow the labeled recently endocytosed vesicles to exchange with the resting vesicle pool (Pyle et al., 2000). Proportions of the recently endocytosed vesicles would then be integrated into the resting vesicle pool. STED movie acquisition was performed exactly as before.

The comparison of the vesicle mobility of non-incubated (recently endocytosed vesicles) with that of incubated neurons showed a tremendous change in vesicle behavior after incubation (see Figure 3.5 A and B, frames #1-5, and Movie A3). The synaptic vesicles actually lost their high mobility state. The decrease in vesicle motion was more obvious when difference images of the non-incubated and the incubated preparations were compared (compare gray panels in Figure 3.5). The dimmer difference image of the incubated neuron indicated less object displacements from the first frame to the second, and thus less vesicle movement (see Methods for calculating difference images).
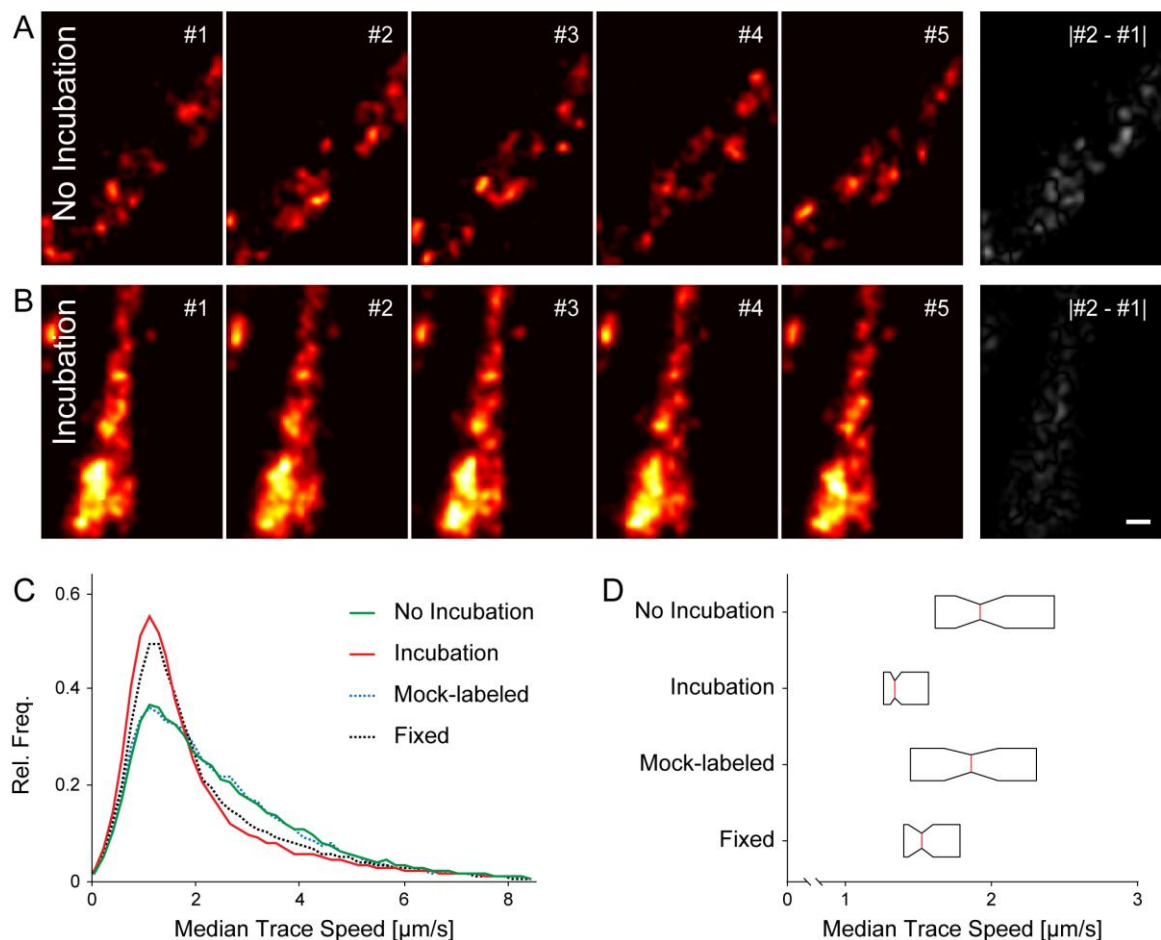
Figure 3.5: Synaptic vesicle mobility decreases after incubation. (A and B) Consecutive STED frames (filtered, 35 milliseconds per frame) of well resolved, live-labeled synaptic vesicles in living hippocampal neurons, imaged after 5 minutes (A) or after 2 hours (B) (see Movie A3). Note the decrease in vesicle mobility after incubation by comparing the difference images calculated from the first and second frames (gray panels in A and B). Scale bar: 250 nm. Voxel size: 15 nm^2; pixel dwell time 0.93 µs at the center, increasing to the side. (C) Illustration of the median trace speeds of synaptic vesicles in the different conditions. The histogram of the non-incubated vesicles is shown in green, the incubated preparations are shown in red, the punctuated blue and black lines show the results of the mock-label condition and the aldehyde fixed samples, respectively. Each histogram consists of 20000-40000 vesicle traces. (D) Boxplot of median trace speeds, showing the statistical variability between the different conditions. The red vertical line is the median of the median trace speed of the respective condition. The left and right endings of each box display the lower and higher quartiles, respectively, showing the interquartile range (dispersion about the median). Boxes whose notches do not overlap have statistically different medians at a 5% significance level.

Tracking of single vesicles in both conditions revealed that the non-incubated, recently endocytosed vesicles (No Incubation) were highly mobile, but the high-mobility state was

lost after incubation (Incubation; Figure 3.5 C, green and red curves, respectively; see Appendix Figure A 1 for the individual histograms with the corresponding standard error of the mean). Interestingly, incubated preparations showed identical vesicle mobility values as aldehyde fixed preparations (compare red with punctuated black curve). Movements in aldehyde fixed samples are due to localization noise in the vesicle assignment from one frame to the next (see Methods). The vesicle mobility between incubated and non-incubated samples changed significantly (Wilcoxon's rank sum test, $p = 2.5$ x 10^{-4}).

To control for the reliability of the incubation protocol mock-labeling experiments were performed, where the neurons were treated as for normal live-labeling, but without the use of antibodies. The preparations were finally live-labeled on ice with anti-synaptotagmin antibodies after placing them back for 2 hours at 37°C (see Methods). The synaptic vesicle mobility of mock-labeled preparations was indistinguishable from non-incubated ones, confirming that the live-labeling itself and the incubation protocol have no affect on the vesicle behavior.

3.1.5 Stabilization and Cluster Integration of Vesicles after Incubation.

The characteristic behavior of synaptic vesicle motion in both the incubated and no-incubated preparations can also be visualized by summing all frames of the individual movies (sum images, as already shown in Figure 3.4 A). Sum images with blurred areas would demonstrate vesicle motion. Areas where vesicles were temporary arrested or moved very little would be characterized by high-intensity spots, or "hot spots". Those hot spots represent pockets within the synaptic vesicle cluster, where vesicles stick to and become stationary (Westphal et al., 2008). Synaptic vesicles trapped in hot spots are consequently members of the synaptic vesicle cluster. The sum images of non-incubated samples show usually blurred vesicle traces. However, sum images of incubated samples are generally described by hot spots (Figure 3.6 A). To characterize the synaptic vesicle behavior in non-incubated and incubated samples, a running average analysis of the movies was performed (see Methods for the running average analysis on hot spots, (Westphal et al., 2008)). The method is based on the analysis of the time a vesicle remained in a hot spot (Figure 3.6 B). Vesicles from non-incubated samples showed high mobility, with most remaining only briefly in hot spots (with only ~18% of the vesicles spending 90% of their total trace time in a hot spot). Incubated

samples showed a much lower vesicle mobility, with vesicles spending most of the time in hot spots (with ~35% of the vesicles spending 90% of their total trace time in a hot spot). The incubated vesicles had identical values to aldehyde fixed samples, demonstrating that they became immobile (Figure 3.6 B).
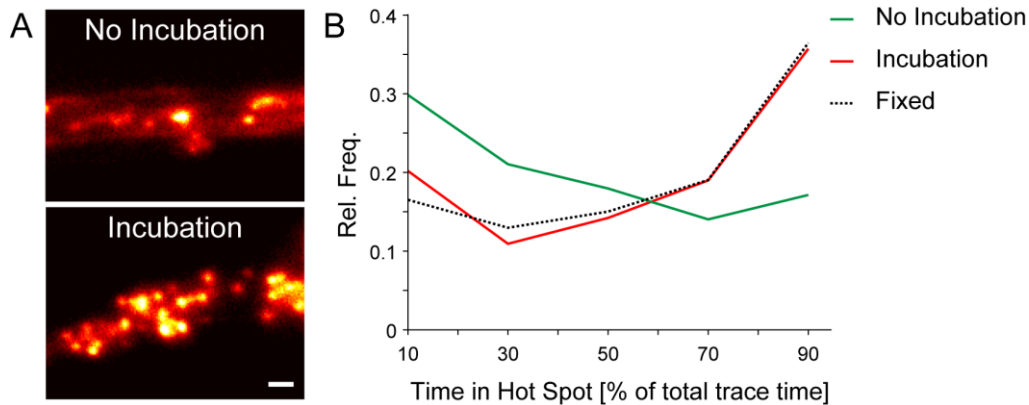
Figure 3.6: Synaptic vesicles become stationary after incubation. (A) Sum images of a non-incubated (upper) and an incubated (lower) preparation. STED movies were acquired and raw movie frames were averaged to get a sum image. Sum images show the preferred localization of the synaptic vesicles. The upper sum image is characterized by blurred parts demonstrating vesicle traces; however the lower sum image is characterized by hot spots. Scale bar: 250 nm. (B) Histograms of the time the vesicles spent in hot spots as the fraction of their total trace time in the three different conditions. Incubated and aldehyde fixed preparations show identical results. Histograms are from 1670–9850 vesicle traces.

Next, I wanted to obtain more information about the localization of the synaptic vesicles before and after incubation in relation to the synaptic vesicle cluster. For this I analyzed the colocalization of live-labeled vesicles to synapse specific proteins of interest. Hippocampal cultures were live-labeled on ice against synaptotagmin as shown above and were then either left in Tyrode at RT for 20 minutes (No Incubation) or placed back into their growth medium at 37°C for 2 hours (Incubation). In both cases the cells were afterwards fixed, permeabilized and immunostained against synaptic proteins of interest. These were general synaptic vesicle markers (synaptophysin, synapsin, Rab3) and AZ markers (Munc 13, bassoon, and the postsynaptic glutamate receptor) (Sudhof, 2004) (see materials). As the neurons were permeabilized during immunostaining, the vesicle markers had access to all synaptic vesicle proteins. The labeling was therefore used as a vesicle cluster marker. The colocalization

analysis was based on the colocalization between the live-labeled synaptic vesicles and the vesicle cluster marker. Imaging was carried out using confocal laser-scanning microscopy for both the live-labeled vesicles and the immunostained markers (see Figure 3.7 A and appendix Figure A 2 for all synaptic marker proteins). The overlays of the live-labeled and the immunostained vesicle marker synaptophysin shown in Figure 3.7 A indicated a higher level of colocalization of the live-labeled vesicles and the common synaptic vesicle cluster after incubation. This impression was also given for all other vesicle markers as well as for the AZ markers (see Appendix Figure A 2). The degree of colocalization was more evident when inspecting line profiles of fluorescence intensity for both the live-labeled synaptotagmin and the immunostained synaptic vesicle marker (Figure 3.7 B). From the intensity profiles the Pearson´s correlation coefficient was generated to compare the degree of colocalization before and after incubation. For all synaptic vesicle and AZ markers the colocalization increased after incubation (Figure 3.7 C). The results depict clearly that the recently endocytosed vesicles were hardly connected with the common synaptic vesicle cluster and the AZ, and were incorporated into the vesicle cluster after incubation. In addition, this argument is in line with the colocalization analysis of the live-labeled vesicles with the cytoskeleton element tubulin. Since tubulin is mainly located in the axon and generally absent within the synaptic vesicle cluster, a decrease in colocalization was observed after incubation (Figure 3.7 C; see also Appendix Figure A 2). Whether the values are correct was demonstrated by a colocalization experiment of live-labeled synaptotagmin with the plasma membrane protein SNAP-25. The SNAP-25 protein is uniformly distributed in the plasma membrane (Punge et al., 2008) and its location is unrelated to the localization of the synaptic vesicle cluster. Hence, the colocalization level was not altered after incubation (Figure 3.7 C).
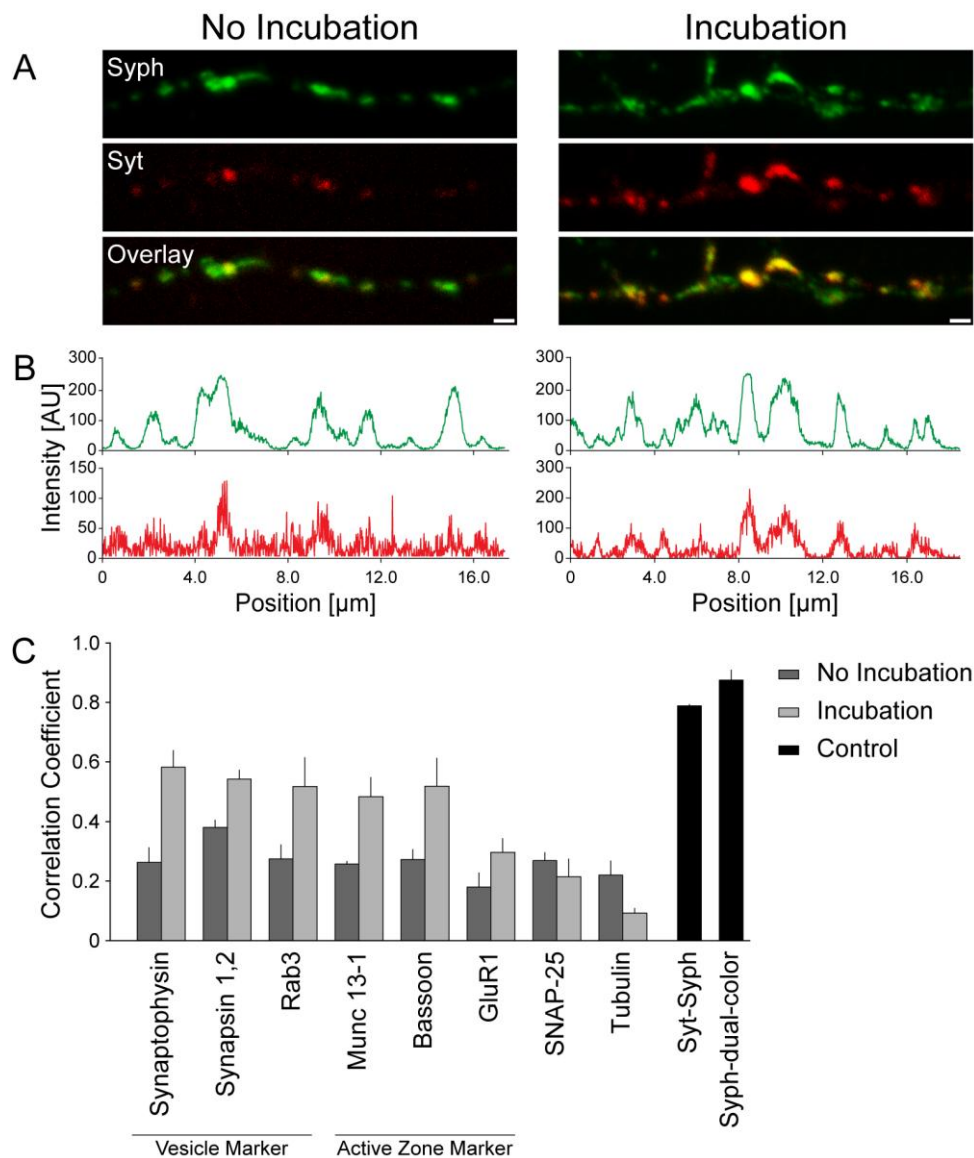
Figure 3.7: Cluster integration after incubation. (A) Colocalization of anti-synaptotagmin live-labeled vesicles with the immunostained synaptic vesicle marker synaptophysin. Live-labeled vesicles with anti-synaptotagmin antibodies (Syt, red) were fixed either after 20 minutes rest at RT (No Incubation, left panel) or after 2 hours of incubation at 37°C (Incubation, right panel), and immunostained (with permeabilization) against the vesicle marker synaptophysin (Syph, green). Comparison of the overlays in both conditions reveals a higher colocalization after incubation. Scale bar: 1 μm. (B) Fluorescence intensity profiles (in arbitrary units, AU) of both the synaptotagmin (red) and the synaptophysin (green) color channels from the corresponding images of (A) were obtained by manually drawing line profiles along the axons through the synaptotagmin channel. (C) The fluorescence intensity profiles were used to calculate the Pearson´s correlation coefficient between the synaptotagmin live-labeled vesicles and the immunostained synaptic vesicle markers (synaptophysin for example in (A) and (B), Synapsin 1,2 and Rab3), AZ markers (Munc 13-1, bassoon and the postsynaptic glutamate receptor GluR1), as well as for the plasma membrane marker SNAP-25 and the cytoskeleton element tubulin. Typical images of all immunostainings are presented in the Appendix Figure A 2. Colocalization results of non-

incubated preparations are shown in dark grey, the results of incubated preparations are presented in light grey. Positive control experiments for the correlation coefficient analysis are shown in black (two most right bars). They represent the colocalization of immunostained synaptotagmin and synaptophysin (Syt-Syph) and the immunostaining against synaptophysin using a mixture of Cy3- and Cy5-labeled secondary antibodies (Syph-dual-color). The control experiments display the best possible colocalization that can be obtained with the analysis program. The results (shown as mean ± SE) are shown from at least three independent experiments for each condition.

3.1.6 Both Vesicle Pools are Exchanged Between Synapses

From the results obtained so far, it can be summarized that the synaptic vesicles are highly mobile after endocytosis (as shown with STED imaging) and colocalize only little with the synaptic vesicle cluster (as shown by the colocalization analysis). They integrate after some time into the vesicle cluster at the AZ (as shown by the colocalization analysis), where they exhibit a low-mobility state (as shown with STED imaging and the hot spot analysis).

As explained in the Introduction, synaptic vesicles are not restricted to particular synapses, but can exchange between neighboring release sites (Darcy et al., 2006; Chen et al., 2008; Staras et al., 2010). A possible hypothesis could be that the recently endocytosed, mobile vesicles are exchanged between synapses and the immobile, resting vesicles are fixed in the synapse. Thus, the effect of the vesicle sequestration on the exchange between synapses was investigated with the fluorescence recovery after photobleaching (FRAP) method. FRAP imaging was carried out either directly after live-labeling (No Incubation) or 2 hours after labeling (Incubation, see above). A fluorescently labeled spot, representing an entire synaptic bouton was bleached and the fluorescence recovery within the bleached synapse was measured (Figure 3.8 A). Fluorescence recovery directly indicated the incorporation of neighboring vesicles in the bleached synapse. Surprisingly, the non-incubated (recently endocytosed) and the incubated (resting) preparations showed no significant difference in fluorescence recovery (Figure 3.8 B). Interestingly, the fraction of incorporated vesicles in the bleached synapses was relatively low with around 30-40% recovery after less than two minutes. This value is identical to that obtained in FRAP-studies on FM dye labeled preparations (Darcy et al., 2006). Nevertheless, the amount is relatively low regarding the high-mobility state of the recently endocytosed vesicles. This indicates that the majority of the vesicles just move through the synapse without the incorporation into the synaptic vesicle

cluster. However, the results are in agreement with previous findings, showing that both the recycling (mobile) (Darcy et al., 2006; Staras et al., 2010) and resting (immobile) pool (Fernandez-Alfonso and Ryan, 2008) exchange inter-synaptically.
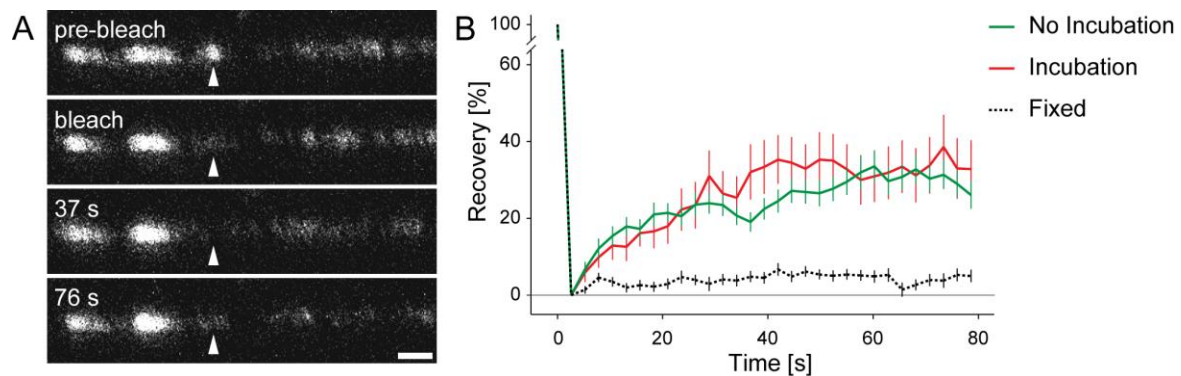
Figure 3.8: Inter-synaptic vesicle exchange. (A) Confocal images of an axon live-labeled with anti-synaptotagmin antibodies presented at different time points of a FRAP experiment (performed 12 minutes after vesicle labeling). A fluorescently labeled spot was bleached (pre-bleach) and fluorescence recovery was recorded inside the bleached synapse (see arrowhead in all four images). Note that some fluorescence reappears in the bleached area, indicating that unbleached vesicles (from neighboring synapses) moved into the existing vesicle cluster (inter-synaptic exchange). Scale bar: 1 µm. (B) Histograms of the fluorescence recovery (corrected for bleaching) for incubated (red line), non-incubated (green line) and aldehyde fixed neurons (punctuated black line). Results are from 4-7 independent experiments (with typically up to 10 FRAP curves per experiment; mean ± SE).

3.1.7 Stimulation Effects on Vesicle Mobility

After incubation the labeled synaptic vesicles exhibit a low-mobility state in the synaptic vesicle cluster at the AZ. Furthermore, they are now perfectly located to perform for what they are made for, to fuse with the plasma membrane and exocytose their neurotransmitter during stimulation. However, the directed movement towards the release site was never monitored. It is still unclear how synaptic activity influences the synaptic vesicle cluster in terms of recruiting single vesicles for exocytosis. What would be the effect of electrical stimulation on both recently endocytosed and resting vesicle mobility states? To test for this, live-labeled cultures were stimulated with 40 action potentials (2 seconds at 20 Hz) during imaging. This stimulation protocol is known to recycle the readily releasable pool of synaptic vesicles in this type of preparation (the docked and primed synaptic vesicles at the AZ

(Schikorski and Stevens, 2001)). STED movie images were acquired with video-rate recording before and during stimulation (start after 1.3 seconds, see Movie A4 and Appendix A.1 for the movie legend). Vesicle tracking was performed for the non-stimulated first 1.3 seconds and during the 2-second stimulation train (Figure 3.9, frames #1-3 of A and B). Comparing the median trace speed of synaptic vesicles before and during stimulation showed identical speed histograms with no change upon stimulation in the vesicle behavior of neither the non-incubated (recently endocytosed) vesicles nor the immobile (resting) vesicles (Figure 3.9 A and B). The synaptic vesicles of both mobility states seemed to be unaffected by the stimulation train.
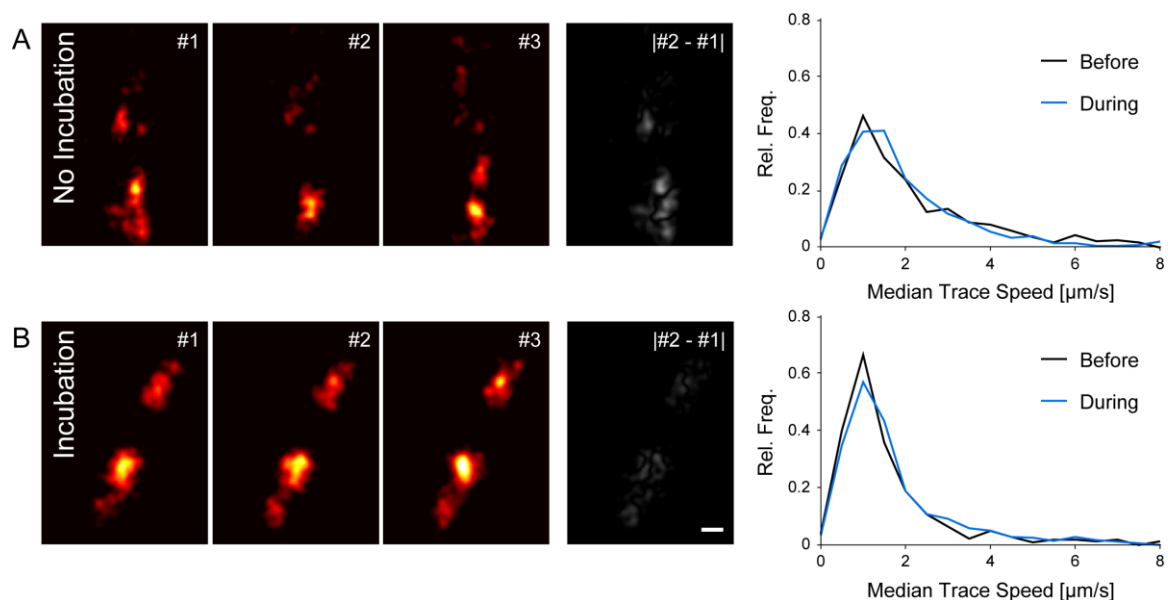
Figure 3.9: Stimulation effects on vesicle mobility. (A and B) Consecutive filtered STED frames of movies form non-incubated (upper panel, A) and incubated (lower panel, B) neurons showing well-resolved synaptic vesicles during electric field stimulation (see also Movie A4). The gray images show difference images from the first and second frames of the respective panels. Scale bar: 250 nm. The histograms show the median trace speed of the vesicles before start of stimulation (black) and during 2 seconds of stimulation at 20 Hz (blue). Histograms are from 550-730 values.

A second type of data analysis was also used, independent of single-particle-tracking methods. For this, difference images were used to display direct measurements of motion, since the displacement of an object from one frame to the next results in more intense difference image than with objects that do not move in consecutive frames (see gray panels in

Figure 3.9 A and B). Thus, difference images for both vesicle states were calculated and normalized to the original intensity of the corresponding movie frame (see Methods). This type of data analysis allowed for the direct visualization of any changes occuring at the beginning and the end of the stimulation period. A change in the intensity of difference images would be directly connected to increased or decreased movement of synaptic vesicles. However, as shown in the histograms of Figure 3.10, no change in difference image intensity can be detected at the beginning, during, or at the end of the 40-action potential stimulation train.

Taken together, two different data processing methods (single-particle-tracking and difference image analysis) showed identical results, with physiological stimulation having no affect on synaptic vesicle mobility of both vesicle states (recently endocytosed and mature vesicles).
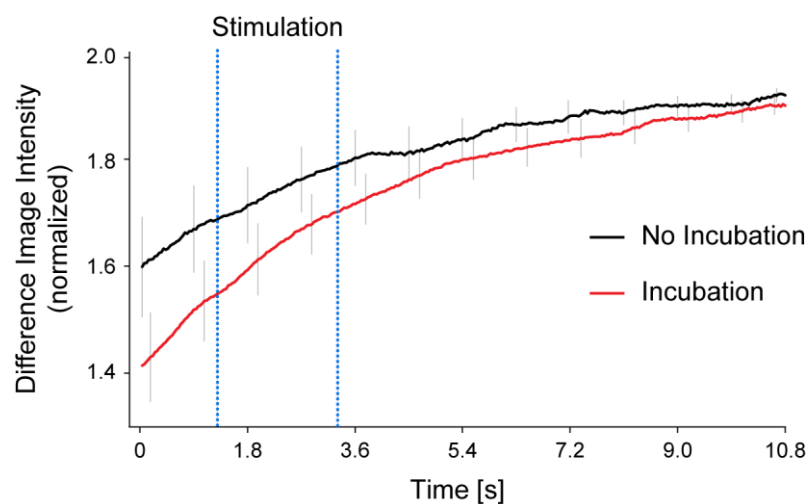
Figure 3.10: Analysis of synaptic vesicle mobility independent of single-particle-tracking methods. The difference image intensity was computed for each movie frame (raw data) and normalized to the intensity of this frame. Bleaching made the frames dimmer and thus the consecutive difference images get proportionally brighter (upward trend in the curves). The histograms were smoothed using a 15-frame moving average. The graphs show the mean ± SE from 20 (No Incubation) and 51 (Incubation) movies.

3.1.8 Synaptic inactivity forces vesicles to integrate into the vesicle cluster

The stimulation experiments may lead to the conclusion that synaptic activity is not directly linked to synaptic vesicle mobility. In the following experiment synaptic activity was inhibited with tetrodotoxin (TTX) to test if this is indeed the case. The poison TTX binds selectively to voltage-gated sodium channels and thus disables their proper functioning. The block of sodium channels inhibits the generation of action potentials, which in turn leads to repressed active neurotransmitter release (the synapse is silence). For the TTX experiments the neurons were live-labeled against synaptotagmin (as shown) and then pre-incubated with TTX (1µM, at RT) for 10 minutes before the start of STED imaging (Figure 3.11, frames #1-3, see Movie A5). Interestingly, the synaptic vesicle mobility of TTX-treated preparations was decreased when compared to untreated recently endocytosed vesicles ((control), histograms in Figure 3.11). The results can be interpreted as a faster vesicle integration into the vesicle cluster in the absence of synaptic activity. This suggests that synaptic activity is needed to maintain the vesicles in a mobile state. Taken together, synaptic activity is thus indeed linked to synaptic vesicle mobility.
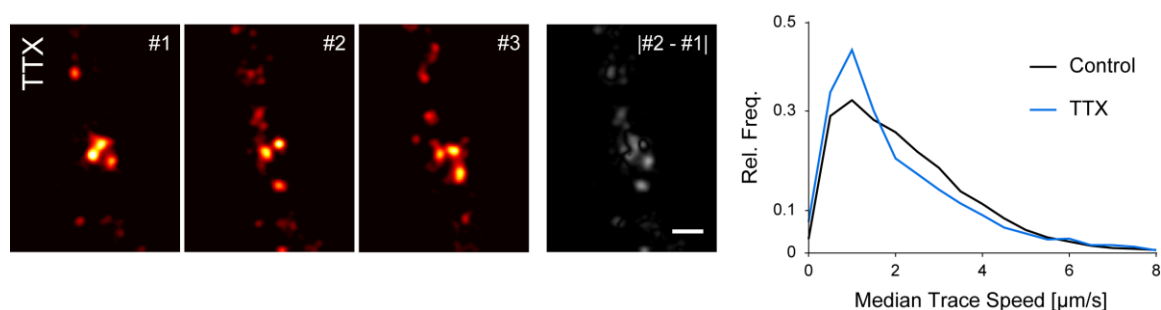
Figure 3.11: Synaptic vesicle motion is linked to synaptic activity. Hippocampal cultured neurons were live-labeled against the vesicle protein synaptotagmin on ice, transferred to RT and pre-incubated in 1 µM TTX in Tyrode buffer for 10 minutes (to block action potentials) before capturing STED movies at 28 frames per second (see Movie A5). Three consecutive frames are shown on the left side (frames #1-3) with well-resolved synaptic vesicles. The gray panel shows the difference image between the first and the second frame (#2-#1). Scale bar: 250 nm. The graph shows histograms of the median trace speed for TTX-preparations (blue) and for control conditions (no treatment, black). Note the lower speed values for the TTX-treated neurons, indicating that synaptic activity keeps the vesicles mobile.

3.1.9 Low-Mobility of Fused Synaptic Vesicles

After synaptic vesicle exocytosis the vesicle material is located on the plasma membrane at the AZ. The vesicle recycling models hypothesize that the vesicle material is mobile in the membrane in order to move to the endocytic periactive zone. As the fused vesicle material recycles rapidly after exocytosis (Westphal et al., 2008) it is difficult to explore its mobility on the membrane.

Several methods can be devised to investigate fused vesicle mobility. The mobility under natural conditions can be recorded in absence of divalent ions in the extracellular buffer. The lack of divalent ions blocks endocytosis and also calcium-triggered exocytosis. The material resides on the plasma membrane at an equilibrium state (Figure 3.12 A; (Zefirov et al., 2006b)). Nevertheless, the amount of fused vesicle material can be increased in the absence of divalent ions by stimulating exocytosis with caffeine (Zefirov et al., 2006a) or with the black widow spider venom (BWSV, (Ceccarelli and Hurlbut, 1980; Henkel and Betz, 1995). Treatment of neurons with caffeine in the absence of divalent ions efficiently causes exocytosis by releasing a minor concentration of calcium from intracellular stores, such as the endoplasmatic reticulum. This concentration is sufficient to trigger exocytosis and results in the addition of a small fraction of vesicle material to the one on the plasma membrane under equilibrium conditions. Quite contrary to caffeine, the BWSV treatment causes massive exocytosis events with almost the entire synaptic vesicle pool being forced to fuse with the plasma membrane. Endocytosis can at the same time be blocked by the lack of calcium in the buffer (Ceccarelli and Hurlbut, 1980). The synaptic vesicle materials are then retained in the plasma membrane of a swollen synapse (Figure 3.12 A).

These three conditions (control (no divalents), caffeine and BWSV) were used on hippocampal cultured neurons to investigate the mobility of the fused vesicle pool on the plasma membrane.
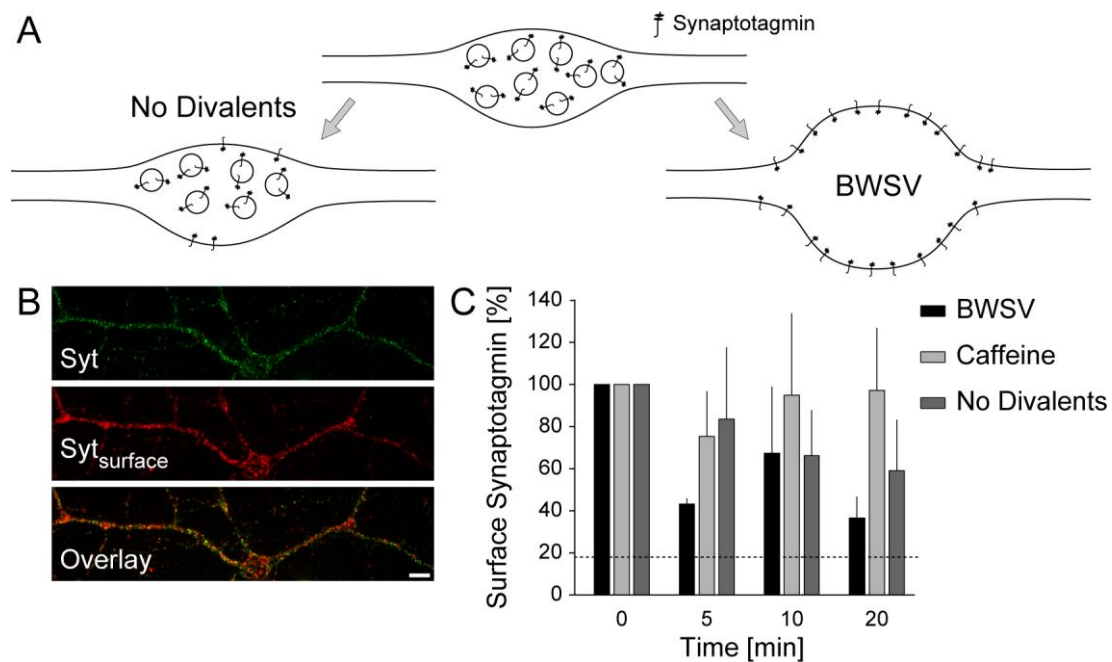
Figure 3.12: Blocking endocytosis allows the investigation of fused synaptic vesicles. (A) Schematic representation of the experimental setup. Endocytosis can be inhibited by decreasing the concentrations of divalent ions in the extracellular medium (no divalents, left) to specifically investigate the mobility of the surface pool of synaptotagmin at equilibrium. The fraction of this pool can be increased by stimulation while simultaneously blocking endocytosis using caffeine (not shown) or BWSV (right). Please consider that BWSV results in an excessive increase in fused vesicle material contrary to caffeine induced stimulation. (B) Hippocampal neurons were treated with BWSV, caffeine or divalent-free Tyrode with a subsequent staining of the surface pool of synaptotagmin with directly fluorescence-labeled Oyster-550 monoclonal mouse anti-synaptotagmin antibodies (Syt, green) on ice. After different incubation times at RT the preparations were fixed and the surface retained monoclonal antibodies were immunostained (without permeabilizaton) using Cy5-tagged secondary antibodies ($Syt_{surface}$, red). Scale bar: 5 µm. (C) The relative amount of antibody on the surface was determined and expressed as the fraction of the control condition (fixed immediately after labeling). The bars show the mean ± SE from three independent experiments for each condition. The dotted line indicates the amount of synaptotagmin left exposed under natural conditions after only 2 min of incubation (Westphal et al., 2008). Note that for all time points considered, all three conditions allow a large fraction of synaptotagmin molecules to remain on the surface instead of being endocytosed.

Before the actual STED imaging was performed the reliability of the three different protocols for blocking endocytosis was tested. The fraction of remaining surface-exposed synaptotagmin was analyzed after different time intervals. To test for this the neurons were first treated using the respective protocols (BWSV: 15 minutes incubation at 37 °C; caffeine: 5 minutes incubation at RT; control: 5 minutes incubation at RT). Afterwards, the fused

synaptic vesicle material was live-labeled on ice with directly fluorescence-labeled Oyster-550 antibodies against synaptotagmin. The neurons were then switched to RT and fixed at different time points (fixation on ice after 0 (control), 5, 10, and 20 minutes), followed by immunostaining (without permeabilization) with Cy5-tagged secondary antibodies for the specific detection of the surface retained synaptotagmin protein. Images of the total labeled synaptotagmin pool (green, Oyster-550) and the surface pool of synaptotagmin (red, Cy5) were acquired (Figure 3.12 B). The amount of fused synaptotagmin left on the plasma membrane after the particular time points was then quantified. The expected block of endocytosis was fulfilled in all three conditions used. Even after 20 minutes approximately two times more material remained on the surface in all three treatments when compared to the amount left on the plasma membrane after 2 minutes under natural conditions (shown as the dotted black line, see (Westphal et al., 2008)). The results revealed the strength of the endocytosis block, with the most efficient inhibition observed for the caffeine treatment.

The mobility of the fused synaptic vesicle material was then investigated using live STED imaging. The neurons were treated using these protocols and the surface-exposed synaptotagmin proteins were live-labeled with directly fluorescence-labeled anti-synaptotagmin antibodies (604.2 tagged with Atto647N obtained from Synaptic Systems, Göttingen). The mobility of the surface pool is shown in Figure 3.13 A (see Movie A6). Note the swollen synapse in the BWSV treated sample, indicating the massive amount of fused synaptic vesicle material (upper row of Figure 3.13 A).
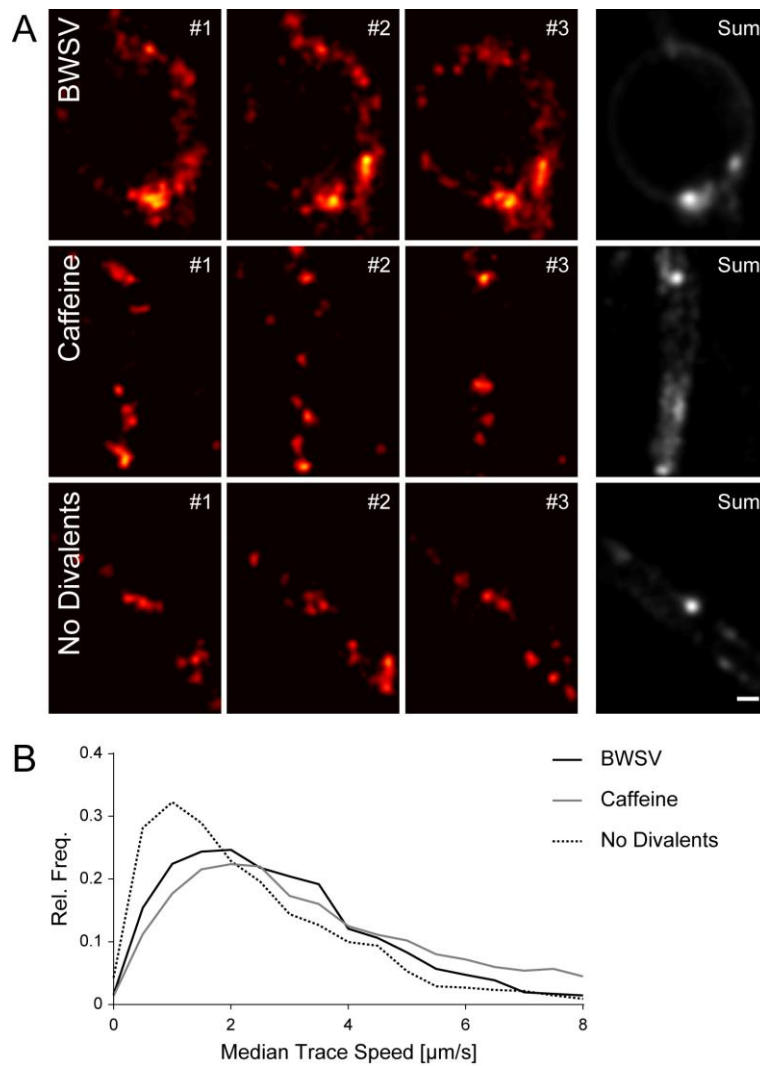
Figure 3.13: Mobility of fused synaptic vesicles. (A) Hippocampal cultures were treated with BWSV, caffeine or divalent-free Tyrode and the surface pool of synaptotagmin was live-labeled. The panels show three typical movie frames (frames #1-3 in each row) from BWSV (upper panel), caffeine (middle panel) or divalent-free (lower panel) preparations (see Movie A6). The gray panels show the sum images (500 frames) of the movies from the respective row. Each sum image has characteristical "hot spots", indicating the preferred location of fused vesicle material. Scale bar: 250 nm. (B) The graph shows histograms of the median trace speed of the fused vesicle material (BWSV: black; caffeine: grey; no divalents: punctuated black). Note that under natural conditions (no divalents) the material on the membrane is limited in mobility. The mobility increased by adding more fused vesicle material to the plasma membrane via stimulation with BWSV or caffeine. The histograms were computed from 2500–3000 values.

Tracking of the fused vesicle material resulted in relatively low speed values under control conditions (no divalents, Figure 3.13 B). Note that the mobility was almost identical to the mobility of recently endocytosed vesicles. Surprisingly, BWSV and caffeine treated

63

preparations showed faster vesicle movements on the plasma membrane compared to the control condition. This indicates that the surface pool of synaptotagmin at normal conditions is somehow hindered in its movements. However, the increased fraction of fused vesicles by BWSV or caffeine resulted in a more unrestricted movement, indicating that these added vesicles escaped the mechanism that is responsible for the low-mobility state under normal conditions (control).

3.1.10 The Fused Vesicle Movement is Restricted

Can a free-diffusion model explain the movement of fused vesicles? As already shown, the initial vesicles in the field of view bleached after some time and unbleached vesicles entered the imaged area continuously from both sides. To investigate the diffusion of fused vesicles, the number of fluorescent particles was determined for each movie-frame (compare with Figure 3.2). In all three conditions the fluorescence was bleached relatively fast, and after approximately 15 seconds only a limited number of particles entered the field of view, regardless of their localization in the neuron (synaptic vesicles of both mobility conditions, or fused vesicles on the plasma membrane; Figure 3.14). Interestingly, comparing these histograms with the one of a non-specific antibody bound to the plasma membrane showed that significantly more unbleached antibodies entered the field of view after 15 seconds (non-specific antibody: 604.2 primary labeled in our laboratory with Atto647N that lost its binding specificity due to the fluorescence labeling, see Appendix Figure A 3 for the specificity of the "specific" and "non-specific" antibodies). Quantifying the fraction of particles entering the imaged area after 15 seconds showed 26% ± 1% (mean ± SE) for the non-specific bound antibodies, which exceeds the 4.1% for the surface pool under control conditions and the 8.6% and 9.8% obtained from the caffeine and BWSV treated preparations, respectively. The results demonstrated that the movement on the surface is restricted by a certain mechanism, as the non-specific antibodies entered much longer the field of view, obviously being in a more free-diffusion state than the fused vesicle material.
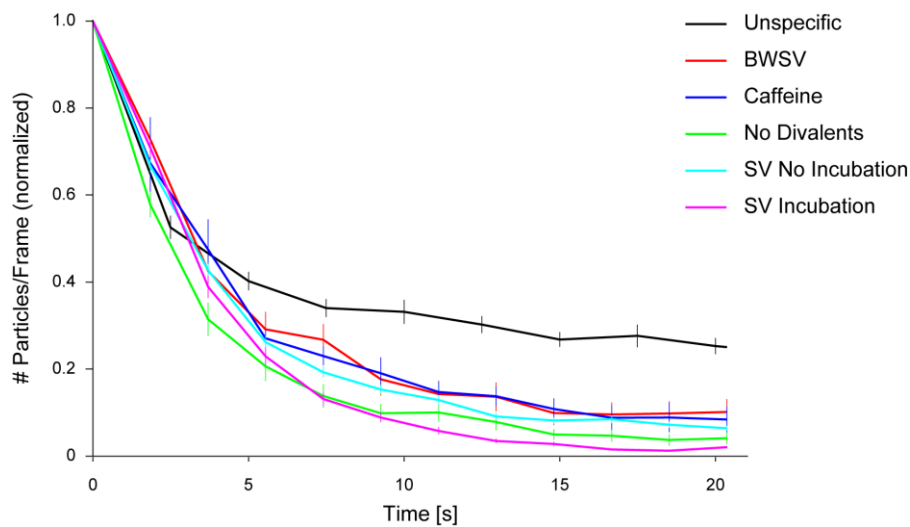
Figure 3.14: Fused motion analysis by bleaching. The amount of fluorescent particles per 50 movie frames was quantified and expressed as a fraction of the particle number in the initial 50 frames. As the particles are bleached during imaging, the amount of fluorescent particles drops quite fast for all conditions analyzed (SV: synaptic vesicles). However, the number of fluorescent particles was much higher in preparations that were labeled with an antibody that binds non-specifically to the plasma membrane (black line). Particles constantly entered the imaged area. The SE was obtained from various movies.

3.1.11 Clathrin-Structures Hinder Free-Motion of Fused Vesicles

Next, the mechanism was analyzed that could be responsible for the low-mobility state of the fused vesicles. The most reasonable candidates were clathrin-coated pits, since they show similar mobility values (0.8 ± 0.06 µm per second on MDCK cells, (Rappoport et al., 2003)). Thus, experiments aimed directly at investigating the colocalization between the surface vesicle pool and proteins of the CME machinery were performed. In principle, the same experimental setup and analysis as for the colocalization experiment shown above were used here (see Figure 3.7). In brief, the neurons were first, treated with one of the three different protocols (BWSV, caffeine, control), second, live-labeled with the anti-synaptotagmin antibodies on ice for surface labeling, and third, fixed and immunostained using Cy5-tagged secondary antibodies. Fourth, neurons were immunostained (with permeabilization) against the clathrin light chain or the clathrin adaptor protein amphiphysin using Cy3-tagged secondary antibodies (Figure 3.15 A). Images were obtained with an epifluorescence microscope, line profiles were manually drawn and the Pearson´s correlation coefficient was generated (see Figure 3.7).

The fused vesicle pool appeared to colocalize to some extent, but significantly (p<0.01, t-test) with the clathrin endocytosis machinery in all conditions (Figure 3.15 B). This provided an indication that a certain number of fused vesicles could move in partially invaginated clathrin-coated pits.
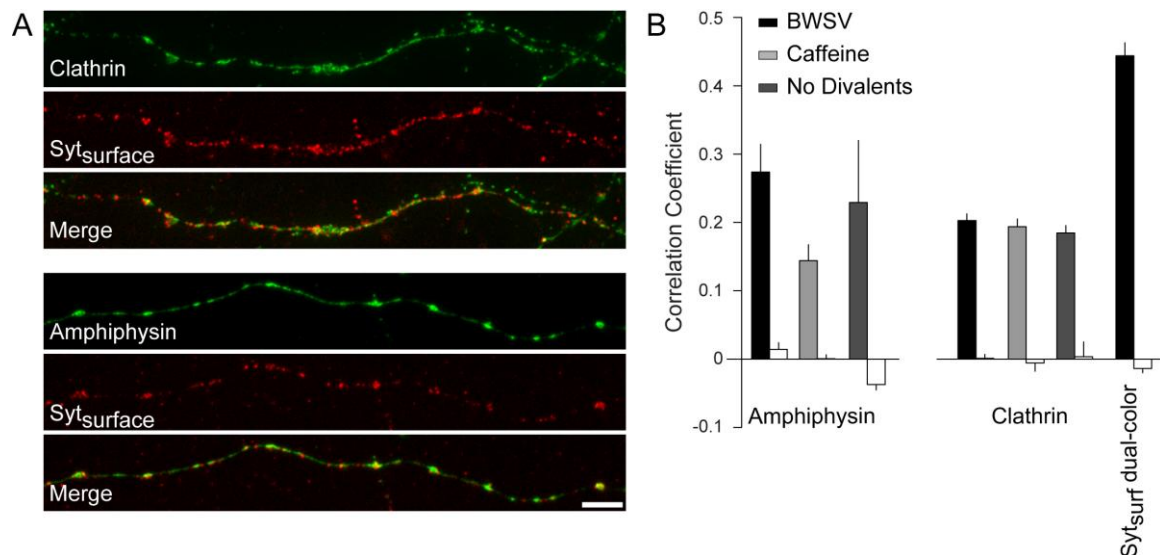
Figure 3.15: Fused synaptic vesicles colocalize with the clathrin machinery. (A) Cultured hippocampal neurons were treated with BWSV, live-labeled with primary antibodies against synaptotagmin and fixed. They were then immunostained using Cy5-tagged secondary antibodies (Syt$_{surface}$, red) and subsequently immunostained (with permeabilization) against clathrin or amphiphysin and Cy3-tagged secondary antibodies (clathrin upper, amphiphysin lower part, green). Scale bar: 5 µm. (B) Analysis was carried out as for Figure 3.7, drawing line profiles for the fluorescence intensity, and the Pearson´s correlation coefficient was determined for the surface pool of synaptotagmin and the clathrin-coat marker. For the indication of a random colocalization, an inversed (mirrored) intensity line profile in the Cy5 channel from each experiment was used for the calculation of the correlation coefficient (white bars). A positive control for the analysis, to receive the best possible correlation, is shown in black and represents an immunostaining of the surface pool of synaptotagmin by a mixture of Cy2- and Cy5-tagged secondary antibodies (neurons were treated with BWSV). A significantly higher level of colocalization was obtained from the surface pool of synaptotagmin with the clathrin-coat markers compared to the random correlation for BWSV- and caffeine- treated neurons (p<0.01, t-test; n=3 independent experiments; only two independent experiments were analyzed for "No Divalents", for which the error bars show the range of values).

3.1.12 Morphological Description of Vesicle Recycling in Conventional Synapses

In the introductory part of this work I already described the different models of synaptic vesicle recycling, with the classical recycling pathway suggested from ultrastructural observations by Heuser and Reese in 1973 (Heuser and Reese, 1973). The classical model is based on vesicle retrieval via clathrin-mediated endocytosis with subsequent coalescence of the recycled vesicles to form cisternae. Finally, the cisternae divide and form new vesicles (Heuser and Reese, 1973). According to the data presented above, the fused vesicle material could use the clathrin-dependent pathway. What would be the fate of the newly formed synaptic vesicle after it lost its clathrin-coat? Is the vesicle retrieved from the surface as a "fusion-competent" synaptic vesicle or is there a sorting step via an endosomal/ cisternal compartment to finally generate a "perfect" vesicle? The intermediate endosomal sorting step in vesicle recycling is controversially discussed (see for example Murthy and Stevens, 1998; Bonanomi et al., 2006; Rizzoli et al., 2006; Hoopmann et al., 2010).

The presented high-resolution imaging of mobile vesicles did not reveal the morphology of the synaptic vesicle cycle. I can hypothesize that only a minor fraction of all synaptic vesicles recycle (under reasonable stimulation). Furthermore, the retrieval mechanism likely uses small vesicle-like organelles, since large cisternae or endosomal structures were never observed with STED imaging.

Thus, in further experiments the morphology of the synaptic vesicle cycle in conventional synapses was investigated. To characterize the morphology of recycling organelles and to be able to localize and discern them from non-recycled organelles, membrane recycling was visualized by labeling the organelles with the styryl dye FM1-43 followed by its photo-oxidation and electron microscopy (see Methods).

Hippocampal cultured neurons were pre-incubated with FM1-43 for 10 seconds before start of stimulation for 2 seconds at 20 Hz (recycling the RRP vesicles). The neurons were left in FM dye to rest for different time intervals of 4, 10 and 30 seconds and were then fixed in ice-cold glutaraldehyde (2.5% in PBS) to stop endocytosis. The different time intervals allowed for the direct comparison of the morphology of the recently endocytosed organelles at various steps in the recycling pathway (Figure 3.16 A). A first visual inspection of the electron micrographs from the three different time points after labeling showed that after 4 seconds the recycled organelles were small, after 10 seconds larger organelles appeared and after 30

seconds again small organelles were present (Figure 3.16 B). The quantification of the diameter of the organelles confirmed this impression. At 4 seconds after stimulation the organelles had small diameters and were consistent in size (around 41 nm). This value is in agreement with previous findings of the diameter of small synaptic vesicles (~41.6 nm, (Takamori et al., 2006)). Interestingly, the second time point (10 seconds after stimulation) was indeed characterized by a fraction of larger organelles with a mean diameter of around 50 nm (see inset of Figure 3.16 C), coming along with a reduction of small organelles (Figure 3.16 C, red). Finally, the 30 second time point again showed small vesicle-like organelles. The decreased number of labeled organelles at 10 seconds (Figure 3.16 D) correlated well with their increased diameter. Furthermore, the total labeled area was equal at all three time points (Figure 3.16 E), showing that the total amount of labeling remained constant over time.

In summary, the results are in agreement with those of Heuser and Reese including the steps shown in their classical vesicle recycling pathway (Heuser and Reese, 1973). Small vesicles fuse with cisternal compartments (or endosomes) leading to larger organelles at 10 seconds after stimulation, from which then small vesicles are generated (hence the small vesicles at 30 seconds after stimulation).

I conclude that the morphological analysis of the vesicle cycle in conventional synapses showed a rather simple recycling mechanism, with at least a partial involvement of endosomal sorting.
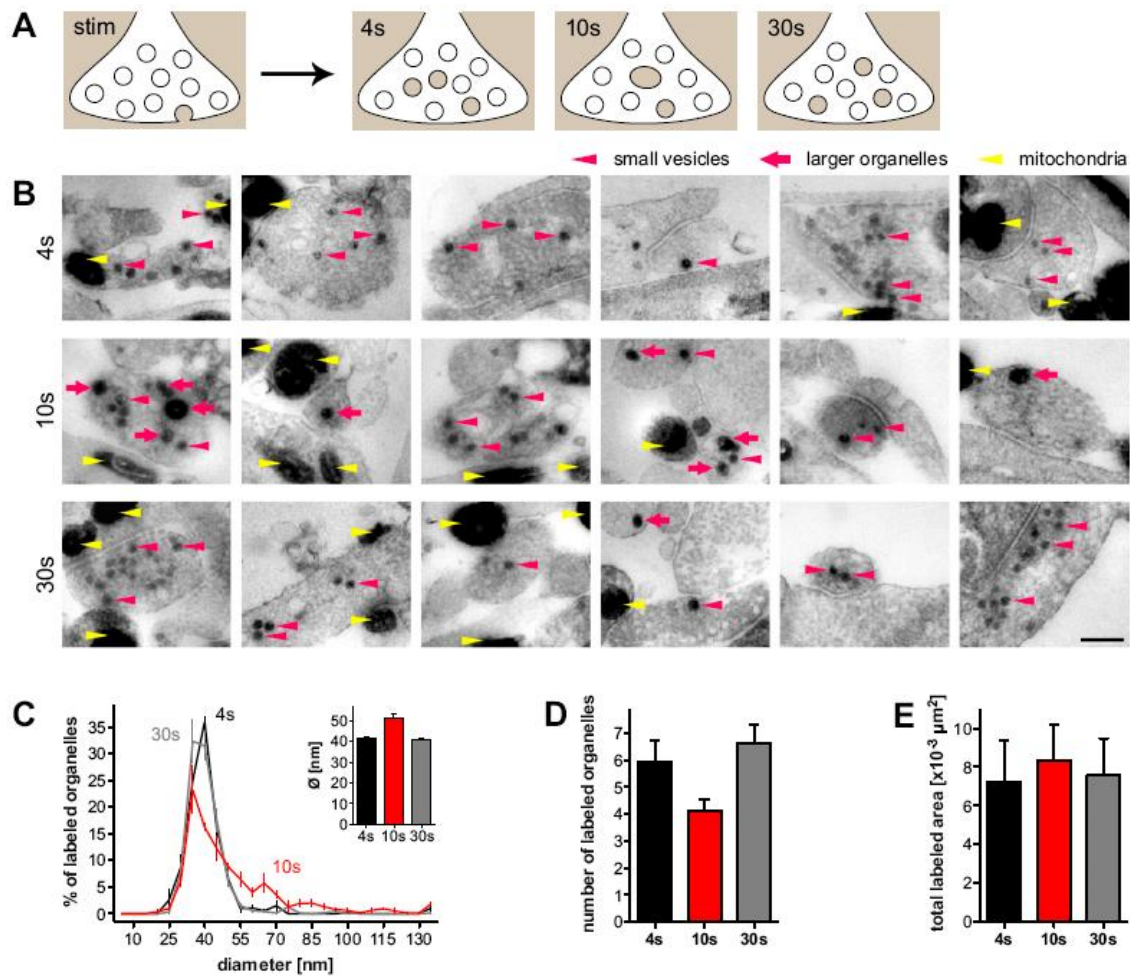
Figure 3.16: FM photo-oxidation reveals morphology of synaptic vesicle recycling. (A) Hippocampal cultured neurons were pre-incubated in FM1-43 for 10 seconds prior to RRP vesicle stimulation (2 seconds at 20 Hz). Neurons were fixed after a resting period of 4, 10, or 30 seconds by dipping them in a large volume of ice-cold glutaraldehyde. The different time points of fixation allowed the characterization of the morphological correlates in the synaptic vesicle recycling pathway. The neurons were then processed for FM photo-oxidation and electron microscopy. (B) Typical electron micrographs of hippocampal cultured synapses taken from the samples with the different fixation time points show labeled (photo-oxidized) small vesicle-like organelles at 4 seconds and 30 seconds after stimulation (red arrowheads), however at 10 seconds after stimulation the amount of small organelles is reduced and larger organelles are observable (red arrows). Mitochondria are marked by yellow arrowheads. Positively photo-oxidized mitochondria are unrelated to synaptic vesicle recycling (Harata et al., 2001; Grabenbauer et al., 2005). Scale bar: 200 nm. (C) Graph shows histograms of the fraction of labeled organelles in relation to their diameter. As visually recognized in (B) the fraction of labeled organelles with larger diameters 10 seconds after stimulation is more evident (~50-100 nm). The inset shows a diagram of the averaged vesicle diameter displaying a significant increase for the 10 seconds time point ($p<0.01$, t-tests). (D) The positive-oxidized organelles were counted for each electron micrograph. At 10 seconds the amount of organelles was significantly smaller ($p< 0.05$, t-tests). (E) Quantification of the total labeled area. No significant differences between the various time points. All graphs show means ±

SE. Experiments and analysis were performed by Dr. S.O. Rizzoli - modified from Hoopmann et al., 2010.

3.2 Sensory Synapses

3.2.1 Live Investigation of Vesicle Recycling in Sensory Inner Hair Cells

Inner hair cells are selectively labeled by FM dyes

While the vesicle recycling mechanism is relatively well explored in conventional synapses, the membrane retrieval pathway in sensory cells is less well understood. I therefore worked on the investigation of vesicle recycling in IHCs of the mouse cochlea.

Most of what is known today on vesicle recycling in conventional synapses (for an overview see Introduction) was achieved by the use of styryl dyes (FM dyes). They have been used for decades to report synaptic vesicle recycling in conventional synapses. The addition of the dye to the bathing solution leads to the partition of the dye into the plasma membrane. Synaptic vesicles that release neurotransmitter during dye incubation come into contact with the dye, which binds to the vesicle membrane and gets thus incorporated upon vesicle endocytosis. The FM dye can also be released from labeled vesicles when these fuse again with the plasma membrane. While conventional synapses are entirely dedicated to vesicle-mediated neurotransmitter release and synaptic vesicle recycling, IHCs also have to deal with vesicle-unrelated endocytic and non-endocytic processes, which would presumably take up FM dyes. Thus, one has to be careful here in interpreting FM studies on IHCs.

As reviewed in the Introduction, immediately after the addition of FM1-43 the FM fluorescence appeared rapidly within hair cells at the apical pole (Seiler and Nicolson, 1999; Gale et al., 2001; Griesinger et al., 2002; Meyers et al., 2003; Griesinger et al., 2004; Griesinger et al., 2005). It is controversially discussed whether this fast FM dye entry is due to endocytosis or to non-selective permeation through pores or channels at the apical pole of the hair cells.

To test for this, I repeated the above-mentioned FM studies on cochlear IHCs. Therefore, the organ of Corti from 14-18 day old mice was dissected and placed into an imaging chamber filled with the standard HEPES-HBSS (calcium-free). To prevent floating of the organ it was fixed in place with nylon fibers. The FM dyes were then applied to the standard HEPES-

HBSS bathing solution (final concentration 10 μM). As shown in Figure 3.17 different FM dyes labeled selectively the sensory IHCs with high intensity, while the surrounding cells did not show any uptake (see Table 1 for details on dyes). Only FM3-25 showed almost no membrane staining of the organ of Corti, not even with increased concentrations of 200 μM. Incubation of FM3-25 on cultured neurons (60 seconds) with subsequent stimulation (20 Hz for 30 seconds plus additional 30 seconds rest in the dye) revealed no uptake into synaptic vesicles when compared to the punctuated synapse-specific staining of FM1-43 (Figure 3.17). Although the fixable analogs of FM1-43 (AM1-43) and FM4-64 (FM4-64FX) are larger in size due to their attached aliphatic amino group on the positively-charged head, they entered the IHCs in the same fashion as the non-fixable FM variants. All FM dyes applied on IHCs (except FM3-25) showed FM fluorescence within the entire hair cells already after 120 seconds, which is in agreement with the literature (Seiler and Nicolson, 1999; Gale et al., 2001; Griesinger et al., 2002; Meyers et al., 2003; Griesinger et al., 2004; Griesinger et al., 2005).
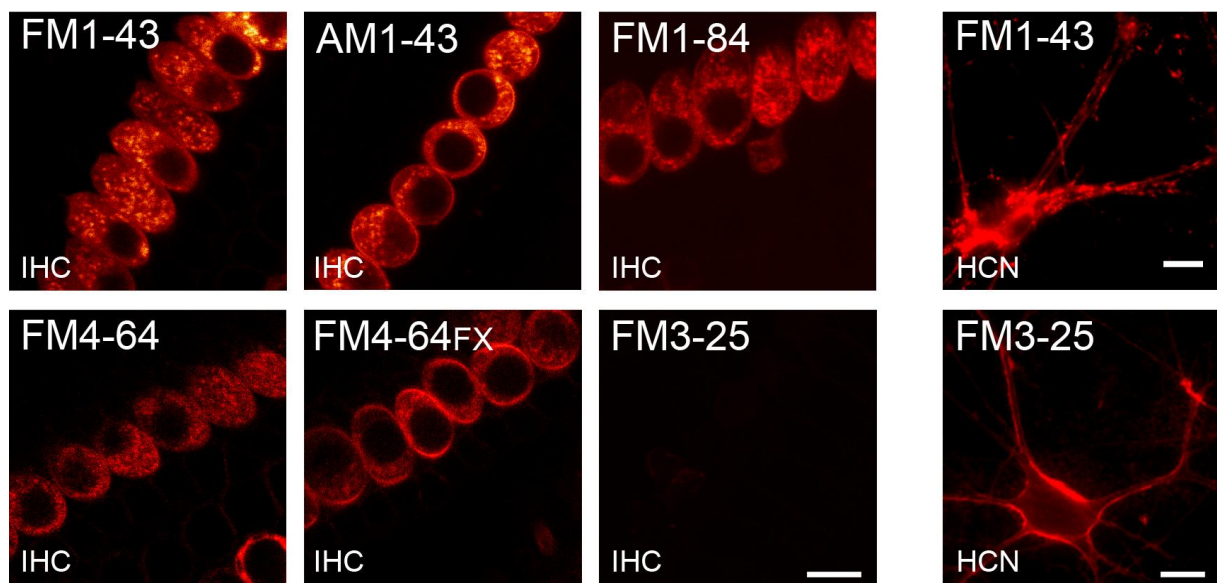
Figure 3.17: FM dye staining on IHCs and cultured neurons. Inner hair cells (IHC, left) of the organ of Corti were labeled with the different FM dyes. Note that the IHCs are selectively labeled (no other cells are labeled), except for FM3-25. This larger FM dye showed almost no membrane staining on IHCs. When testing FM3-25 on hippocampal cultured neurons (HCN, right) under electrical stimulation conditions (20 Hz for 30 seconds with additional 60 seconds rest in the dye), the dye was not taken up into synaptic vesicles as observed for the

classical FM dye FM1-43 (compare the synaptic-like labeling pattern of FM1-43 with the membrane staining of FM3-25). Scale bars: 10 μm; HCN/ FM3-25: 5 μm.

FM dyes enter IHCs at the apex in a fast non-endocytic process

Furthermore, time-lapse z-stack series were recorded during dye application and its washout showing that FM dyes rapidly entered the IHCs at the apical pole as shown previously (Figure 3.18) (Gale et al., 2001; Griesinger et al., 2002; Meyers et al., 2003; Griesinger et al., 2004; Griesinger et al., 2005). Apparently, FM1-43 bound immediately to the plasma membrane of the stereocilia after FM dye application (FP1, second series). The FM fluorescence signal was already observable between the stereocilia and the nucleus in the next z-stack series (FP2, 20 seconds later), while the basal part still showed no FM dye uptake. After some time the fluorescence also became visible at the nucleus (FP3) and later on at the basal pole (FP4).

Figure 3.18: Characteristics of FM dye entry into living IHCs. FM1-43 entry into IHCs was investigated using time-lapse z-stack series during dye application and its washout (*FP: focal plane*). The first focal plane (FP1) was placed at the stereocilia level, FP2 between the stereocilia and the nuclei, FP3 at the level of the nuclei and FP4 at the basal pole. Z-stack series were imaged every 20 seconds. FM1-43 was applied between the first and the second z-stack series (large Arrow).

To directly address the issue of labeling through endocytosis or non-selective permeation through ion channels, the labeling of fixed IHCs was investigated. The organ of Corti was fixed in 4% PFA for 60 minutes and afterwards imaged exactly as the living preparations (time-lapse z-stack series during dye application and its washout). Surprisingly the fixed preparations showed a similar IHC labeling with FM dye as the living ones (Figure 3.19). The FM fluorescence was first visible at the stereocilia and then spread to the nucleus and

later to the basal pole. With this simple experiment I demonstrated that endocytic processes do not mediate the apical FM dye entry into the IHCs as they were fixed (dead). The uptake was rather caused by the rapid permeation of the FM molecules through non-selective channels.
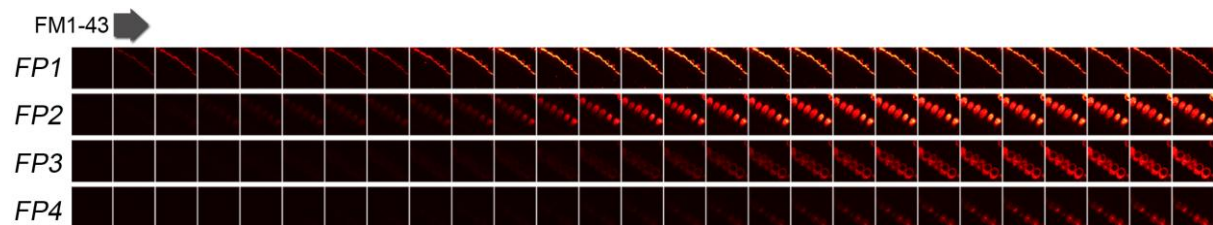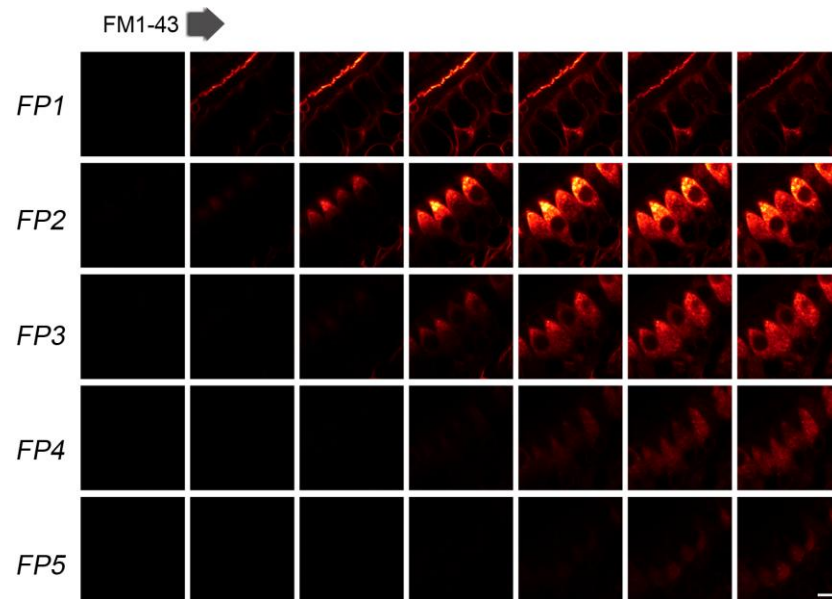

Figure 3.19: Characteristics of FM dye entry into fixed IHCs. FM1-43 entry into aldehyde fixed IHCs was investigated using time-lapse z-stack series during dye application and its washout. FM1-43 was applied as on living organs of Corti and z-stacks were acquired every 10 seconds (random z-stacks are displayed in chronological order). The appearance of the FM dye in fixed IHCs is identical to live ones. Scale bar: 10 μm.

The same experiments were also performed on fixed and permeabilized (3 minutes with 0.1% TX100 at RT) organs of Corti to induce additional pores in the plasma membrane. Interestingly, identical labeling results were obtained as for only fixed or living preparations (Figure 3.20). Note that here also neighboring cells of the IHCs were labeled, as the dye could penetrate through the pores induced by permeabilization.
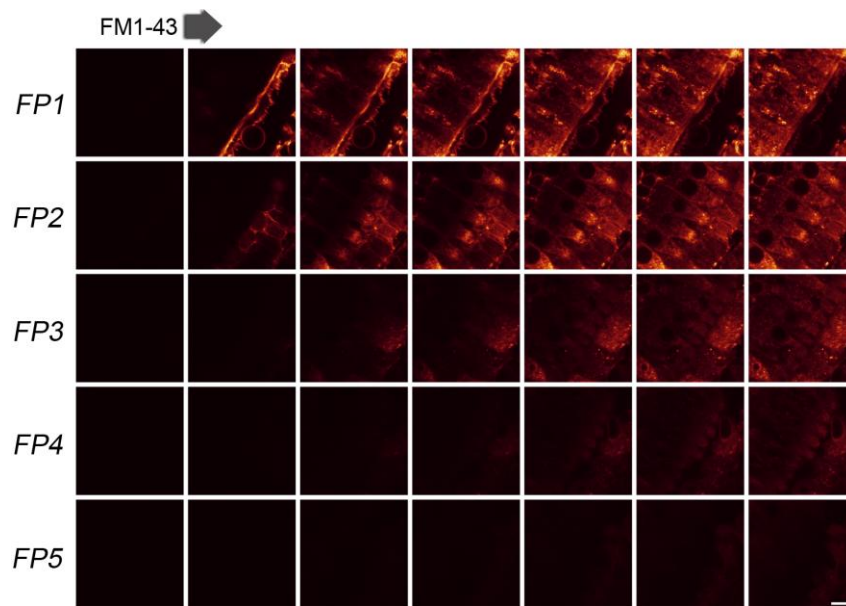
Figure 3.20: Characteristics of FM dye entry into fixed and permeabilized IHCs. FM1-43 entry into aldehyde fixed and TX-100 (0.1%) treated IHCs was investigated using time-lapse z-stack series during dye application and its washout. FM1-43 was applied (large arrow) and z-stacks were captured (random z-stacks are displayed in chronological order). The appearance of the FM dye in fixed and permeabilized IHCs is identical to live and "only fixed" ones (no permeabilization). Note the appearance of FM fluorescence in the neighboring cells. Scale bar: 10 μm.

Interestingly, in none of the conditions (alive, fixed, or fixed and permeabilized) the nuclei of the IHCs showed FM fluorescence, since membranes are absent within the nuclei.

The so far obtained results on investigating vesicle recycling in IHCs by styryl dyes, indicated that the various species of FM dyes enter the IHCs at the apex through ion channels in a non-selective fashion. The rapid FM dye appearance within the IHCs is therefore unrelated to vesicle recycling. Consequently, the use of FM dyes to investigate synaptic vesicle recycling in living IHCs as performed on conventional synapses is not recommendable - the results would be distorted by the non-selective passage of the dye into the cytosol of the cells.

In further experiments attempts to block the unspecific permeation of FM dyes through ion channels known to be located at the apical pole were conducted. All tested inhibitors (d-tubocurarine to block the mechanotransduction channels and at higher concentrations P2X

receptor channels (Crumling et al., 2009); EGTA to break the tip-links of the stereocilia to inhibit mechanotransduction; suramin to block the P2X receptors (Meyers et al., 2003; Crumling et al., 2009)) still showed permeation of FM1-43 into IHCs. With some of the inhibitors the intensity of FM fluorescence was partially reduced (data not shown; EGTA showed no effect). The results of suramin are of secondary interest for the further work here, but reveal important findings to its action in combination with FM dye labeling investigations (please see the Appendix (Section A.5) for the additional experiments on blocking P2X receptors by the pharmacological reagent suramin).

Other dyes used for vesicle recycling studies in inner hair cells

Whether other dyes than styryl dyes are suitable for studying vesicle recycling in living IHCs was also tested (Table 1). First, dodecanoyl fluorescein, a small lipid-like molecule with a fluorescent head group was used. Application of the dye on hippocampal cultured neurons only showed the staining of the outer plasma membrane (1 mg/ml in Tyrode buffer for 60 seconds at RT), indicating no flipping or penetration (not shown). After high potassium stimulation (~30 seconds, 70 mM KCl; 1 mg/ml dodecanoyl fluorescein) a clearly punctuated synaptic-like pattern was visible, indicating the labeling of recycled synaptic vesicles (Figure 3.21, compare with FM1-43 pattern in Figure 3.18). Nevertheless, when the dye was added to the organ of Corti, it labeled the IHCs in the same fashion as FM dyes, pointing also to the penetration through channels (Figure 3.21).

The next tested dye was the fluorescent carbocyanine dye DiO. It has a positively charged ring system (head group) that builds the fluorophore with two attached uncharged tails, which make the dye extremely lipid-soluble. The dye appeared to be insoluble in an aqueous environment and thus showed precipitation on membranes of cultured neurons, leading to their partial labeling (Figure 3.21). Hence, it was not further tested on IHCs.

In a new attempt of testing dyes that should not be able to permeate through ion channels, the cell impermeant, and polyanionic fluorescein derivative calcein was used. The small molecule dye calcein (100 μM) showed spontaneous fluorescence in solution in contrast to FM dyes. Therefore, standard confocal imaging was impossible in presence of the dye, as the illumination light was absorbed along the lightpath in fluid, and fluorescence was not

detectable. Thus, multi-photon imaging was used to decrease absorbance. The IHCs appeared as dark areas in a highly fluorescent background when the dye was present during imaging (Figure 3.21). Calcein has an identical molecular weight as FM1-43 (622 and 612, respectively) but showed no permeation into hair cells, likely due to its different behavior in binding/ interacting with membranes (Figure 3.21).
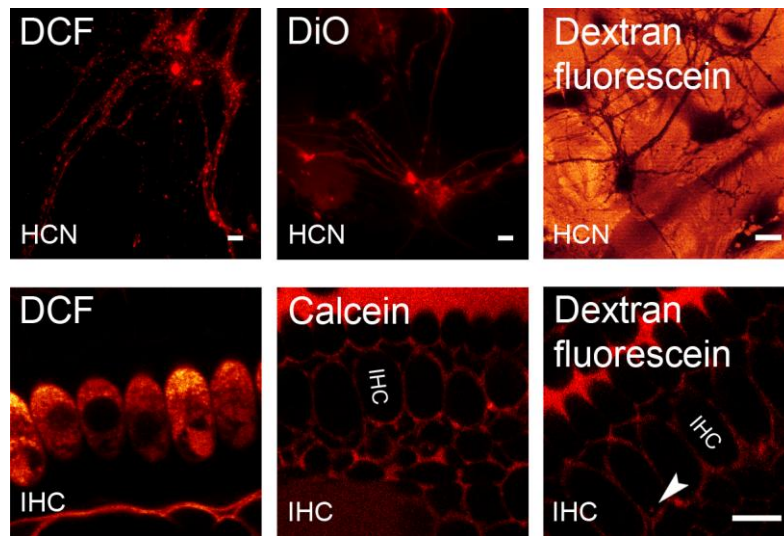
Figure 3.21: Labeling of hippocampal cultured neurons (HCN) and inner hair cells (IHC) using different fluorescent markers. Upper panel from left to right shows epifluorescence images of hippocampal cultured neurons tested with the following dyes: dodecanoyl fluorescein (DCF), DiO (from the carbocyanine family), and 3000 Dalton dextran fluorescein (multi-photon image). Lower panel from left to right shows multi-photon images of IHCs tested with the following dyes: dodecanoyl fluorescein (DCF, confocal image), calcein, and 3000 Dalton dextran fluorescein. Note the appearance of a fluorescent spot at the basal pole of the dextran labeled IHCs representing endocytosed dextran (white arrowhead). Scale bar for HCN: 10 μm, dextran HCN: 20 μm; scale bar for IHCs: 10 μm.

Identical results were achieved for the fluorescein-labeled 3000 Dalton dextran. The 3000 Dalton dextran is small enough to get incorporated in synaptic vesicles of synaptosomes (Rizzoli et al., 2006 used 10 kDa dextran), or the difficult to access neuromuscular junction (Rizzoli and Betz, 2004). Multi-photon imaging was used to image the anionic (lysine fixable) dextran fluorescein as it is also highly fluorescent in solution, as shown by the high extracellular fluorescent background staining of cultured neurons in presence of the dye (0.25 mg per ml)(Figure 3.21). The imaging of IHCs after 4 minutes of dextran fluorescein

incubation (1 mg per ml in standard HEPES-HBSS) showed no permeation of the dye through ion channels. A subsequent acquisition of a single z-stack uncovered a labeled spot at the basal pole inside one IHC, indicating an organelle that took up dextran during incubation (Figure 3.21, white arrowhead). As the experiment was performed under zero calcium conditions, one has to be careful in interpreting the result.

Both the fluorescein derivative calcein and the 3000 Dalton fluorescein labeled dextran seem to be promising for live investigations of vesicle recycling in IHCs but need a more precise testing.

Live-labeling of vesicles in inner hair cells using antibodies

In an additional approach I tested whether the vesicles of IHCs could be live-labeled with antibodies as shown above for conventional synapses (see also (Matteoli et al., 1992; Kraszewski et al., 1995)). For live-labeling anti-otoferlin antibodies that recognize the intra-vesicular domain of the IHC-specific vesicle protein otoferlin were used (Roux et al., 2006; Schug et al., 2006). The live-labeling protocol was adapted from the conventional labeling protocol. Primary anti-otoferlin antibodies were applied for 10 minutes in high potassium HEPES-HBSS buffer at RT. The organ of Corti was fixed and immunostained (with permeabilization) with Cy2-tagged secondary antibodies.

Subsequent imaging of the embedded preparations using confocal optics revealed no labeling of IHCs. Problems with the approach could be due to a slow binding affinity of the antibodies to its antigen, or the antibody cannot penetrate through the tissue to reach the release sites of the IHCs. Moreover, vesicle labeling also failed when the organ of Corti was incubated with collagenase to clean the preparations from connective tissue prior to antibody application (25 µg per ml in calcium HEPES-HBSS for 5 minutes at 37°C). The correct function of the anti-otoferlin antibodies was tested with immunostainings of IHCs (with permeabilization) (see Appendix Figure A 9).

Table 1: Fluorescent dyes tested as potential vesicle recycling markers in IHCs.

Dye Name	Dye Type	Testing	Comments
FM1-43 (synaptogreen C4; Biotium) FM1-84 (synaptogreen C5; Biotium) FM4-64 (synaptored C2; Biotium)	"Classical" FM dyes	Cultured neurons, Organ of Corti (IHCs)	Synaptic vesicle recycling marker in conventional synapses (cultured neurons, NMJs). Permeate non-selective through ion channels at the apical pole of IHCs – disabling them for vesicle recycling studies as on conventional synapses.
AM1-43 (Biotium) FM4-64FX (Invitrogen)	Fixable analogs of "classical" FM dyes	Cultured neurons, Organ of Corti (IHCs)	Larger in size compared to the "classical" analogs – nevertheless penetrating into the IHCs.
FM3-25 (synaptogreen C18; Biotium)	Large FM dye	Cultured neurons, Organ of Corti (IHCs)	Labels the plasma membrane of cultured neurons, however it is not taken up into small synaptic vesicles during stimulation. Organ of Corti showed no response to bath application, leaving all membranes mostly unlabeled.
Dodecanoyl fluorescein	Fluorescent lipid-like molecule	Cultured neurons, Organ of Corti (IHCs)	Shows identical results on hippocampal cultured neurons as FM dyes, with a synaptic-like pattern after stimulation. Staining behavior on IHCs looks alike to that of FM dyes, indicating its permeation through channels.
DiO	(Dialkyl-) Carbocyanine family	Cultured neurons	Highly lipophilic and non-solvent in water, leading to its precipitation when added to the aqueous buffer.
Calcein (Invitrogen)	Polyanionic fluorescein derivative	Organ of Corti (IHCs)	Shows no permeation through ion channels or flipping in the membrane of IHCs and thus can be used as a fluid phase marker.
Dextran fluorescein 3000 MW	Labeled dextran	Cultured neurons, Organ of Corti (IHCs)	This small inert fluid phase marker is unable to enter the IHCs through ion channels and seems to be endocytosed.
Otoferlin antibodies (Synaptic Systems)	Polyclonal antibodies	Organ of Corti (IHCs)	The antibody functions well in immunostainings (see appendix). Live-labeling needs further testing.

Up to now live-imaging of vesicle recycling in IHCs showed limited success. In summary, first, the classical synaptic activity reporter dyes, like FM1-43 label the IHCs by a non-selective entry through ion channels at the apical pole. Second, the antibody-based live-labeling approach as used for vesicle labeling in vivo in conventional synapses showed no results of any antibody uptake into vesicles. Third, some other dyes like calcein and the 3000 Dalton dextran fluorescein are promising in using them as recycling markers in IHCs. However, they need further testing since the labeling efficiency in the first tests was very low. Both calcein and dextran are described as fluid phase markers; their minor uptake into organelles may be due to their weak binding affinity to membranes or lipids. Thus, the incorporation into endocytic organelles is less effective than in the case of FM dyes or antibodies, which present direct molecule-lipid or protein-protein interactions, respectively, making them relatively difficult to use.

3.2.2   Ultrastructural Analysis of Recycling Organelles in Inner Hair Cells

Regarding the results of FM dye application on IHCs, one could conclude that FM dyes are not applicable for investigating vesicle recycling in IHCs. However, while the FM dyes permeate into IHCs through non-selective channels, they may also be taken up into organelles via endocytic processes. This plausible hypothesis was tested by incubating the IHCs with the styryl dye FM1-43 followed by its photo-oxidation and electron microscopy, as performed on hippocampal cultured neurons (Figure 3.16) (Rizzoli and Betz, 2004; Denker et al., 2009). The photo-oxidation technique allowed me to localize and discern the endocytosed labeled organelles from the background and from non-recycled objects. Moreover, it enabled me to perform the first morphological characterization of vesicle recycling in IHCs. Thus, I can describe where vesicle retrieval is located and what type of organelles participate in this process.

The organ of Corti was pre-incubated in standard buffer at physiological temperature for 5 minutes, incubated for ~60 seconds in FM1-43 (5 μM in the appropriate buffer, see below), and fixed with ice-cold glutaraldehyde (2.5%). The preparations were then quenched and prepared for the FM photo-oxidation process (see Methods).

Subsequently the preparations were continuously illuminated in presence of DAB which resulted in photobleaching of the FM dye, while at the same time it generated reactive

oxygen species that precipitated (through oxidation) the DAB in the close proximity of the FM dye. As the FM dye was present in the entire hair cell (shown above) one could assume that the endocytosed FM dye will be indistinguishable from the background precipitate (cryptozoic FM dye). However, the DAB precipitation within the cytosol of the IHC resulted in an almost homogeneously dispersed precipitate, as it was not captured in small membrane-enclosed organelles. The organelles with endocytosed FM dye appeared darker than the background, as the DAB precipitate is retained and concentrated inside the membrane-enclosed organelles. Thus, the entire hair cell became a bit darker than the neighboring tissue (due to the dispersed precipitate) and contained dark (black) structures in the cytoplasm, representing the organelles that took up the FM dye during incubation. In conclusion, the cytosolic FM dye did not cause difficulties for the electron microscopy analysis, as it was the case for the recycling investigations *in vivo*.

For the morphological characterization of the membrane recycling pathway I investigated membrane retrieval at different time intervals after labeling (similar to the morphological characterization of the conventional synapses in Figure 3.16). The different time intervals allowed for the direct comparison of the morphology of the recently endocytosed organelles at various steps in the recycling pathway. The different steps were investigated under zero calcium and high potassium stimulation conditions. FM incubation was performed as described above, for approximately 60 seconds at physiological temperature in standard or high potassium HEPES-HBSS, respectively. The organ of Corti was then either fixed immediately to stop endocytosis ("zero calcium" and "high potassium/ stimulation"), or the high potassium stimulation preparations were subsequently washed rapidly and left at rest for different time intervals of 5 and 30 minutes (under physiological temperature and constant exchange of the buffer).

Afterwards, the IHCs were photo-oxidized and processed for electron microscopy. Sections of 100 nm were cut longitudinally and imaged using a transmission electron microscope. The positive photo-oxidized structures (organelles that took up FM dye during incubation) for the "zero calcium" IHCs are shown in Figure 3.22, and for the "stimulated" IHCs are shown in Figure 3.23. Both figures show typical electron micrographs of 6 different IHCs, at the apical pole (at the cuticular plate), the nucleus-area and the basal pole.

In both conditions, labeled recently endocytosed organelles were observed at the apical part, with small vesicle-like and larger endosomal-like organelles (upper panel). At the baso-lateral side positive-oxidized tubules were visible (middle panel). A visual observation gave the impression that the stimulation condition (Figure 3.23) had more vesicle-like and larger endosomal-like organelles in the basal part compared to the zero calcium IHC (lower panel). Note that the vesicles in the efferent synapses were not positively oxidized under zero calcium conditions, but showed dye uptake in the stimulated preparations (Figure 3.23), indicating the correct function of the buffers.

The electron micrographs in Figure 3.24 and Figure 3.25 show the "5 minutes" and "30 minutes" IHCs, respectively. Endocytosed FM dye was still located at the apical part as it was the case for the "zero calcium" and "stimulated" IHCs. The most obvious disparity between the resting IHCs (5 and 30 minutes rest) and the zero calcium/ stimulated IHCs was the absence of the tubular-like structures at the baso-lateral side. Instead of these elongated organelles high frequencies of small vesicle-like organelles were present, suggesting that the large tubules disintegrated into small organelles. At the basal part of the IHCs almost only small vesicle-like organelles and fewer larger endosomal-like structures were observed, with more numerous small organelles, compared to the immediately fixed stimulation conditions. This suggests an origin of the vesicle-like organelles from the larger endosomal-like structures. The efferent synapses of both conditions contained labeled vesicles as well.

Figure 3.22: FM photo-oxidation of IHCs. Typical electron micrographs of 6 different IHCs labeled with FM1-43 under zero calcium conditions showing labeled (photo-oxidized) round (red arrowheads) and tubular-like organelles (red arrows). Upper panel: micrographs of the apical pole of IHCs (SC: stereocilia; CP: cuticular plate). Middle panel: micrographs taken at the baso-lateral side of IHCs (at nucleus (N)). Lower panel: micrographs of the basal pole of IHCs (ES: efferent synapse). Mitochondria are indicated by yellow arrowheads. Scale bar: 200nm.

Figure 3.23: FM photo-oxidation of IHCs. Typical electron micrographs of 6 different IHCs labeled with FM1-43 under high potassium stimulation. The micrographs show labeled (photo-oxidized) round (red arrowheads) and tubular-like organelles (red arrows). Note that here also the basal pole is characterized by labeled organelles. Upper panel: micrographs of the apical pole of IHCs (SC: stereocilia; CP: cuticular plate). Middle panel: micrographs taken at the baso-lateral side of IHCs (at the nucleus (N)). Lower panel: micrographs of the basal pole of IHCs (ES: efferent synapse; white arrowhead indicates labeled efferent synaptic vesicles). Mitochondria are indicated by yellow arrowheads. Scale bar: 200nm.
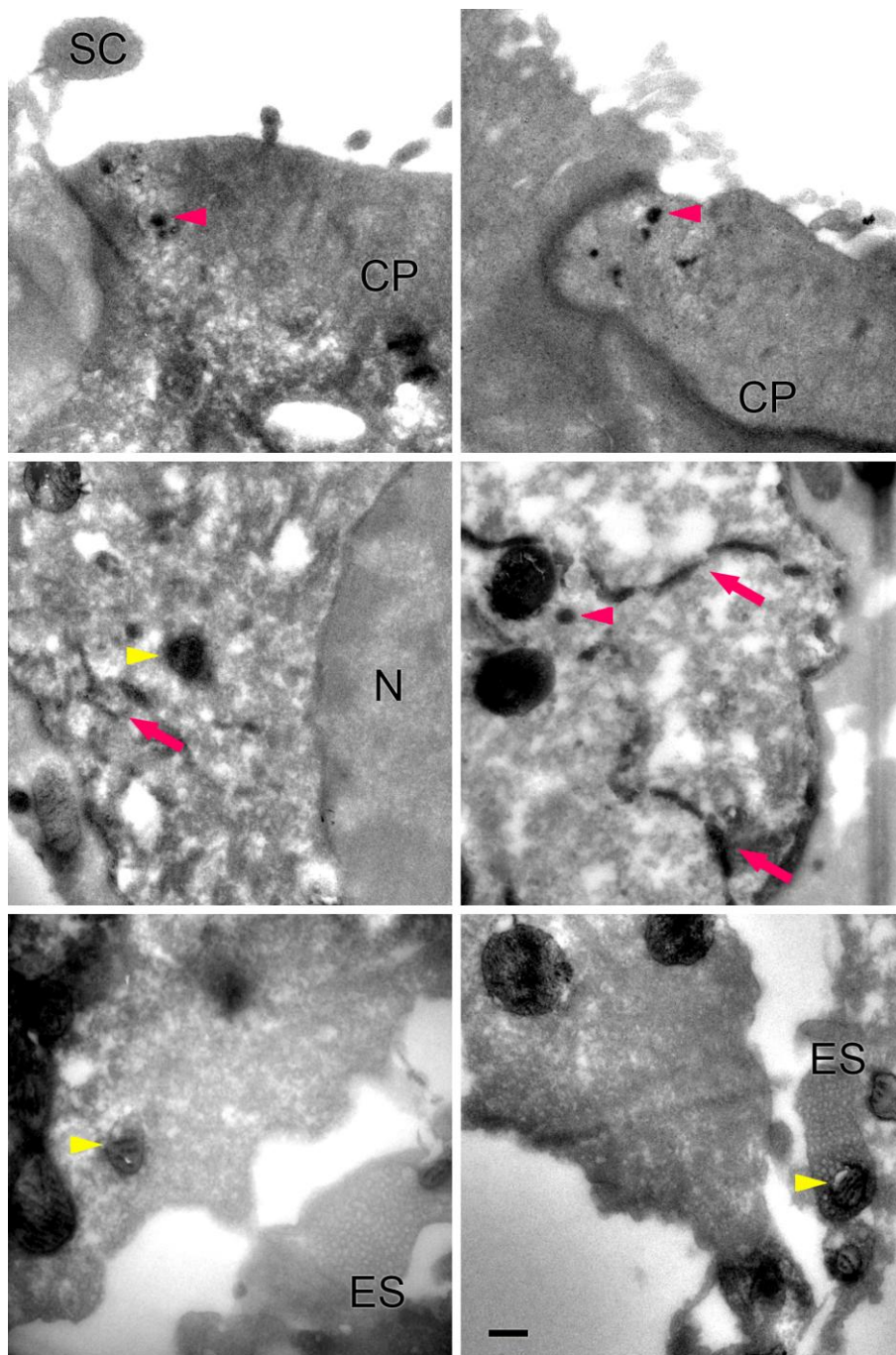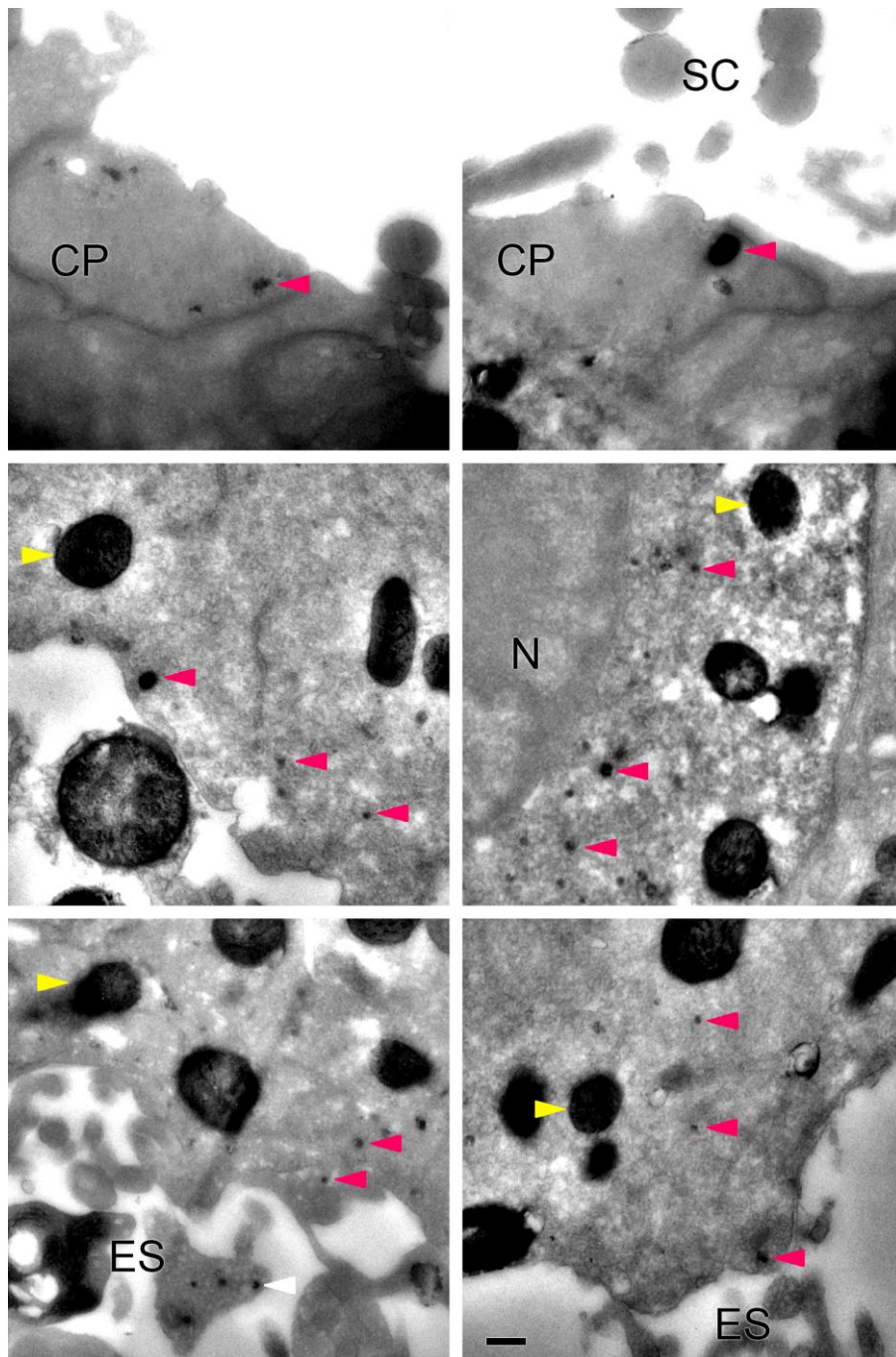
Figure 3.24: FM photo-oxidation of IHCs. Typical electron micrographs of 6 different IHCs labeled with FM1-43 under high potassium stimulation and left for rest additional 5 minutes. The micrographs show only labeled (photo-oxidized) round organelles (red arrowheads). Note that labeled tubular organelles are absent. Upper panel: micrographs of the apical pole of IHCs (SC: stereocilia; CP: cuticular plate). Middle panel: micrographs taken at the baso-lateral side of IHCs (at the nucleus (N)). Lower panel: micrographs of the basal pole of IHCs (ES: efferent synapse; white arrowhead indicates labeled efferent synaptic vesicles). Mitochondria are indicated by yellow arrowheads. Scale bar: 200nm.
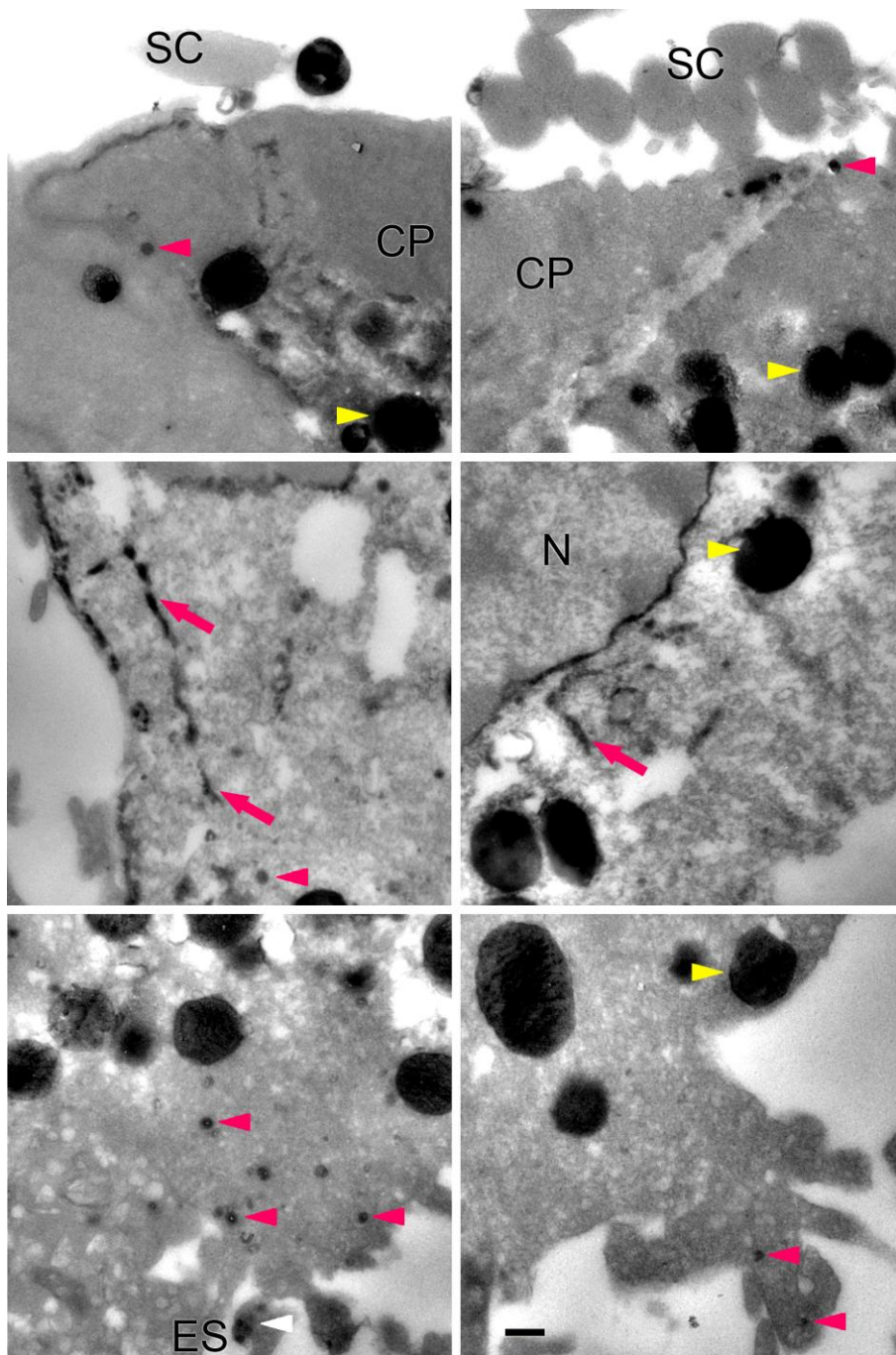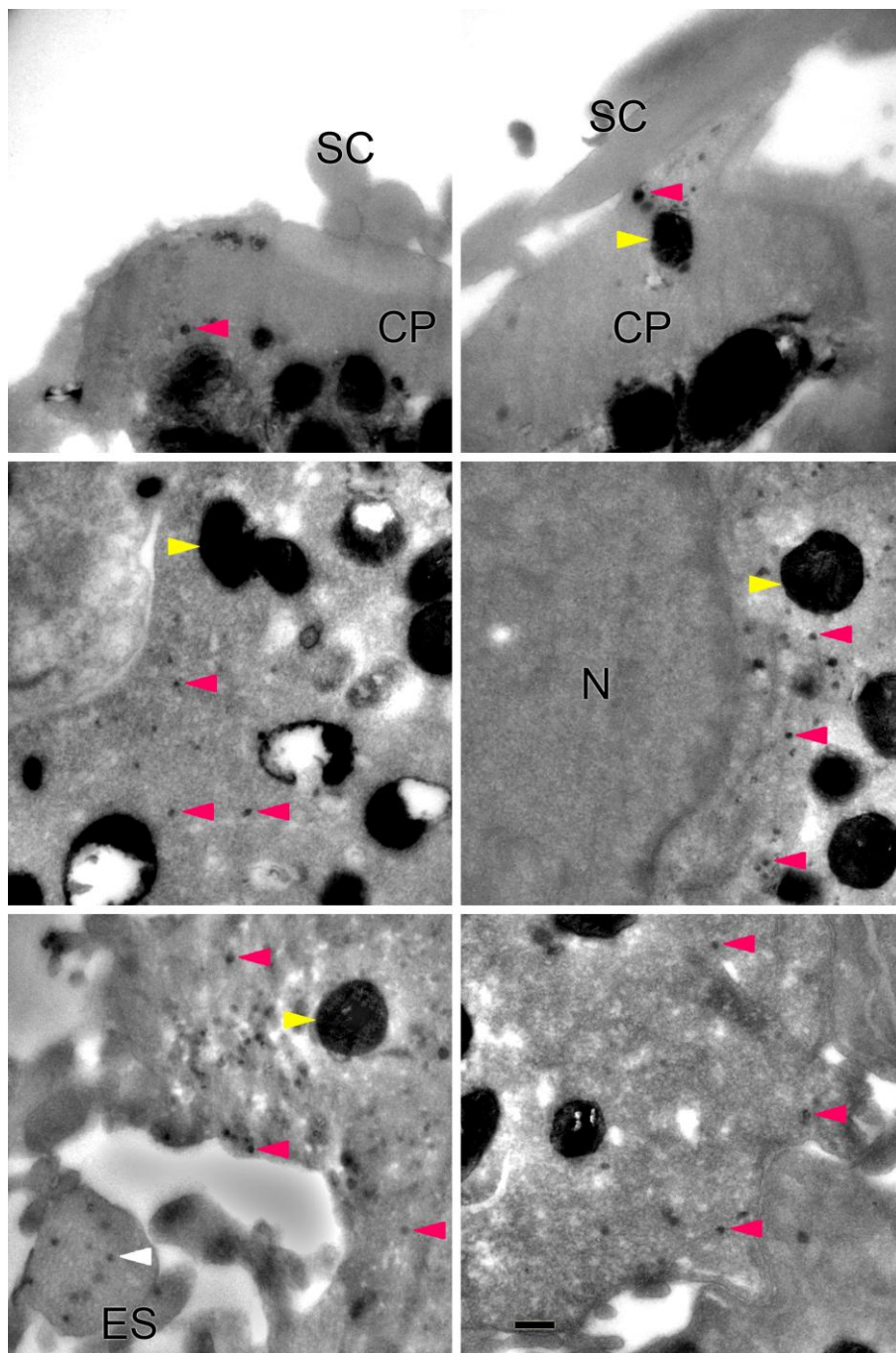
Figure 3.25: FM photo-oxidation of IHCs. Typical electron micrographs of 6 different IHCs labeled with FM1-43 under high potassium stimulation and left for rest additional 30 minutes. The micrographs show labeled (photo-oxidized) round organelles (red arrowheads). Upper panel: micrographs of the apical pole of IHCs (SC: stereocilia; CP: cuticular plate). Middle panel: micrographs taken at the baso-lateral side of IHCs (at the nucleus (N)). Lower panel: micrographs of the basal pole of IHCs (ES: efferent synapse; white arrowhead indicates labeled efferent synaptic vesicles). Mitochondria are indicated by yellow arrowheads. Scale bar: 200nm.

3.2.3 Three-Dimensional Reconstruction of Inner Hair Cells Reveals the Vesicle Recycling Pathway

The analysis of typical electron micrographs from the different time intervals (zero calcium, high potassium stimulation, 5 minutes, 30 minutes) allow a rather vague interpretation of the morphology of the vesicle recycling process in IHCs. Thus, I reconstructed three-dimensional images of the different treated IHCs to better describe the morphological nature of the organelles that are involved in the vesicle retrieval process.

As a first step I cut serial cross-sections of 100 nm from the organ of Corti and imaged the IHCs using a transmission electron microscope. The individual micrographs of a single serial section were afterwards merged to obtain full image of the entire IHC. All merged serial sections were aligned using Photoshop. See Figure 3.26 for aligned serial sections of the "zero calcium" (A) and "stimulated" (B) IHCs and Figure 3.27 for "5 minutes" (A) and "30 minutes" (B) IHCs. The shape of the IHCs is almost identical for all conditions (bottle-like structure). The cuticular plate is visible as a dense area at the apical tip of the IHCs (from where the stereocilia emerge). Additionally, in all sections mitochondria are visible as black spots (note that the photo-oxidized darkening of the mitochondria was not related to vesicle recycling (Grabenbauer et al., 2005)). The nuclei are visible in each single section in the middle of the IHCs.
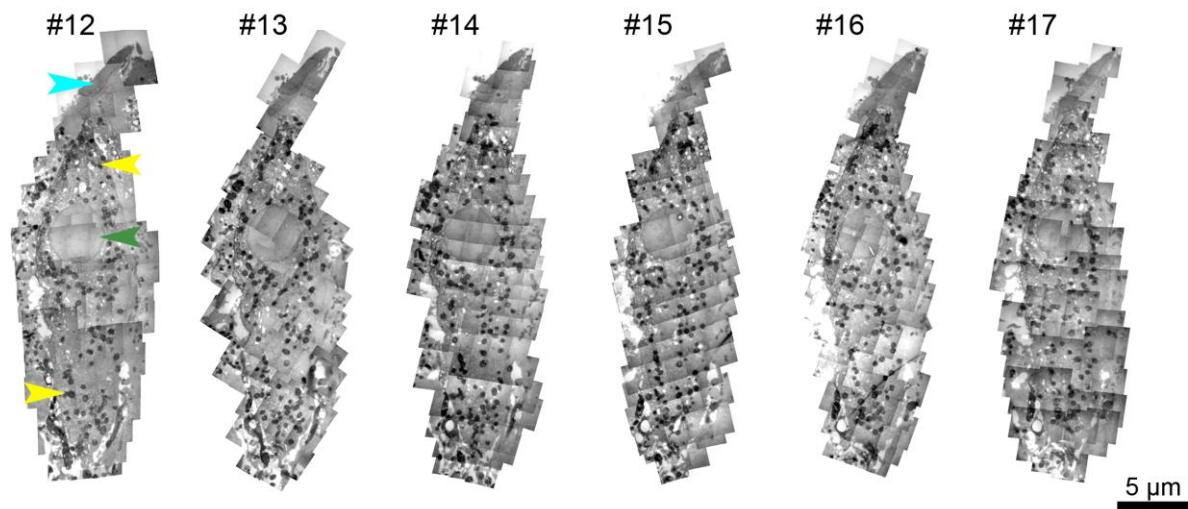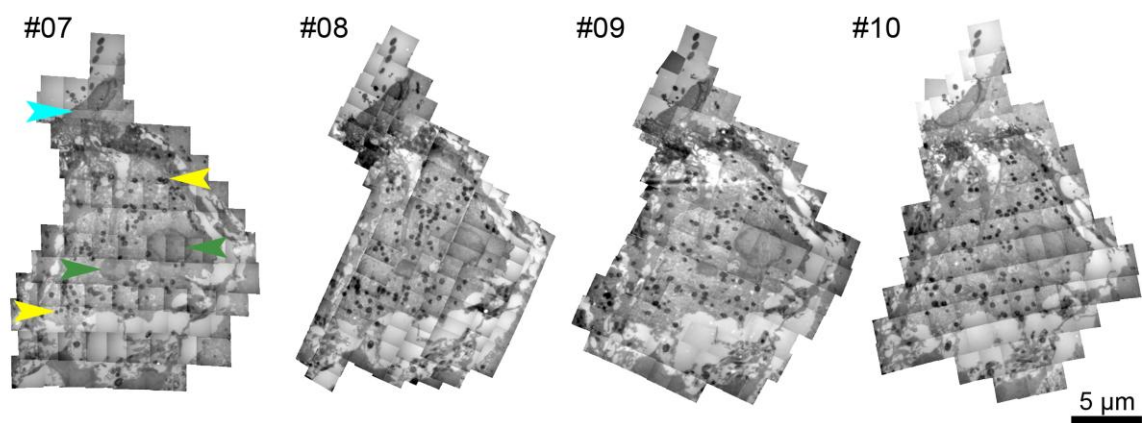
Figure 3.26: Three-dimensional processing of IHC sections. Aligned IHC serial cross-sections build from merged individual electron micrographs (# indicate the section number). Yellow arrowheads indicate the darkened mitochondria, cyan arrowheads the cuticular plate, and green arrowheads indicate the nucleus. (A) Zero calcium condition. (B) High potassium stimulation. Note that the serial sections of the "stimulated" preparation (B) show two adjoining hair cells (the nucleus of the left cell disappears with deeper cutting).
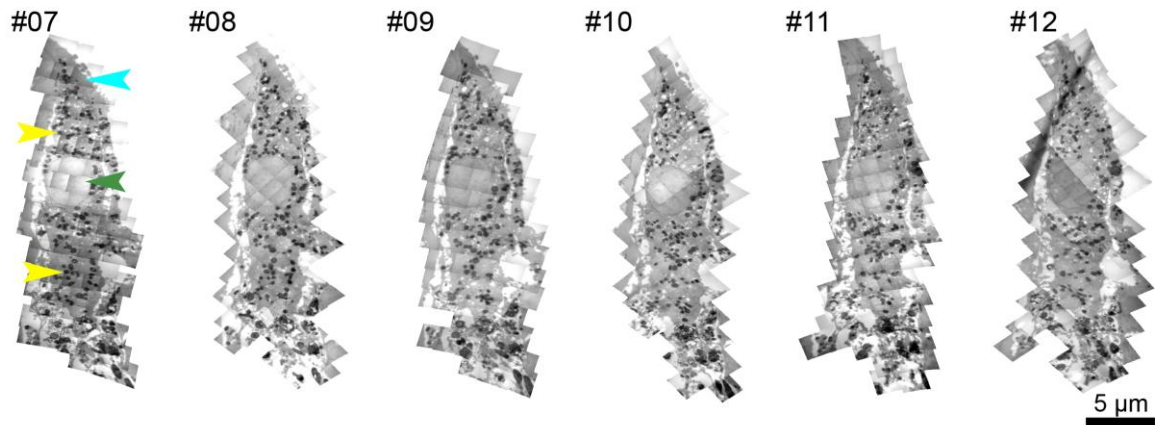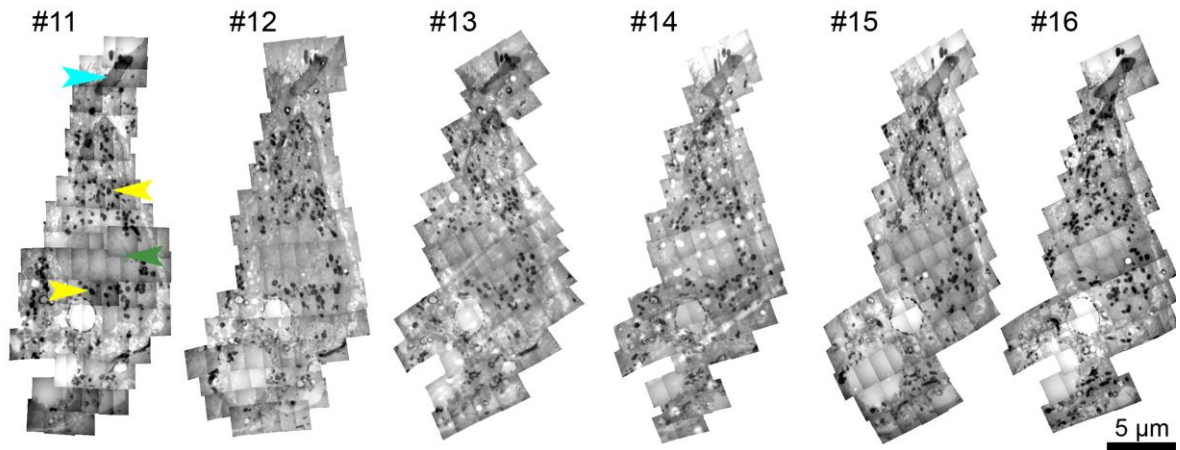
Figure 3.27: Three-dimensional processing of IHC sections. Aligned IHC serial cross-sections build from merged individual electron micrographs (# indicate the section number). Yellow arrowheads indicate the darkened mitochondria, cyan arrowheads the cuticular plate, and green arrowheads indicate the nucleus. (A) Stimulated IHC after 5 minutes rest. (B) Stimulated IHC after 30 minutes rest.

In the further processing I used the serial sections to generate three-dimensional reconstructions of the individual IHCs. Cochlear IHCs of the mouse typically have a diameter of around 5-10 μm and a length between approximately 30-40 μm. These dimensions made it difficult to reconstruct entire IHCs and thus the reconstruction was limited to around 20±1 sections per condition (resulting already in approximately 2000 electron micrographs per IHC). With a section depth of 100 nm in total, more than 2 μm along the longitudinal axis of

one hair cell was reconstructed (the true thickness of a single section was slightly bigger than 100 nm, as the preparations shrink by approximately 25% during electron microscopy processing (Gaffield et al., 2006)). For the three-dimensional reconstruction the plasma membrane, the nucleus, the cuticular plate, the active zones, and the labeled organelles were manually redrawn with Photoshop and saved as single images (see Methods for example images of redrawn structures). The IHCs were then reconstructed from these images assuming a thickness of 100 nm for each section, using routines written in Matlab.

Figure 3.28: Three-dimensional reconstruction of the FM1-43 labeled and photo-oxidized zero calcium IHC. The plasma membrane is represented in yellow, the cuticular plate in cyan, the nucleus in green, the labeled organelles in purple, and the active zone in red (red arrowhead indicates the location of the ribbon). The reconstruction is made of 21 serial cross-sections, each with a section depth of 100 nm.

The three-dimensional reconstructions of the IHCs under zero calcium and stimulation conditions (Figure 3.28 and Figure 3.29, respectively) displayed an involvement of large

cisternae (and not tubules) in the membrane recycling process. Their primary location was essentially at the baso-lateral site. Interestingly, as already observed from single electron micrographs they disappeared in the IHCs with the resting periods (compare Figure 3.30 (5 minutes) and Figure 3.31 (30 minutes) with Figure 3.28). The reconstructed stimulation IHC, as observed before, showed a more numerous appearance of round organelles at the basal part, compared to the zero calcium IHC. All reconstructed IHCs showed labeled organelles at the cuticular plate (apex). Nevertheless, in all reconstructions the major membrane labeling was located below the nucleus, suggesting that the apical membrane retrieval might be just a minor recycling route. Interestingly, by comparing the control (zero calcium) and the 5 minutes conditions by eye the baso-lateral sites were characterized in the former by cisternae and in the latter by high frequencies of small labeled organelles. This indicates that a morphological change of the organelles has occurred. The large elongated cisternae likely disintegrated into round vesicle-like organelles. A morphological analysis of the reconstructions is presented below.
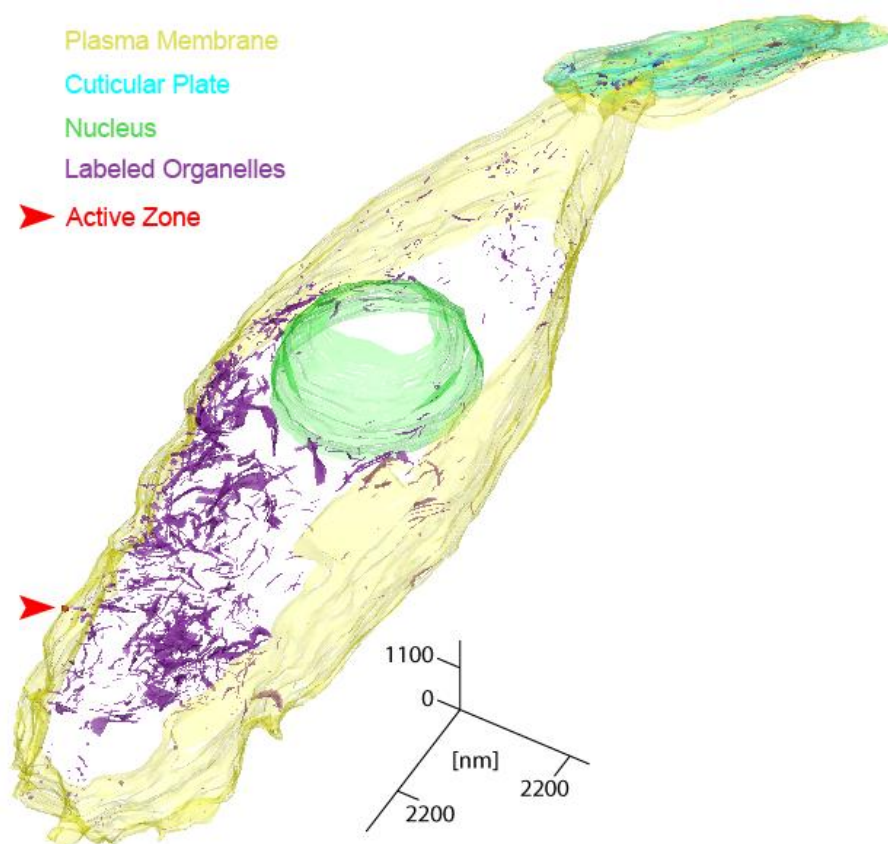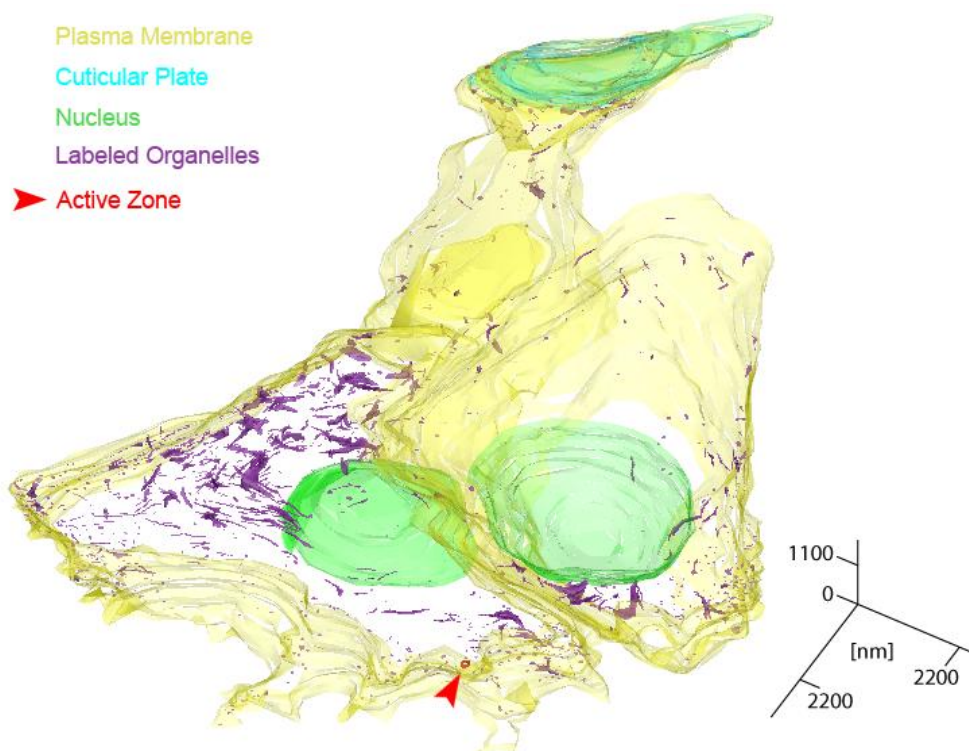

Figure 3.29: Three-dimensional reconstruction of the FM1-43 labeled and photo-oxidized high potassium stimulation IHC. The plasma membrane is represented in yellow, the cuticular plate in cyan, the nucleus in green, the labeled organelles in purple, and the active

zone in red (red arrowhead indicates the location of the ribbon). The reconstruction is made of 19 serial cross-sections, each with a section depth of 100 nm. Note that here two neighboring IHCs are partially reconstructed.
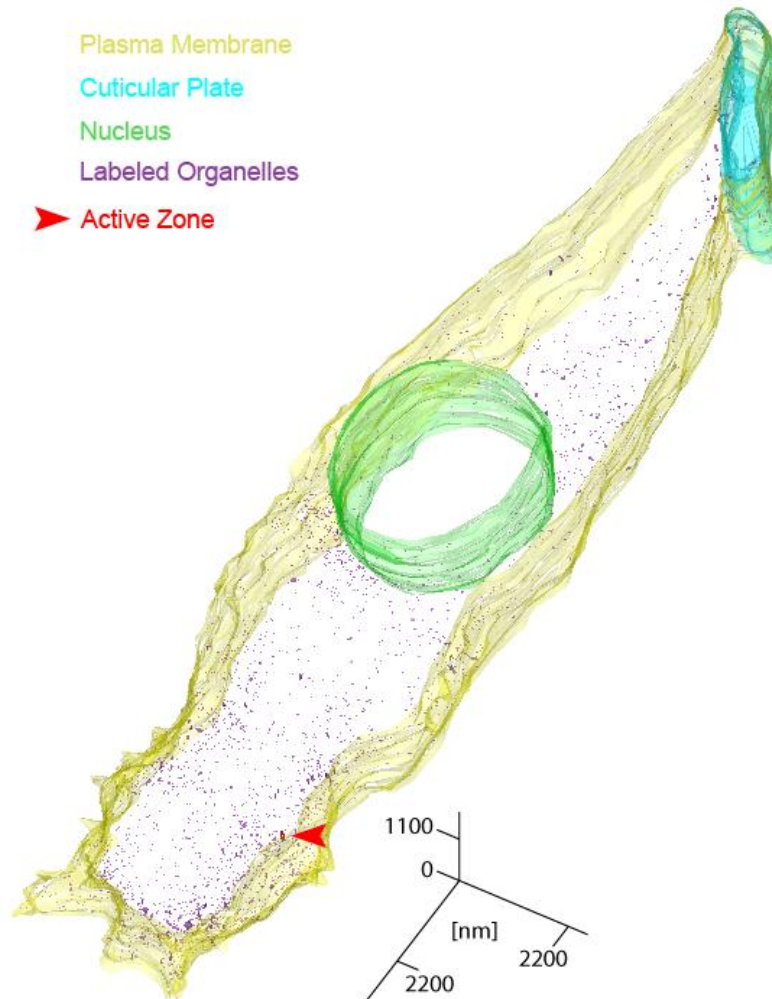
Figure 3.30: Three-dimensional reconstruction of the FM1-43 labeled and photo-oxidized high potassium stimulation and 5 minutes rest IHC. The plasma membrane is represented in yellow, the cuticular plate in cyan, the nucleus in green, the labeled organelles in purple, and the active zone in red (red arrowhead indicates the location of the ribbon). The reconstruction is made of 21 serial cross-sections, each with a section depth of 100 nm.
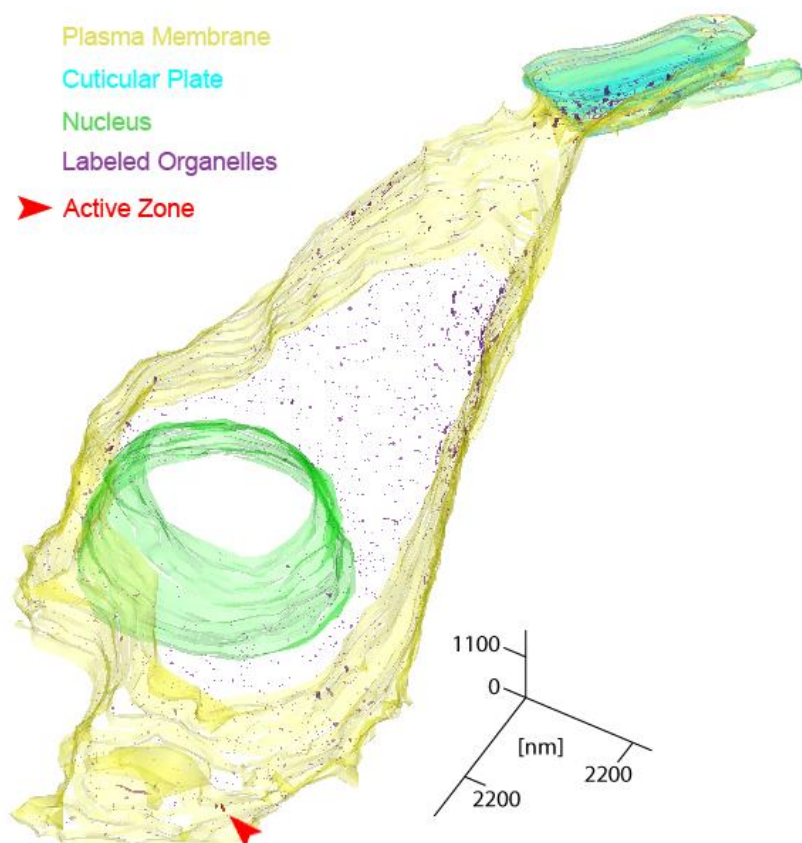
Figure 3.31: Three-dimensional reconstruction of the FM1-43 labeled and photo-oxidized high potassium stimulation and 30 minutes rest IHC. The plasma membrane is represented in yellow, the cuticular plate in cyan, the nucleus in green, the labeled organelles in purple, and the active zone in red (red arrowhead indicates the location of the ribbon). The reconstruction is made of 21 serial cross-sections, each with a section depth of 100 nm.

3.2.4 Morphological Analysis of Recycling Organelles in Inner Hair Cells

The three-dimensional reconstructions revealed already much information about the morphology of the vesicle recycling pathway in IHCs. However, for a more detailed view on the morphological changes of the endocytosed organelles I performed a morphological analysis of the recycling organelles. The analysis should address the questions (1) of what nature are the recycling organelles and (2) where are the different organelles located? Thus, I used different tools to analyze the distribution and the size of the organelles.

In a first step the positive photo-oxidized organelles were counted to describe the average density. The IHC at 5 minutes showed approximately twice as many labeled organelles (on average ~4 organelles per μm^2) compared to the zero calcium and the stimulated IHCs (2.1

and 1.6 organelles per μm^2, respectively; Figure 3.32). However, after 30 minutes rest fewer labeled organelles were present compared to the 5 minutes time point (on average around 2.6 organelles per μm^2). One can infer from the density increase after 5 minutes and its decrease after 30 minutes that the membrane was retrieved via large infoldings (large membranes exhibit lower organelle densities), from which then small vesicles bud off, which results in the higher density of labeled organelles at 5 minutes. These vesicles could then participate again in neurotransmitter release and thus lose the FM dye, which is shown by the decrease of labeled organelles after 30 minutes.
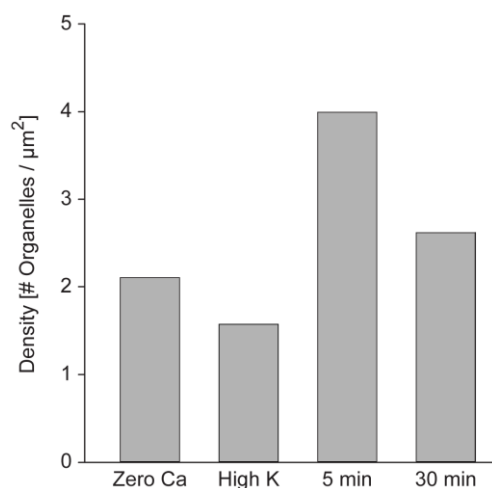
Figure 3.32: Density of labeled organelles. Shown are the numbers of organelles present per μm^2 for the four three-dimensional reconstructed IHCs.

Furthermore, I analyzed the size and shape of the labeled organelles. Two histograms present the results. The first illustrates the size of the organelles where the fraction of labeled organelles was plotted against the area they occupied (Area histogram, Figure 3.33). The second shows the fraction of labeled organelles, which was plotted against the axis ratio (major axis versus the minor axis of the organelles; Ratio histogram, Figure 3.34). The histograms reflect clearly the observed impressions from the three-dimensional reconstructions above. Before dye wash-off (+/- stimulation), most of the labeled organelles occupied large areas (Figure 3.33) and were elongated in shape (Figure 3.34), while at 5 and 30 minutes after stimulation the organelles were small in size (Figure 3.33) and almost round in shape (Figure 3.34).
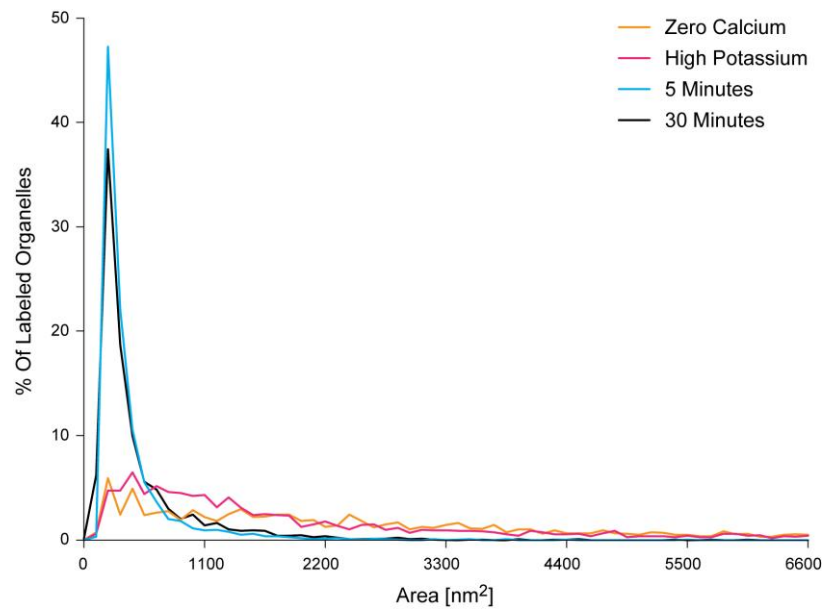
Figure 3.33: Area histograms of labeled organelles. The histograms show the area the organelles occupied in the different IHCs. The organelles in the zero calcium (orange) and the high potassium stimulation (red) IHCs are larger in size than the organelles of the 5 (blue) and 30 (black) minutes rest IHCs.
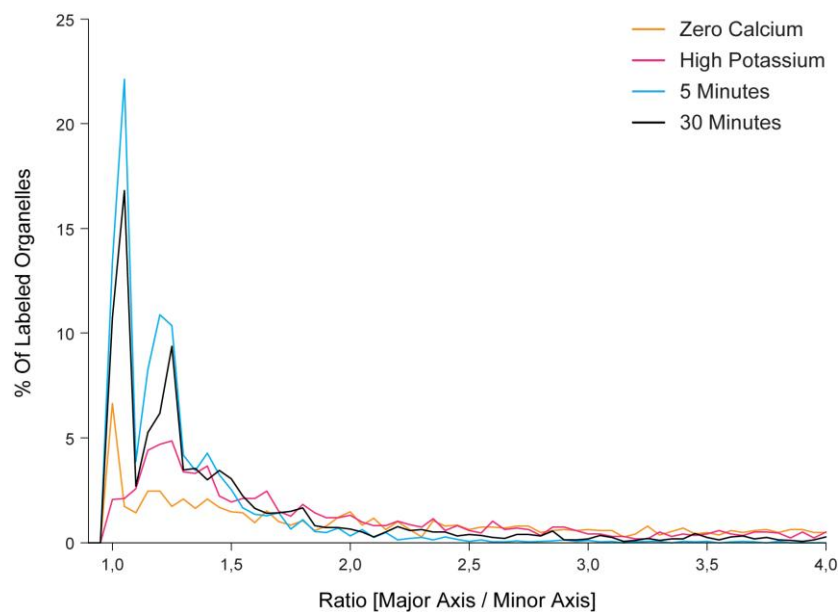
Figure 3.34: Axis ratio histograms of labeled organelles. The ratio of the major axis against the minor axis of labeled organelles was calculated and plotted as the fraction of labeled organelles. The axis ratio depicts the nature of the organelles, with spherical objects having a ratio of one while elongated structures (with a larger major axis) exhibit higher ratios. The organelles of the zero calcium IHC (orange) and the stimulated IHC (high potassium, red) are characterized by higher axis ratio values compared to the 5 and 30-minute time points (blue and black, respectively).

94

The shape of the organelles became also clear when analyzing scatterplots, where the values from the major axis and the minor axis of the organelles were presented (Figure 3.35). Both rested IHCs (5 minutes: blue, 30 minutes: black) showed clustered values with primarily low major and minor axis values, indicating that most of the organelles were small and round shaped. However, the plots of the zero calcium and the stimulated IHCs showed both a broad value distribution, which verified that many types of organelles were present (large and round, large and elliptic, elongated).
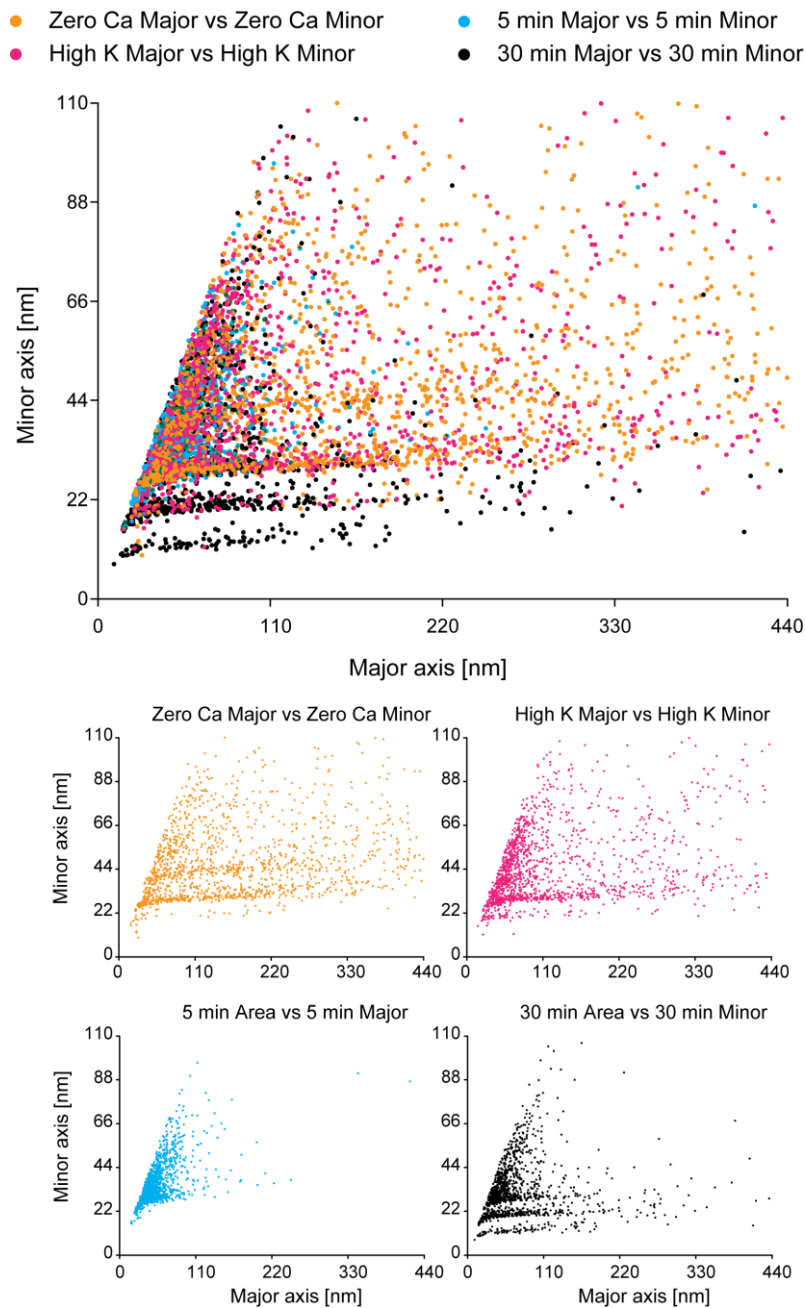
Figure 3.35: Scatterplots of major versus minor axis values of labeled organelles. The scatterplots present the nature of the organelles in the different treated IHCs. The "zero calcium" (orange) and the "high potassium" IHCs (red) had broad variations of organelles, with high values for the major and the minor axis. The "5 minutes" (blue) and the "30 minutes" (black) IHCs had organelles with smaller major and minor axis values, indicating small and round organelles.

A second scatterplot analysis represents the area an organelle occupied related to the previously calculated ratio (major axis vs. minor axis) (Figure 3.36). The graphical illustration clearly showed the characteristic morphology of the labeled organelles at the different time points in the recycling pathway. The zero calcium and high potassium stimulated IHCs contained lots of large elongated organelles, as could be seen from the correlation of high area and ratio values. In contrast the 5 minutes and 30 minutes time points were characterized by only small organelles, as large area and ratio values were almost absent. Only few elongated objects were present after 30 minutes. However, they were still smaller in size compared to the organelles from the zero calcium and the stimulation IHCs.

Taken together, the non-stimulated and the stimulated IHCs were both characterized by large elongated and also round organelles, occupying large areas. In contrast, the IHCs at 5 and 30 minutes after stimulation can be described by mostly small spherical organelles.
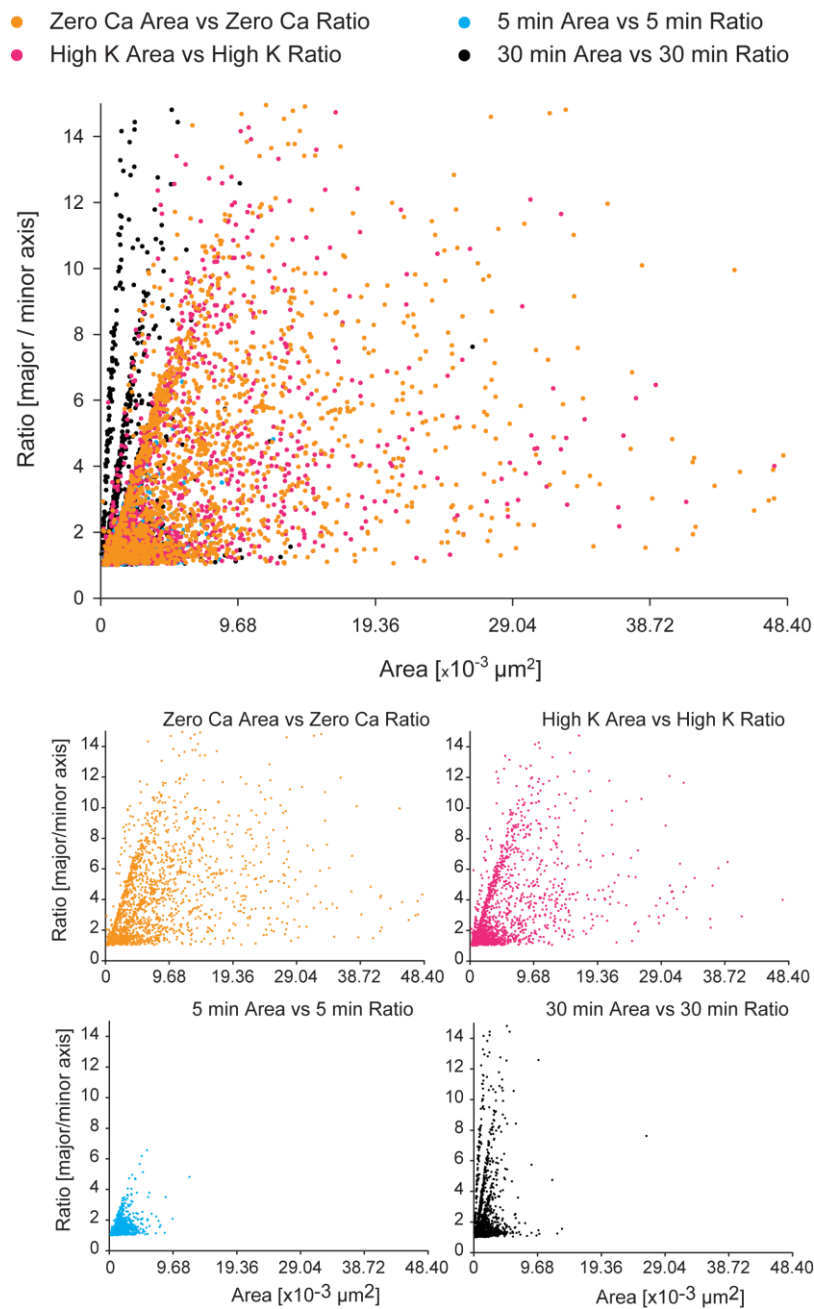
Figure 3.36: Scatterplots of the area occupied by the organelles versus their axis ratio. The scatterplot shows that the "5 minutes" IHC (blue) had small and round organelles (low area values correlate with low ratio values), similar to the "30 minutes" IHC (black), which had some more elongated tubular structures (low area values correlate with some higher ratio values). The "zero calcium" (orange) and "high potassium" (red) IHCs show both high area values correlating with high ratio values, reflecting the existence of large cisternal organelles.

97

3.2.5 Morphological Separation of Labeled Organelles

In the next step the organelles were separated by their morphological nature to demonstrate and compare their appearance at the different steps in the recycling pathway. Thus, the organelles were separated into classes like the following: "elongated organelles" were characterized by a major axis that was two times larger (or more) than the minor axis; "larger elliptic organelles" had a ratio between 1.2 and 2; "larger round organelles" had a ratio of < 1.2; "small vesicles" are characterized by a ratio of < 1.2 and a size of < 60 nm. The characteristic organelle classes were plotted as the fraction of all labeled organelles (Figure 3.37). The non-stimulated IHC contained mainly elongated organelles (> 95% of the occupied area, gray) and a few larger elliptic organelles (~3%, green). The fractions of small vesicle-like organelles and larger round organelles were very low in relation to the area they occupied (both ~0.4%). A similar distribution of the organelle classes was found in the stimulated IHC. While large elongated organelles were predominant (~88%, Figure 3.37 B), a higher fraction of large elliptic organelles (~7%) and small vesicle-like organelles (~1-2%) were present. Importantly, the stimulated IHC had the highest proportion of large round organelles (~2%, Figure 3.37 B). As shown before, the morphology separation pattern completely changed after 5 and 30 minutes rest. After 5 minute an almost negligible fraction of elongated organelles was present with less than 1% of all labeled organelles (Figure 3.37 B), and only few elliptic organelles existed (< 3%). Interestingly, the small vesicle-like organelles accounted for the highest fraction of labeled organelles with around 95%. After 30 minutes the distribution was similar to the 5 minutes time point.
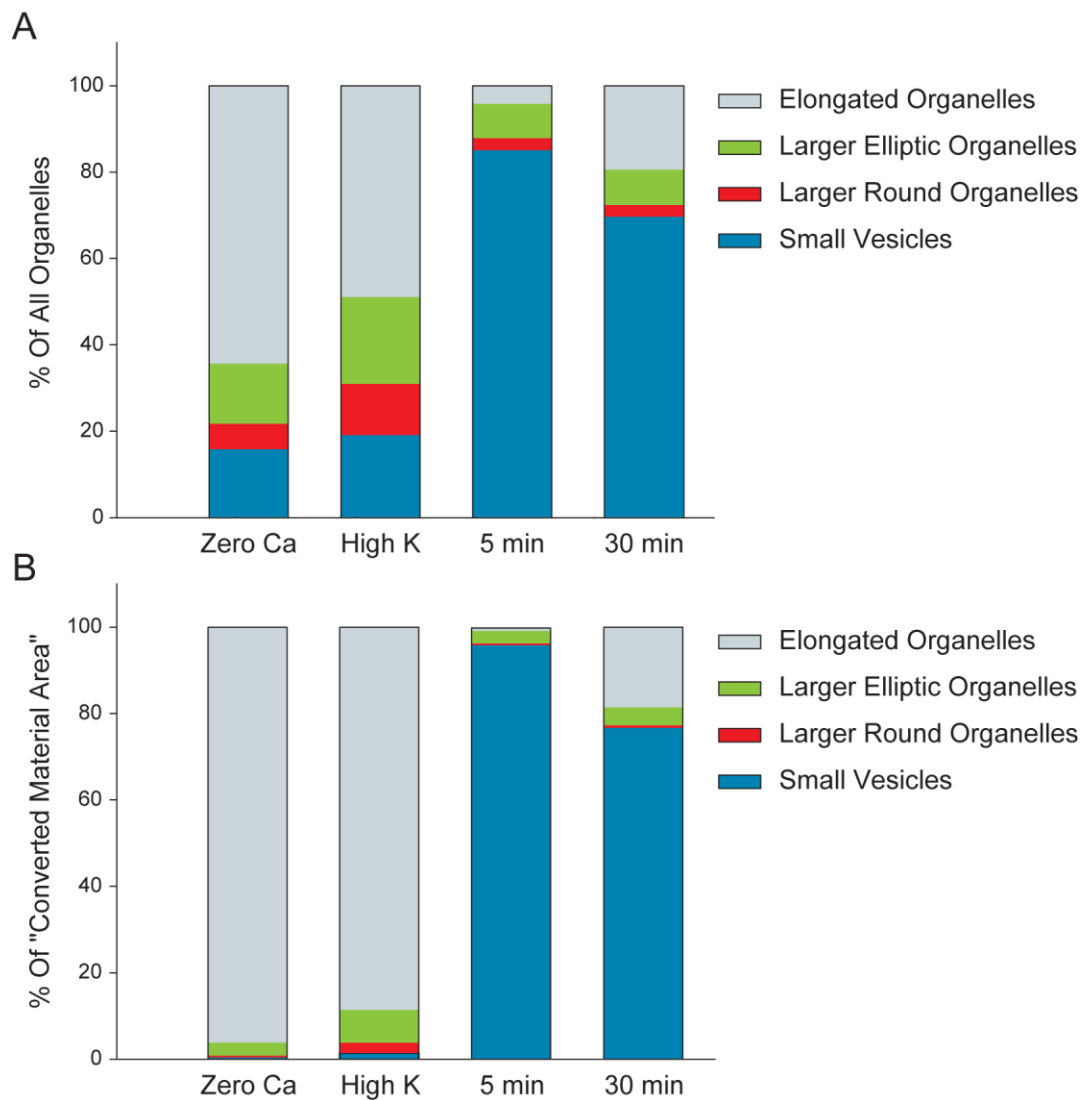
Figure 3.37: Organelle morphology separation. (A and B) The separation was performed related to the classes of organelles in the different IHCs. The small vesicle-like organelles (blue) and the elongated organelles (grey) change their proportion in the recycling process. The fraction of larger elliptic organelles (green) was almost identical in all four IHCs. Larger round organelles (red) were most abundant in the high potassium IHC.

Furthermore, I specifically analyzed the localization of the organelle classes to make assumptions concerning their preferred areas. For this, the length of each entire IHC (apical to basal) was divided into sections of 1100 nm (Figure 3.38). Additionally, for each section the organelle morphology was separated, as presented above, to describe the distribution of the organelles in the respective segment of the cell. In the case of the zero calcium IHC the main position of the elongated organelles in the cell (the main organelle structure here) was between 8800 and 26400 nm, at the baso-lateral site. These areas were almost free of small

vesicles, which were only found at the basal pole, (last sections in Figure 3.38 A). The comparison with the stimulated IHC showed that with stimulation the proportion of larger round and elliptic organelles increased substantially at the basal release site, indicating a possible role for endosomal-like organelles in a basal recycling process (last three elements in Figure 3.38 B). The distribution of large elongated organelles was identical to the zero calcium condition. Both hair cells show vesicle-like structures at the apical part (each ~50% (first sections from left in Figure 3.38 A and B)). After 5 minutes rest the IHC contained almost only small vesicle-like organelles (Figure 3.38 C). Just the apical part was characterized by small, elliptic and a few elongated organelles. The organelle morphology separation after 30 minutes revealed identical results. Small vesicles dominated the middle segments and a small fraction of elongated organelles was present at the apical part (Figure 3.38 D; see also the three-dimensional reconstruction).
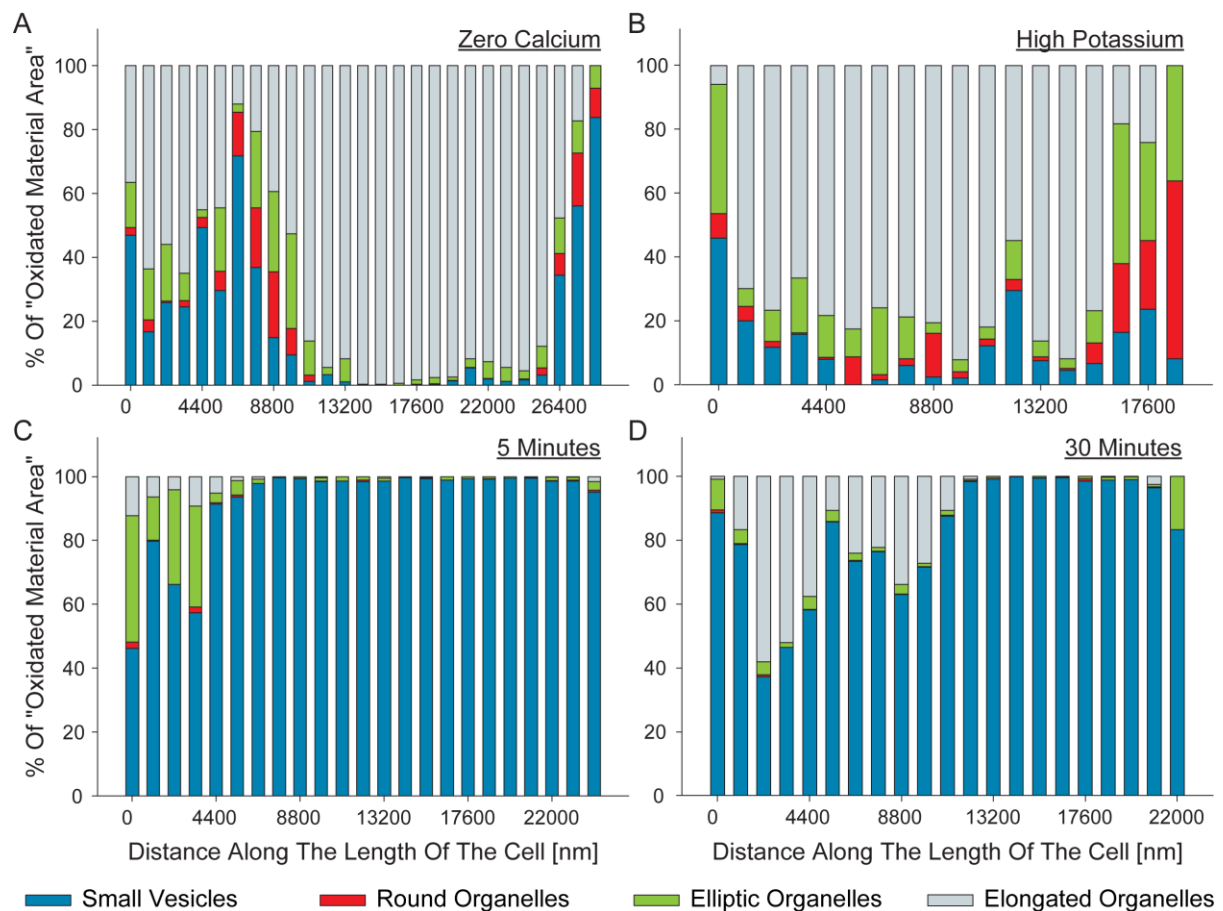
Figure 3.38: Organelle morphology separation along the cell. (A-D) IHCs were separated in 1100 nm sections and the organelle classes in each section were determined and corrected for the area the labeled organelles occupied. (A and B) Both the zero calcium and the high potassium IHCs were characterized by high fractions of elongated organelles (grey) at the baso-lateral side (middle sections). At these locations only small vesicles (blue) were abundant after 5 and 30 minutes (C and D). Note that the high potassium IHC (B) shows high fractions of larger round and eliptic organelles at the basal pole (red and green, respectively).

A less quantitative but more visual presentation about the morphological variability of the stimulated (high potassium) IHC is displayed in Figure 3.39. The projection of the serial sections shows color-coded organelles according to the ratio the individual organelle exhibits (see color scale at the bottom). It is clearly obvious that high fractions of larger round and elliptic organelles are present at the basal release site (compare Figure 3.38, red), indicating most likely endosomal-like organelles that are used in parallel to the cisternae for vesicle recycling upon stimulation.
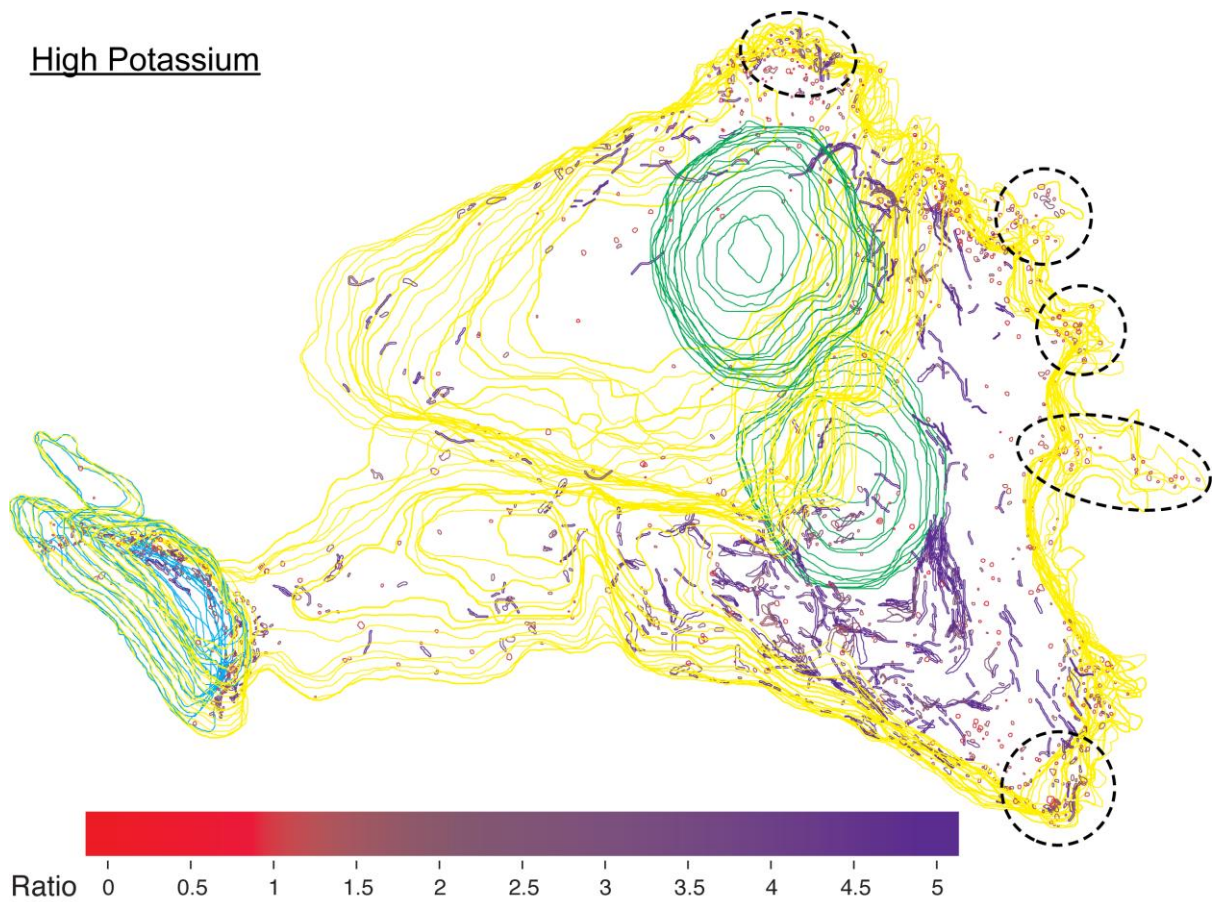
Figure 3.39: Axis ratio variability along the stimulated IHC. Serial section projection of the high potassium IHC illustrates the axis ratio variability of the organelles. High ratio organelles (elongated organelles) are presented in purple, low ratio organelles (round) are depicted in red (see ratio colorscale). Note that high fractions of larger round organelles can be seen at the basal pole (highlighted by dashed black circles), indicating endosomal intermediates in the recycling pathway upon stimulation.

4 Discussion and Conclusions

As reviewed in the Introduction of this work the steps of the vesicle cycle in conventional synapses are relatively well understood, although the general mobility of synaptic vesicles has so far only been studied using indirect measurements using sparse vesicle labeling (Gandhi and Stevens, 2003; Lemke and Klingauf, 2005; Zhang et al., 2009), indirect mobility measurements with FRAP (Kraszewski et al., 1995; Henkel et al., 1996b; Kraszewski et al., 1996; Gaffield et al., 2006) or correlation spectroscopy (Jordan et al., 2005; Shtrahman et al., 2005; Yeung et al., 2007). With these diffraction-limited imaging techniques only the averaged synaptic vesicle mobility was investigated resulting in insufficient vesicle behavior informations. In the present work I therefore studied specifically the mobility of single synaptic vesicles in living cultured neurons using high-resolution stimulated emission depletion fluorescence microscopy, as well as conventional microscopy techniques. STED microscopy allowed me to visualize moving single synaptic vesicles in living cultured neurons. Thus, I was able to give a thorough description of the vesicle behavior during the individual steps in the synaptic vesicle cycle. As one of the most important observations I found that upon endocytosis a small pool of highly mobile synaptic vesicles is generated – the recently endocytosed vesicles. The mobility of the recently endocytosed vesicle pool differs heavily from the resting vesicle pool, which exhibits a low-mobility state, as previously reported (Gaffield et al., 2006). In almost every model of synaptic vesicle recycling the endocytosed vesicle is thought to move directly back to its original vesicle cluster (see for example Südhof, 2004). In contrast, I observed that the endocytosed vesicles spend tens of minutes in a mobile state before they integrated into the vesicle cluster and became thus immobile. Interestingly, both vesicle pools showed no change in their mobility upon physiological stimulation. However, the vesicle mobility decreased with the inhibition of synaptic activity, indicating that synaptic activity keeps the vesicles in a mobile state. Finally, after transmitter release the membrane-fused synaptic vesicles were relatively slow in their movement, which is possibly restricted by the clathrin machinery.

The here presented vesicle mobility in the synaptic vesicle cycle finally differs from the general vesicle recycling models. Nevertheless, the recycling pathway seems to be very simple in morphological terms. As shown by the FM photo-oxidation method in combination

with electron microscopy a small pool of vesicles (the readily releasable vesicles) may need to fuse with an endosomal compartment to get perfectly recycled, largely in agreement with the literature (Heuser and Reese, 1973; Sudhof, 2004).

In contrast to conventional synapses, the non-neuronal derived sensory IHCs seem to use a much more complex membrane recycling mechanism. As there is only little information available on presynaptic function of IHCs and almost nothing about their vesicle recycling pathway, the first aim was to investigate what organelles participate in vesicle recycling. Thus, I used as well the FM photo-oxidation technique in combination with high-resolution electron microscopy to be able to discern the labeled organelles from unlabeled ones. By generating three-dimensional reconstructions of IHCs I showed that they primarily use particularities for their membrane retrieval. From these cisternae then likely new vesicles are formed and spread throughout the entire IHC. This retrieval mechanism most likely allows these cells to compensate for their substantial vesicle release. However, upon stimulation vesicle recycling also occurs locally via endosomal intermediates at the basal release sites.

4.1   Mobility in the Conventional Synaptic Vesicle Cycle

4.1.1   A New Model of the Synaptic Vesicle Cycle

From the presented work I generated a new model of the synaptic vesicle mobility in the vesicle cycle of conventional synapses that is more complex compared to the classical hypothesized one (Figure 4.1). In the following I will discuss the novel findings of the individual stages separately.
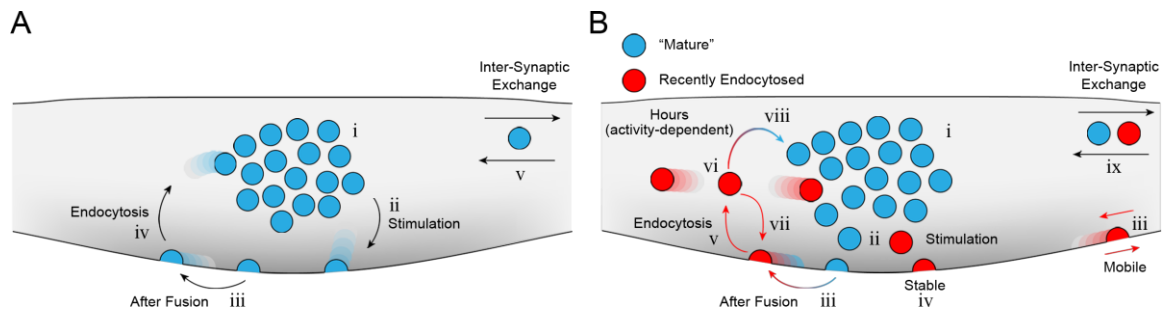
Figure 4.1: Models of synaptic vesicle mobility in the vesicle cycle of conventional synapses. (A) Model of vesicle motion as proposed in the past 40 years of synaptic research. The vesicles in the cluster are immobile at rest (i) and move toward the AZ during stimulation (ii). Vesicle material may diffuse in the membrane after fusion (iii) before endocytosis brings the vesicles back to the cluster (iv). Vesicles may also move from one cluster to another in the axon (v). (B) Model of vesicle motion generated from this work. Resting ("mature") vesicles are immobile (blue, i) and recently endocytosed vesicles are mobile (red, iv). Stimulation does not affect the mobility of both vesicle states (ii). Vesicle material may move after fusion (iii), but a substantial fraction has low mobility (iv). Endocytosis (v) generates the recently endocytosed mobile vesicles (red, vi). Repeated recycling keeps these vesicles in the mobile pool (vii), but eventually they integrate into the resting vesicle cluster (viii). Both the resting and recently endocytosed vesicles move between clusters/ synapses (ix).

The classical proposed model defines four stages in the synaptic vesicle cycle (Figure 4.1 A): (i) the vesicles in the cluster are immobile at rest; (ii) stimulation causes the vesicles to move towards the AZ and fuse with the plasma membrane; (iii) the fused vesicle material moves laterally across the membrane; (iv) the vesicles get endocytosed and move back to the vesicle cluster.

The new model from the main results of this work, however, is characterized by additional steps in the synaptic vesicle cycle. Importantly, two sorts of vesicles are involved. The resting vesicles (blue) are immobile (i) – with the low-mobility state as previously reported (Betz and Bewick, 1992; Ryan et al., 1993; Gaffield et al., 2006), and the recently endocytosed vesicles (red) with a high-mobility status (vi). Since recycling vesicles and resting vesicles are intermixed within the synapse (hippocampal cultured neurons (Schikorski and Stevens, 2001); frog NMJ (Rizzoli and Betz, 2004)) the actual "mission" of the resting vesicles remains unknown, even though resting vesicles are docked at the AZ and can exocytose under non-physiological stimulation conditions (Rizzoli and Betz, 2004). However, physiological stimulation (ii) does not affect both vesicle pools in contrast to the classical model. A possible explanation for this is that the mobile vesicles are already in a high-

mobility state that enables them to easily reach the AZ, and thus, stimulation would only affect their fusion ability and not their motion behavior. Another explanation is that the resting vesicles located at the AZ will simply collapse (fuse) into the membrane without a detectable change in vesicle movement. The finding that resting vesicles are docked at the AZ in hippocampal neurons is in agreement with the findings that of the totally 10-20 docked vesicles (Schikorski and Stevens, 2001) on average only around one vesicle fuses per action potential (Hanse and Gustafsson, 2001; Gandhi and Stevens, 2003). Additionally, while antibody labeling used here targets only a small population of vesicles – the surface pool (~30 vesicles (Fernández-Alfonso et al., 2006)) – it is difficult to predict how many of them will certainly be docked at the AZ and thus would eventually report a stimulation-induced change in mobility.

Interestingly, the different mobility states have also been found at the frog NMJ where recycling vesicles were mobile at rest and only the resting (reserve) pool vesicles were immobile (Gaffield et al., 2006). Moreover, the mobility state of the recycling vesicles never changed upon stimulation, but the mobilization of the resting vesicles increased during strong stimulation. I never tested the effect of non-physiological stimulation on resting vesicles. However, STED imaging also reported no change in the mobility of recently endocytosed vesicles with prolonged high potassium stimulation (Westphal et al., 2008).

Most of the presented studies were performed at RT. However, one study of Gaffield and Betz showed that in the frog NMJ the vesicle cluster is immobile at RT, but vesicle mobility increased substantially with the rise to physiological conditions (Gaffield and Betz, 2007). Moreover, they observed no change in vesicle mobility after disturbing the actin cytoskeleton with Latrunculin (Gaffield and Betz, 2007). This is in disagreement with the presented STED data on cultured neurons, which point to a partial involvement of active transport mechanisms in vesicle motion. Unfortunately, in this work the cytoskeleton was never totally disrupted by using both Latrunculin against actin and nocodazole against microtubules at the same time. Since actin is present in the synapse and tubulin in the axon, both drugs together would block all motor-driven movements. Thus, it would be of interest whether under these conditions vesicle motion is completely inhibited.

Interestingly, the inhibition of synaptic activity by TTX decreased the mobility of recently endocytosed vesicles (Figure 3.11), which is the first time that mobility is directly linked to synaptic activity. The result indicates a faster cluster integration of the vesicles in absence of

synaptic activity (viii), and suggests that synaptic activity maintains the vesicles mobile. Moreover, one can conclude that the process of cluster integration (maturation, see below), which may usually occur within the timescale of minutes to hours is activated more rapidly with synaptic inactivity (viii).

After vesicle fusion, the vesicle material moves across the plasma membrane (iii) as it is also hypothesized in the classical model. I found that the vesicle material resided in a low mobility state (iv) and that it moved partially out of the synapse. Other groups have shown that the vesicle identity gets lost upon vesicle fusion, with the dispersion of vesicle molecules in the plasma membrane and their intermixing with other "stranded" proteins (Sankaranarayanan et al., 2000; Li and Murthy, 2001; Fernández-Alfonso et al., 2006; Wienisch and Klingauf, 2006). However, I showed that the fused vesicles do not move faster than the recently endocytosed vesicles (under control conditions). The finding indicates that the surface exposed synaptotagmin proteins are not diffusing freely, but presumably remain in multi-molecular patches as demonstrated before (Willig et al., 2006). Moreover, a comparative STED analysis of fused native vesicle proteins (synaptotagmin, synaptophysin, VGAT) versus fused GFP-tagged ones (pHluorins) as used in the above-mentioned studies (synaptotagmin-citrine, synaptophysin-pHluorin and synaptobrevin-pHluorin) showed that the native proteins have a clustered distribution in contrast to the GFP-tagged proteins that disperse in the plasma membrane (Opazo et al., 2010). Only with high frequency stimulation the native synaptotagmin protein diffuses out of the boutons, but it recycles locally at physiological stimulations. The synaptotagmin patches (Opazo et al., 2010) may also contain other synaptic vesicle proteins as synaptotagmin forms a complex with other vesicle transmembrane proteins *in vitro* (synaptophysin and SV2 (Bennett et al., 1992b)). And, as demonstrated here with live STED imaging, several low-mobility spots were present on the plasma membrane, which largely contradicts a free-diffusion model. This would only exist if the molecules are dispersed in the membrane after fusion. In addition, the fused vesicle material is to some extent associated with the clathrin machinery (Figure 3.15), favoring the movement in clathrin-coated pits of a multi-molecular protein cluster. Finally, the free-diffusion model can only be accepted when the fused vesicle material would continuously enter the imaged area, which was not the case (Figure 3.14). Taken together, the fused vesicle material is not moving as individual molecules, but moves most likely in multi-protein clusters of low-mobility that are targeted by the clathrin machinery. To have the vesicle

material accumulated in low-mobility clathrin-coated membrane pits has the advantage that the material could get rapidly endocytosed upon stimulation (Gandhi and Stevens, 2003). Such an action potential triggered retrieval mechanism would only occur if the vesicle material is located at endocytosis sites, which was indeed observed as "hot spots" in the sum images of all three conditions, representing the preferred locations for vesicle retrieval (BWSV, caffeine, control, Figure 3.13). The increase in fused vesicle mobility after BWSV or caffeine treatments is likely the result of vesicles that are not captured during the formation of the clathrin-pit, because generally after extensive stimulation the vesicles may escape the clathrin mechanism (Miller and Heuser, 1984).

After endocytosis (v) the vesicles are affiliated to the recently endocytosed vesicle pool and exhibit a high-mobility state (red, vi), especially when compared to the resting vesicle pool. This observation is entirely in agreement with the findings of Gaffield and colleagues (2006), who demonstrated that, unlike the resting pool, the recycling pool of the frog NMJ is mobile (Gaffield et al., 2006). Interestingly, all models of vesicle recycling hypothesized so far that the endocytosed vesicle will move back to the vesicle cluster as a bona fide synaptic vesicle (see for example Sudhof, 2004). This process would be finished after a few minutes. However, the presented results here point towards a different mechanism, where the vesicles remain in a high-mobility state for a significant amount of time (tens of minutes at RT), before they lose their mobility upon the incorporation into the vesicle cluster (viii). The advantage of the extended high-mobility state allows repeated recycling of the vesicles, which in turn would remain in the mobile recycling pool (vii). Nevertheless, at some point (after minutes to hours) they eventually "mature" and become affiliated to the resting vesicle cluster (viii). It is the first time that a change in vesicle mobility has been observed after endocytosis.

Both the immobile resting vesicles and the mobile recently endocytosed vesicles exchange between neighboring vesicle clusters (ix). These findings are in agreement with many previous studies, which demonstrated the exchange of recycling vesicles between release sites using FM dye loading (Darcy et al., 2006; Staras et al., 2010). These observations were complemented with the results of pHluorin experiments, which showed that also the resting vesicles exchange between neighboring synapses (Fernandez-Alfonso and Ryan, 2008).

4.1.2   Changes in Vesicle Mobility

One of the most important findings of this work is the change in vesicle mobility. "How" can the changes in vesicle mobility take place over time, or what makes the vesicles become stationary and fixes them in place?

First of all, the pool allocation of the synaptic vesicle is rather non-permanent in the vesicle lifetime, as the endocytosed vesicles become resting vesicles after a specific period of time. The process from the recently endocytosed mobile state to the cluster integrated resting state can be termed as "maturation". Recycling vesicles may maintain their affiliation by releasing once in a while, but will finally "mature" to attain the resting status. In contrast, the resting vesicles cannot themselves switch to the recycling status. The resting vesicles that are docked at the AZ can become recycling vesicles upon fusion and their subsequent endocytosis. Thus, they will refill the recycling vesicle pool, which loses vesicles by cluster-integration. Consequently, the resting pool status is the final stage of this maturation process, with endocytosis being the first step. The resting vesicles are therefore termed mature vesicles in this model, and simply represent the "older" vesicles.

Secondly, the maturation from the recycling status to the resting status indicates that a molecular change of the vesicles may drive their mobility restriction. The most likely molecular anchor is the vesicle cross-linking protein synapsin. As reviewed in the Introduction the vesicle-associated protein synapsin binds to both actin and synaptic vesicles, and cross-links especially the resting pool (Pieribone et al., 1995). It is hypothesized that vesicle clustering depends on the phosphorylation status of synapsin. Dephosphorylation of synapsin immobilizes the synaptic vesicles at rest by binding them to each other and to actin (Hirokawa et al., 1989; Siksou et al., 2007). Synaptic activity results in its phosphorylation. Phosporylated synapsin binds off the vesicles, moves into the axon (Chi et al., 2001), and consequently regulates synaptic vesicle mobility (Fernández-Busnadiego et al., 2010). This is in agreement to the finding that synapsin is absent from fused vesicles (Torri Tarelli et al., 1992; Bloom et al., 2003).

Furthermore, it has been shown that the knockout of all neuronal synapsin genes (triple knockout) results in altered synaptic transmission, in the decrease of the pool of resting vesicles (Gitler et al., 2004), and a reduction of recycling pool vesicles (synapsin I knockout (Ryan et al., 1996)). It also has been shown that the vesicles in the cluster are still tethered by

other filamentous structures (Siksou et al., 2007). Moreover, the vesicle mobility, as observed from FRAP experiments on motor nerve terminals, is identical in synapsin wildtype and triple knockout mice (Gaffield and Betz, 2007). Taken together, one could hypothesize that the vesicles become unleashed from synapsin during or after exocytosis, and the recently endocytosed vesicles would be free of it and therefore mobile. As long as the vesicles exhibit a synapsin-free status, or bind just a minor amount of synapsin molecules, they remain in the high-mobility state (a synaptic vesicle contains ~8 copies of synapsin (Takamori et al., 2006)). The vesicle will lose its mobility with increasing synapsin association as it gets "glued" by synapsin onto the resting vesicle cluster. However, synapsin alone does not necessarily account for the vesicle cross-linking (Siksou et al., 2007); it may only be the initiator of the clustering process by acting as the molecular anchor, which starts the vesicle stabilization process onto the resting cluster.

4.1.3 The Importance of Mobile Vesicles

In the presented work I demonstrated that synaptic vesicles exhibit high- and low-mobility states in the vesicle cycle. Low-mobility values of the vesicle cluster have already been found in the past; however, vesicles with a high-mobility state have only been observed after non-physiological treatments (e.g. okadaic acid treatment). The importance of mobile vesicles can only be surmised. The mobile recycling pool vesicles can without any difficulties reach the AZ for repeated neurotransmission. This in turn also keeps them in the recycling pool and thus mobile (see above). It was shown here that synaptic activity does not explicitly guide the vesicles towards the release site, indicating that (random?) vesicle movements guarantee reaching the AZ and the subsequent release, i.e. synaptic neurotransmission.

Furthermore, it has been hypothesized that synapses work as individual units with the synaptic vesicles being restricted to their host synapse. This view changed as substantial exchanges of synaptic vesicles or complete vesicle clusters between neighboring synapses have been observed (Krueger et al., 2003; Darcy et al., 2006; Chen et al., 2008; Staras et al., 2010). These studies all took advantage of FM dye labeling, and therefore investigated only the movements of recycling vesicles. However, it has also been shown that resting vesicles are shared between synapses (pHluorin experiments from Fernandez-Alfonso and Ryan, 2008). Moreover, with an ultrastructural analysis of FM dye labeled recycling vesicles (via

FM photo-oxidation and electron microscopy) Darcy and co-workers showed that unlabeled vesicles colocalize with labeled recycling vesicles, possibly belonging to moving vesicles of the resting pool. These results are in full agreement with the presented work, showing the movement of both the recently endocytosed and the immobile resting vesicles along the axon, and their integration into pre-existing vesicle clusters at neighboring release sites. The substantial lateral exchange of both the recycling pool vesicles and the resting pool vesicles across neighboring release sites can in principle represent an additional multi-synapse vesicle pool. This extra-synaptic pool was previously named "superpool" (Westphal et al., 2008; Staras et al., 2010). The superpool hypothesis is based on observations from recycling pool vesicles which are dynamically exchanged with a turnover rate of >4% of the total synaptic vesicle pool of a synapse (Staras et al., 2010). As presented in this work, between 1-3 vesicles entered the imaged area per second. Taking this observation at its lowest value, if only one vesicle moves through a synapse, then in 3 minutes around 180 vesicles would have passed through which equals the amount of vesicles that are housed in the synaptic bouton of these type of neuron (Schikorski and Stevens, 1997). Furthermore, the vesicles participate with normal kinetics in neurotransmission at their new release site (Krueger et al., 2003; Darcy et al., 2006; Staras et al., 2010), indicating that the synapses of the nerve cell are intensely inter-linked.

Consequently, one can assume that the mobile superpool vesicles may be simply an additional supporting reserve pool that helps to sustain neurotransmission at individual release sites - the vesicles travel across multiple boutons and (where necessary) they fuse or integrate into the existing vesicle cluster. However, the resting vesicles are also shared between synapses (Fernandez-Alfonso and Ryan, 2008). Thus, it is questionable whether the exchange of recycling vesicles and resting vesicles is used for distinct purposes. In general, as vesicles disappear or get incorporated in the vesicle clusters the exchange may balance the vesicle populations of the inter-linked synapses over a longer period (Darcy et al., 2006).

What would cause the release of the resting vesicles from the cluster and make them move along the axon? A simple explanation for this is missing, but some observations made clear that additional molecules other than synapsin might be present to manage the migration from and the entry into the cluster (as shown by additional cross-linking filaments (Siksou et al., 2007)).

Surprisingly, the vesicle exchange was exclusively observed in cultured hippocampal neurons. It may thus thought to be an effect of synapse maturation or neuron development rather than of importance for native tissues (Matteoli et al., 1992). However, one recent investigation strengthened the superpool hypothesis as also vesicles are exchanged in hippocampal tissue slices (Staras et al., 2010). Moreover, Shepherd and Harris performed serial sectioning of the connection between the CA3-CA1 hippocampus area of adult rat CNS slices (Shepherd and Harris, 1998). Their three-dimensional reconstructions revealed loose clusters of vesicles in the axons, indicating the existence of vesicle packages traveling between release sites in mature neurons. Nevertheless, it is not known if vesicle exchange is limited to the hippocampus or whether it also takes place in other parts of the CNS.

Although synaptic vesicles are shared inter-synaptically across multiple boutons, synaptic vesicle membrane proteins are as well exchanged after strong stimulation by lateral movements across the axonal plasma membrane (Li and Murthy, 2001). Vesicle or protein exchange may therefore be an additional way to redistribute synaptic vesicle components across several release sites.

Finally, not only synaptic vesicles or their components are constitutively exchanged between neighboring nerve terminals. Also components of the cytomatrix at the AZ are transported from one synaptic release site to the next, e.g. bassoon (Tsuriel et al., 2009), but also synapsin 1 (Tsuriel et al., 2006). Furthermore, entire orphan release sites (fully functional release sites formed in the absence of axon-dendritic contacts) arise from or coalesce with stable vesicle clusters (Krueger et al., 2003). This illustrates the importance of mobile presynaptic components for the organization and the maintenance of the functional and structural properties of the synapse.

Taken together, individual synapses cannot be seen anymore as autonomous units, as previously believed. Synapses are even more inter-linked with a substantial fraction of their vesicles (recycling and resting pool vesicles) being affiliated to a common mobile "superpool" to serve multiple release sites.

4.2 Conclusions on Vesicle Recycling in Conventional Synapses

In conclusion, the high-resolution investigation allowed me to provide a thorough view of the vesicle behavior during the individual steps in the vesicle cycle. Related to this I was able to generate a new model of the synaptic vesicle cycle including new aspects on vesicle mobility. I conclude from this work that high- and low-mobility stages are important properties for the synaptic vesicle cycle in CNS synapses. Most important, vesicles are highly mobile after endocytosis (recycling vesicles) and "mature" over time to become resting vesicles with a low-mobility, indicating that their pool affiliation is non-permanent. Furthermore, besides the different mobility states both vesicle types are exchanged between release sites and are thus affiliated with an extra-synaptic "superpool". In most experiments the surface pool of synaptotagmin, belonging to the pool of "stranded" vesicles was selectively labeled. This pool participates actively in vesicle recycling as shown before (Gandhi and Stevens, 2003; Wienisch and Klingauf, 2006; Willig et al., 2006). Moreover, the surface pool exhibits a low-mobility state, as it moves partially in clathrin-coated pits of multi-molecular protein clusters. Thus, I hypothesize that the vesicle material likely recycles via clathrin-mediated endocytosis. On the morphological basis the recycling pathway is characterized by the involvement of an endosomal-like compartment. However, as the vesicles usually do not lose their identity after fusion (Willig et al., 2006; Opazo et al., 2010) they may not need an endosomal sorting step and could be retrieved as a fusion-competent synaptic vesicle. Nevertheless, the RRP vesicles undergo repeated recycling more often than other vesicles and may therefore need an intermediate sorting step.

4.3 Vesicle Recycling in the Sensory Synapse

4.3.1 Conclusions on FM Dye Labeling of Inner Hair Cells

It was hypothesized that FM dyes enter the hair cells via endocytosis at the apical pole. The labeled vesicles would then move down, fuse with the Golgi complex from which new vesicles are transported to the basal pole to refill the vesicles at the ribbon synapse (Griesinger et al., 2002; Griesinger et al., 2004; Griesinger et al., 2005). In contrast, it has been observed that FM dyes block the mechanotransduction channels at the stereocilia, and thus it has been concluded that FM dyes permeate non-selectively through these channels and label all membranes inside the hair cell (Gale et al., 2001; Meyers et al., 2003). As it was the aim of this work to investigate vesicle recycling in IHCs it was of high interest to solve the FM dye controversy.

I used various styryl dyes and other lipophilic dyes and observed the same labeling behavior on the cochlear IHCs of the mouse as shown before (Figure 3.18). However, finally I could show that FM-based IHC labeling is identical on aldehyde fixed and thus dead IHCs (Figure 3.19). I therefore conclude that the substantial FM dye labeling inside the IHCs is not due to endocytosis, but rather mediated by a non-selective permeation through channels. Whether they do so through the mechanotransduction channels of the stereocilia (Gale et al., 2001; Meyers et al., 2003; Crumling et al., 2009) or via other apex located receptor channels remains unknown (e.g. ATP-gated ion channels (P2X receptors) (Glowatzki et al., 1997; Meyers et al., 2003; Crumling et al., 2009)). The attempt to block those channels with diverse chemical treatments failed as possibly these dyes permeate more than one type of channel (see also Appendix).

Taken together, I conclude that the rapid appearance of FM fluorescence within the apical part of the IHCs is not mediated by endocytic processes, but rather by non-selective entry through ion channels. Nevertheless, I do not *per se* rule out that endocytosis takes place at the apical pole.

4.3.2 Vesicle Mobility in Sensory Synapses

Since vesicle live-labeling in IHCs fails with general labeling techniques used on conventional synapse I can only discuss reported findings from the literature on this topic. In the ribbon-type synapse of retinal bipolar cells the vesicles were found to be highly mobile throughout the whole terminal, which is largely in contrast to conventional synapses (Holt et al., 2004). FRAP experiments in ribbon-type cone photoreceptors revealed high recovery values, showing that also in these cells a highly mobile vesicle fraction exists (Rea et al., 2004). Their movement was also unaltered after actin cytoskeleton disruption, which is in agreement with the findings on mouse motor nerve terminals (Gaffield and Betz, 2007), but in disagreement with the presented results on cultured neurons. Likewise, cytoskeleton disruption had also no effect on the rate of exocytosis during sustained stimulation or the refilling of the RRP vesicles at the ribbon, indicating that active transport mechanisms do not play a role in vesicle movement and release (Holt et al., 2003). Moreover, synapsin, the vesicle cross-linking protein in conventional synapses, is absent in most ribbon-type synapses, which may explain the high mobility (Mandell et al., 1990). Nevertheless, some cross-linking structures are present in ribbon synapses that dock the vesicles to the ribbon (Lenzi et al., 1999).The treatment of ribbon type goldfish bipolar cells with the phosphatase inhibitor okadaic acid surprisingly slowed the movement of vesicles, suggesting that their mobilization mechanism differs from that in conventional synapses (Guatimosim et al., 2002). The recently endocytosed mobile vesicles of cultured neurons as shown here are also free of synapsin, and thus, likely comparable to the mobile vesicles of ribbon synapse (Bloom et al., 2003). Similar findings have been obtained from FM dye experiments on ribbon-type cone photoreceptors of the lizard where vesicles appear to diffuse freely in the cone terminal, with diffusion coefficients as high as from vesicle-like spheres in solution (Rea et al., 2004). However, the vesicle motion in cone terminals was still 10 times faster than in the retinal bipolar cells. Moreover, these cells may have no resting pool as even after 1 hour 87% of the FM labeled vesicles are still mobile (Rea et al., 2004). Holt and colleagues calculated that the large amount of mobile vesicles in the cytoplasm (~300000) would cause ~900 collisions per second against the ribbon. This calculation indicates that the high vesicle mobility would guarantee ribbon refilling, and thus high neurotransmission over long periods (Holt et al., 2004).

Whether the vesicles of the IHCs are also highly mobile remains unknown. However, as also the IHCs lack the cross-linking protein synapsin, this might indeed the case (Lenzi and Von Gersdorff, 2001).

Taken together, the ribbon-type synapses host large amounts of highly mobile vesicles to sustain their enormous needs of vesicle release. Compared to conventional synapses the vesicles of the ribbon synapse could be readily affiliated to a "superpool" of conventional synapses (i.e. they are mobile and very numerous).

4.3.3 Vesicle Recycling in Cochlear Inner Hair Cells

As it was presented above vesicle recycling studies on IHCs *in vivo* failed due to the disability of vesicle staining. Therefore, I used the FM photo-oxidation method in combination with high-resolution electron microscopy to investigate the steps involved in vesicle recycling in IHCs. In the following I will give a detailed description of the findings:

First, I found that indeed apical endocytosis takes place and observed that large and small organelles do exist (Figure 3.22). However, the amount of incorporated FM dye at the apex was for all IHCs relatively low and does not reflect the major membrane retrieval site. Second, I found that also at rest conditions (zero calcium) vesicle retrieval occurred, even though vesicle recycling was blocked at efferent synapses (Figure 3.22). Third, stimulation did not increase the amount of apical labeled organelles, however, more labeled organelles, mostly larger in size were present at the basal pole (Figure 3.29 and Figure 3.38). Fourth, the most important finding, in both the non-stimulated (Figure 3.28) and the stimulated IHCs (Figure 3.29) the majority of FM labeled organelles was located at baso-lateral sites and appeared as large elongated cisternae (Figure 3.28 and Figure 3.29). Fifth, after 5 minutes rest no cisternal compartments were present. However, high frequencies of small synaptic-like vesicles existed at the baso-lateral sites (Figure 3.30). Sixth, after 30 minutes rest synaptic-like vesicles were dispersed throughout the entire cytoplasm of the IHC with a lower density than in the 5 minutes rest IHC (Figure 3.31).

My observations can be explained with the help of a relatively simple model of vesicle recycling (Figure 4.2). The endocytosed organelles at the apex were found in all four IHCs, suggesting that they presumably play a minor role for compensatory vesicle recycling. Their further role remains unknown and needs to be clarified. FM photo-oxidation studies on hair

cells of the lateral line organs of Xenopus larvae have also revealed apical labeled organelles and it has been suggested that they represent endosomes (Nishikawa and Sasaki, 1996). However, the major location of membrane recycling occurred at the baso-lateral site via large elongated cisternae. They may represent bulk membrane retrieval that is known from other synapses mostly appearing during intense stimulation (Clayton et al., 2007). In parallel to a rapidly recycling pathway of small vesicles Richards and colleagues for example showed in the frog NMJ a slower one that retrieves the membrane via large infoldings from which cisternae get internalized (Richards et al., 2000). Such bulk retrieval has also been observed in terminals of ribbon-type bipolar retina cells after prolonged stimulation (Holt et al., 2003; Holt et al., 2004). New vesicles were slowly generated from these deep membrane invaginations, or the entire infolding was retrieved as a cisterna. However, cisternae have been rarely detected in resting terminals, although they have also been found in saccular hair cells of the frog and the goldfish (Hama and Saito, 1977; Lenzi et al., 2002). Moreover, the latter study reported that the cisternae have their origin in tubular invaginations of the plasma membrane.

My work also revealed the involvement of larger organelles (cisternae) in both the stimulated and the non-stimulated IHCs. However, with stimulation larger labeled organelles were more abundant at the basal site, likely indicating endosomes, similar to the work of Paillart and colleagues on isolated bipolar neurons of the goldfish retina. They used cationized ferritin and stimulated either briefly or with higher intensities. Positive ferritin-labeled larger endosomal organelles were in both conditions substantially more abundant compared to the low amount of small 30 nm vesicles (Paillart et al., 2003).

What mechanism is accountable for the proper membrane retrieval in sensory cells – is clathrin involved in this process? In saccular hair cells of the goldfish Hama and Saito have shown evidence for the involvement of clathrin-coated vesicles in the recycling process (Hama and Saito, 1977). Furthermore clathrin-coated pits and coated vesicles were also found close to the ribbon-type AZs of cochlear hair cells of gerbils and chinchillas (Siegel and Brownell, 1986). In contrast, the bipolar terminals of the retina did not reveal a clathrin-mediated vesicle retrieval mechanism (Paillart et al., 2003). This would be in agreement with the results of Heidelberger who observed that blocking dynamin fission in these synapses does not disturb endocytosis (Heidelberger, 2001). In contrast, in conventional synapses and NMJs clathrin-mediated budding has been reported to be essential for vesicle retrieval from

cisternae (Takei et al., 1996; Teng and Wilkinson, 2000). Nevertheless, it remains unknown what molecules participate in the invagination and fission of the cisternal membrane. In this work I showed by generating three-dimensional IHC reconstructions that new vesicles were generated from the cisternae. Whether clathrin is involved in this step needs to be clarified.

After 30 minutes the recycled vesicles were dispersed throughout the entire cytoplasm, where they probably mix with the non-recycled vesicles as it has been shown for the bipolar nerve terminal (Paillart et al., 2003; Holt et al., 2004) and the gerbil cochlear hair cells and may also refill the vesicles at the ribbon synapses (Siegel and Brownell, 1986). Finally, there is no direct evidence from this work that the Golgi complex is involved in membrane recycling as proposed before (Nishikawa and Sasaki, 1996; Griesinger et al., 2005)).

In contrast to my findings the above-mentioned studies showed that membrane retrieval appears near the ribbon-type active zones. However, for the large IHCs it seems reasonable to separate the substantial membrane retrieval from the location of the ribbon synapses. Essentially, two arguments would favor the spatial separation between release and retrieval sites. First, the cisternae occupy large areas far away from the release sites and appear to dissipate into small organelles locally. Second, it was shown at the bipolar retina synapse that the pool of cytoplasmic vesicles and not the recycled ones replenish the vesicles at the ribbon (Holt et al., 2004). This suggests that the separation of both sites allow the free dispersion of the new formed vesicles within the cytoplasm, and in turn enables the free movement (see above) of the cytosolic vesicles towards the basal located ribbon-type active zones. This hypothesis is supported by the findings of FM photo-oxidation studies on hair cells of the lateral line organs of Xenopus larvae (Nishikawa and Sasaki, 1996). Nishikawa and Sasaki also found tubular structures at baso-lateral sites and small vesicles close to the synaptic ribbon at the basal part. Thus, vesicle replenishment and consequentially neurotransmission at the IHC ribbon synapses may be perfectly guaranteed by free vesicle movements (see above) (Holt et al., 2004).
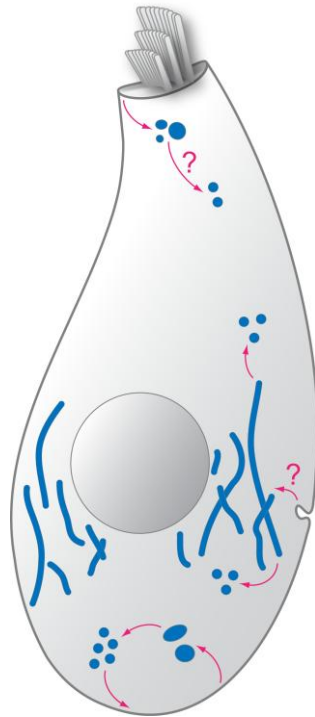
Figure 4.2: Model of vesicle recycling in cochlear IHCs generated from FM photo-oxidation and three-dimensional reconstructions. Vesicle recycling occurs at various parts of the IHC. At the apex large and small organelles are endocytosed (independent of stimulation). The fate of these organelles is unknown. Large elongated cisternae are used to recycle massive amounts of membrane at the baso-lateral side. Their endocytic origin is unidentified, but they may be connected to the cell membrane. Small vesicles are generated from the cisternae and dispersed throughout the IHC. Vesicle recycling also takes place at the basal pole near the locations of the release sites. High neurotransmission rates (stimulation) lead to the formation of larger round organelles, reflecting most likely endosomal intermediates from which vesicles are generated (identical to the classical model of vesicle recycling (Heuser and Reese, 1973)).

In parallel to the major vesicle recycling at the baso-lateral site recycled organelles appeared at the basal pole. However, here only small synaptic-like vesicles and larger round and elliptic organelles were present (Figure 3.38). These results are in agreement with the above-mentioned FM photo-oxidation studies from Nishikawa and Sasaki who also showed evidence for parallel retrieval pathways in hair cells. They observed as well small labeled vesicles at the basal part coexistent to apical endocytosed organelles and tubular structures at the baso-lateral site (Nishikawa and Sasaki, 1996). As here the larger round and elliptic organelles were more abundant after stimulation suggests that they may represent endosomal intermediates from which new vesicles are generated (compare to Paillart et al., 2003). The

basal retrieval mechanism therefore corresponds to a local recycling pathway, which is in agreement to the retinal bipolar cells (Holt et al., 2003; Paillart et al., 2003), and furthermore to the classical recycling pathway in conventional synapses (Heuser and Reese, 1973).

However, the question of why sensory IHCs do require cisternae for recycling remains.

A possible explanation comes along with the concept of the graded receptor potential of cochlear ribbon synapses used for neurotransmission. IHCs can release hundreds of vesicles per second over extended time periods (Beutner et al., 2001; Nouvian et al., 2006). As a consequence, the local recycling machinery is likely overwhelmed with the substantial amount of vesicle material that is added to the plasma membrane. Therefore, the IHC invaginates the excessive membrane in form of cisternae akin to a conventional synapse after strong stimulation (bulk retrieval). From these large membranes new vesicles can be generated more slowly. In that way, the bulk uptake may maintain the hair cells structural plasticity, as also proposed for the retinal bipolar cell (Holt et al., 2003).

Thus, I conclude that the IHCs use cisternae as a slow compensatory recycling route to constantly retrieve the vesicle material that is added to the plasma membrane (due to the continuous transmitter release at high rates). The endosomes at the basal pole therefore reflect a fast recycling pathway, which is only activated upon stimulation.

4.4 Conclusions on Vesicle Recycling in Cochlear Inner Hair Cells

Synaptic vesicle recycling in the model system of a sensory synapse, the cochlear inner hair cell is different from that of a conventional synapse. While the conventional synapse is under physiological conditions characterized by a local clathrin-mediated retrieval pathway, the IHCs use a variety of recycling organelles. I found that several classes are involved in the vesicle recycling process, which is largely in contrast to conventional synapses. Thus, I conclude that the basic mechanisms of vesicle recycling in conventional and sensory synapses are related, but that sensory synapses, and especially IHCs contain particularities (cisternae). The IHCs likely form deep infoldings to compensate for the large increase in the surface area from the continuous transmitter release. Therefore, the cisternae may reflect the necessity of the much stronger membrane recycling in IHCs compared to conventional synapses. In parallel to the slow recycling pathway by cisternea, a fast retrieval mechanism exists at the basal pole, which is only activated upon stimulation.

5 Outlook

5.1 Conventional Synapses

In this work I demonstrated that STED microscopy has the power of dissecting single synaptic vesicles *in vivo* using video-rate imaging. The resolution of the vesicles was limited to approximately 60 nm by the STED laser power, increasing the resolution by a factor of around 18 compared to confocal imaging. To further increase the resolution one could use higher STED laser power, but this would in turn substantially enhance photobleaching, which was already the case with the used settings. In addition, higher STED laser power would cause problems in collecting enough emitted photons from the reduced effective focal spot, and consequently, in separating the moving vesicles from background noise. Related to this, the fluorescent dyes and laser technologies need to be improved in parallel to reliably enhance resolution. Moreover, STED lasers with continuous wave beams would excite the fluorophores continuously, and thus allow for capturing more photons. Consequently, imaging of weaker signals, as well as imaging/ scanning with higher speeds over the sample would be possible. During this work it has been shown that STED with continuous wave beams can be applied to video-rate imaging on conventional synapses (Lauterbach et al., 2010).

However, as the resolution of the microscopes will presumably at some point achieve the size of proteins and antibodies, labeling methods need to be revisited. A gigantic primary and fluorescently-tagged secondary antibody complex used in immunofluorescence imaging would hinder the precise colocalization of two in principle exactly colocalizing proteins as their fluorophores could be separated some tens of nanometers.

In addition, protein colocalization studies would also need two-color STED imaging, which was already demonstrated for fixed cells, but awaits its application on living samples (Donnert et al., 2007). The application of a multi-color STED microscope with the ability of video-rate imaging would allow the investigation of the two vesicle pools simultaneously and would by far expand the here presented work. Questions one could address with a video-rate two-color STED are:

1. What can we learn on the synaptic vesicle mobility when the two different pools (such as the recycling and resting vesicles) are investigated in parallel?
2. How do the vesicles move in relation to cellular elements like the AZ, is their movement more directed towards the AZ upon (strong) stimulation?

Video-rate STED imaging used in this work was only performed on cultured hippocampal neurons. As already mentioned STED microscopy is difficult to use in tissue, as it has a low penetration depth. However, it would be of great interest to have nanoscale resolution available for deep tissue imaging to allow vesicle mobility studies in native brain slices. One recent study used STED two-photon laser scanning microscopy to investigate spine morphology deep inside acute brain slices (Ding et al., 2009). By applying a pulsed two-photon excitation laser and a one-photon STED continuous wave laser they achieved at an imaging depth of around 100 μm a 3-fold increase in resolution compared to confocal imaging. Nevertheless, this resolution enhancement would not be sufficient for vesicle mobility studies as presented here.

A great advantage would be nanoscale resolution in all three dimensions *in vivo*. Three-dimensional STED imaging was already performed on fixed cultured cells by the implementation of a second STED laser, the z-doughnut. The microscope allowed nanoscale imaging of immunostained neurofilaments with a resolution of 45 x 45 x 108 nm (Wildanger et al., 2009). However, capturing a single image frame (10 μm^2, pixel size 10 nm) takes 4 minutes – which is unfeasible for fast *in vivo* investigations as most biological processes are very short lived.

Moreover, three-dimensional optical sectioning was applied to image the endoplasmatic reticulum inside a living cell, but not at high frame-rates (Hein et al., 2008).

Another form of three-dimensional nanoscale imaging can be achieved with an isoSTED microscope. This technique relies on the 4Pi microscope system (Hell and Stelzer, 1992). A 4Pi microscope is equipped with two opposing objective lenses that focus into the same focal area. The molecules in the focal spot are illuminated by both lenses, which also collect the emitted fluorescence. Consequently, the interference of the two opposing light beams results in the resolution increase along the optical z-axis of about 5-7 fold (Bewersdorf et al., 2006). Since this method only increases the z-axis resolution one is still left with a poor lateral resolution. Thus, Schmidt and colleagues combined STED microscopy with 4Pi microscopy

(Schmidt et al., 2008). The focal spot in the resulting isoSTED microscope thus has x,y,z-resolution of around 40-50 nm. Three-dimensional nanoscopy was only once applied to single synaptic vesicle investigations of fixed hippocampal cultured neurons (Wilhelm et al., 2010), and is awaiting its application on living specimens.

5.2   Sensory Inner Hair Cells

The here presented results of membrane recycling in IHCs were achieved with high-resolution electron microscopy of FM dye labeled and photo-oxidized preparations. The investigations were based on morphological observations of the recycling organelles to uncover the vesicle retrieval pathway on the single organelle level. Since vesicles in hair cells cannot be live-labeled without difficulties with FM dyes or antibodies as used for conventional synapses, vesicle recycling studies on IHCs *in vivo* are challenging (FM dyes (Gaffield and Betz, 2006), antibodies (Kraszewski et al., 1995)). However, electron microscopy allowed me to perform the first morphological identification of the endocytic pathway in these cells.

Nevertheless, the data presented here needs to be strengthened by defining the properties of the large cisternae and their vesicle budding mechanism. The next steps are therefore aimed at investigating the protein complement of the recently endocytosed organelles (cisternae, organelles at the apex and bottom). Related to this, correlative microscopy could be used, in which the IHCs are stained by a fluorescent fixable marker (e.g. dextran, see Results) and immunolabeled against proteins of interest. The preparations will then be embedded in a plastic matrix, which can be processed in 50-80 nm thin-sections before imaging in high-resolution STED mode and subsequently with electron microscopy (see for example Grabenbauer et al., 2005; Watanabe et al., 2010). This would allow to characterize simultaneously both the morphology and the protein identity of the recycling organelles. Moreover, this technique would also allow to perform three-dimensional nanoscopy on fixed IHCs with a resolution of less than 80 nm in all directions (Punge et al., 2008).

In general the questions one should address are:

1. Which organelles contain synaptic vesicle proteins (and are thus directly involved in vesicle recycling)?

2. Are proteins of the clathrin machinery (clathrin, AP2, amphiphysin) involved in vesicle recycling (at cisternae as well as at the other recycling organelles)?

3. Is dynamin used for the fission step of the recycling organelles?

4. Are Golgi complex or endoplasmic reticulum markers present on the recycling organelles?

5. Do recycling organelles contain endosome markers?

Although high-resolution fluorescence microscopy techniques (such as STED) are not applicable to study deep inside tissues STED imaging was performed on fixed IHCs with less than 100 nm resolution at a tissue depth between 15 to 25 µm (Frank et al., 2010). A great advantage also for IHC studies would be three-dimensional optical sectioning at nanoscale resolution, as the dimensions of an IHC are much larger compared to that of a small conventional synapse. Finally, after finding the proper vesicle marker the application to *in vivo* studies would be optimal to precisely localize the vesicle and traffic them inside the IHC.

Recently, a pH-sensitive green fluorescent protein (GFP)-based sensors, termed pHluorin, was introduced which allows the optical monitoring of vesicle cycling (exo-/ endocytosis) during synaptic activity (Miesenböck et al., 1998). When the pH-sensitive GFP is tagged to a protein domain in the synaptic vesicle lumen its GFP-fluorescence is quenched by the acidic environment inside the vesicle (pH ~5.6). In contrast to the vesicle lumen the extracellular space has a neutral pH at around 7.4. Vesicles that fuse with the plasma membrane during stimulation expose their lumen to the extracellular space (to a neutral pH) and consequently the pHluorin fluorescence has a higher quantum yield compared to the quenched situation. Upon endocytosis the protein gets incorporated into the lumen of the vesicle, where the environment becomes acidic from the activity of a vesicular proton pump (ATPase) and suppresses its fluorescence, hence the vesicles become dark again. While the so far generated constructs of the general synaptic vesicle proteins synaptophysin (pHluorin construct: sypHy (Granseth et al., 2006)), synaptobrevin-2 (synapto-pHluorin (Miesenböck et al., 1998)), the vesicular glutamate transporter-1 (vGlut-pHluorin (Voglmaier et al., 2006)) and synaptotagmin 1 (pHluoro-tagmin (Fernández-Alfonso et al., 2006)) are all absent from IHCs, new pHluorin variants need to be specifically generated for sensory inner hair cells.

The expression of a pHluorin-tagged protein in IHCs would allow *in vivo*-studies on vesicle recycling to analyze exo-/ endocytosis kinetics in IHCs, as well as the mobility of fused vesicles and the site of their retrieval.

A. Appendix

1. Movie Legends

Movies can be found on the attached CD or downloaded from the particular web-sites as stated below.

i.   Movie A1

Video-rate STED microscopy dissects synaptic vesicle movements. Movie of single labeled synaptic vesicles acquired at 28 frames per second in a hippocampal axon in culture. The field of view has a dimension of 1.8 x 2.5 µm. Left: first frame of the movie in confocal mode. Middle: STED raw movie frames. Right: Gaussian filtered STED movie frames to increase the signal-to-noise ratio (see Methods). (Movie was published in Westphal et al., 2008 and can be downloaded at http://www.sciencemag.org/cgi/content/full/1154228/DC1)

ii.   Movie A2

Synaptic vesicle motion within an axon. Recently endocytosed synaptic vesicles are shown in red (see main text for details on vesicle labeling). Mitochondria (shown in green) are labeled by pre-incubation with 100 nM MitoTracker Green FM. STED (synaptic vesicle) frames were acquired at 28 frames per second; after each 18 frames in the vesicle channel, two frames in the mitochondria channel were acquired with confocal resolution. The movie can be downloaded at http://www.cell.com/biophysj/supplemental/S0006-3495(10)00552-7

iii.   Movie A3

Mobility of synaptic vesicles before and after incubation. Filtered STED movies of preparations stained against synaptotagmin, and imaged within 5 minutes (No Incubation, right) or after two hours of incubation (Incubation, left). Movies were acquired at 28 frames per second. The movie can be downloaded at http://www.cell.com/biophysj/supplemental/S0006-3495(10)00552-7

iv.   Movie A4

Influence of stimulation on vesicle mobility. Filtered STED movies (acquired at 28 frames per second) of preparations stained against synaptotagmin, and imaged within 10 minutes (No Incubation) or after two hours of incubation (Incubation). After 1.3 seconds of imaging, the preparations were stimulated at 20 Hz for 2 seconds. The movie can be downloaded at http://www.cell.com/biophysj/supplemental/S0006-3495(10)00552-7

v.   Movie A5

Influence of tetrodotoxin on vesicle mobility. Filtered STED movie (acquired at 28 frames per second) of a preparation labeled as described and imaged after a 10-minute incubation with 1 μM tetrodotoxin. The movie can be downloaded at http://www.cell.com/biophysj/supplemental/S0006-3495(10)00552-7

vi.   Movie A6

Vesicle material on the surface. Filtered STED movies of preparations treated with BWSV, caffeine or incubated shortly in absence of divalent ions, before anti-synaptotagmin labeling and imaging at 28 frames per second. The movie can be downloaded at http://www.cell.com/biophysj/supplemental/S0006-3495(10)00552-7

2. Synaptic Vesicle Motion Statistics

Illustration of the median trace speed with the corresponding error bars of synaptic vesicle motion in the different conditions from Figure 11. Each histogram consists of 20000-40000 vesicle traces.
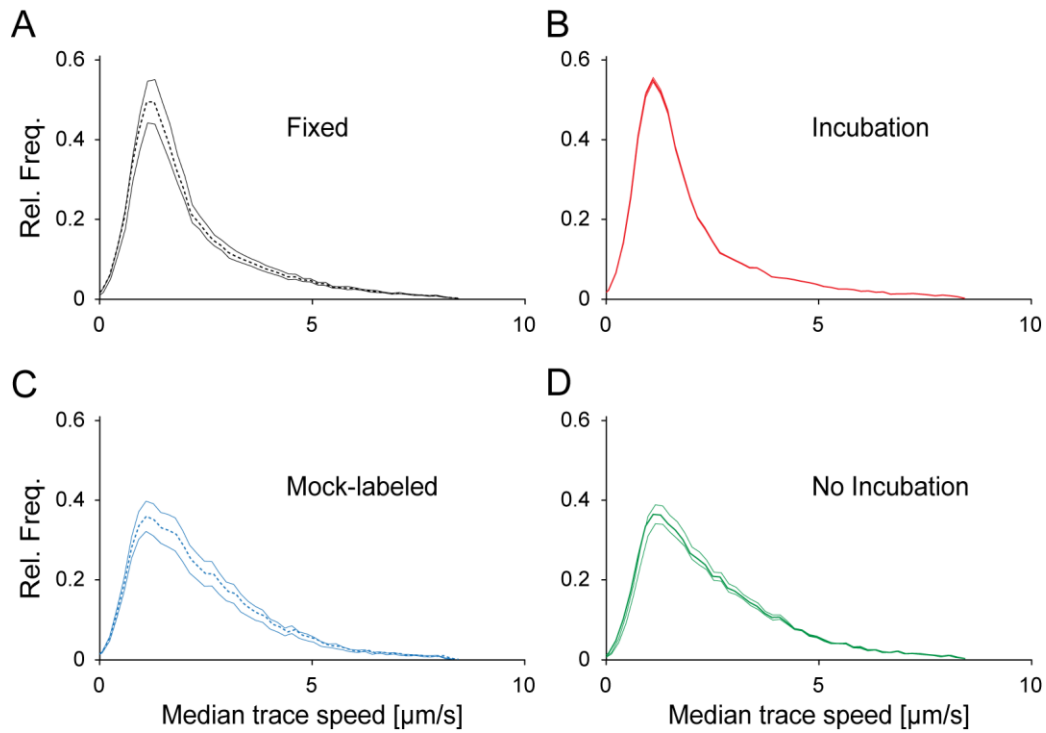

Figure A 1: Synaptic vesicle motion statistics. (A-D) The individual histograms from Figure 3.5 with the corresponding error bars, shown as the standard error of the mean.

3. Colocalization of Recently Endocytosed and Incubated Synaptic Vesicles with Different Neuronal Markers

Primary cultured hippocampal neurons were live-labeled against synaptotagmin (shown in red) as described in Methods, and fixed with paraformaldehyde (4% in PBS) either after a rest period of 20 minutes at room temperature (No Incubation) or after incubation for two hours at 37°C (Incubation). The neurons were then immunostained (after permeabilization) against different synapse specific proteins (shown in green), including synaptic vesicle markers or AZ markers. Imaging was done by confocal fluorescence microscopy.
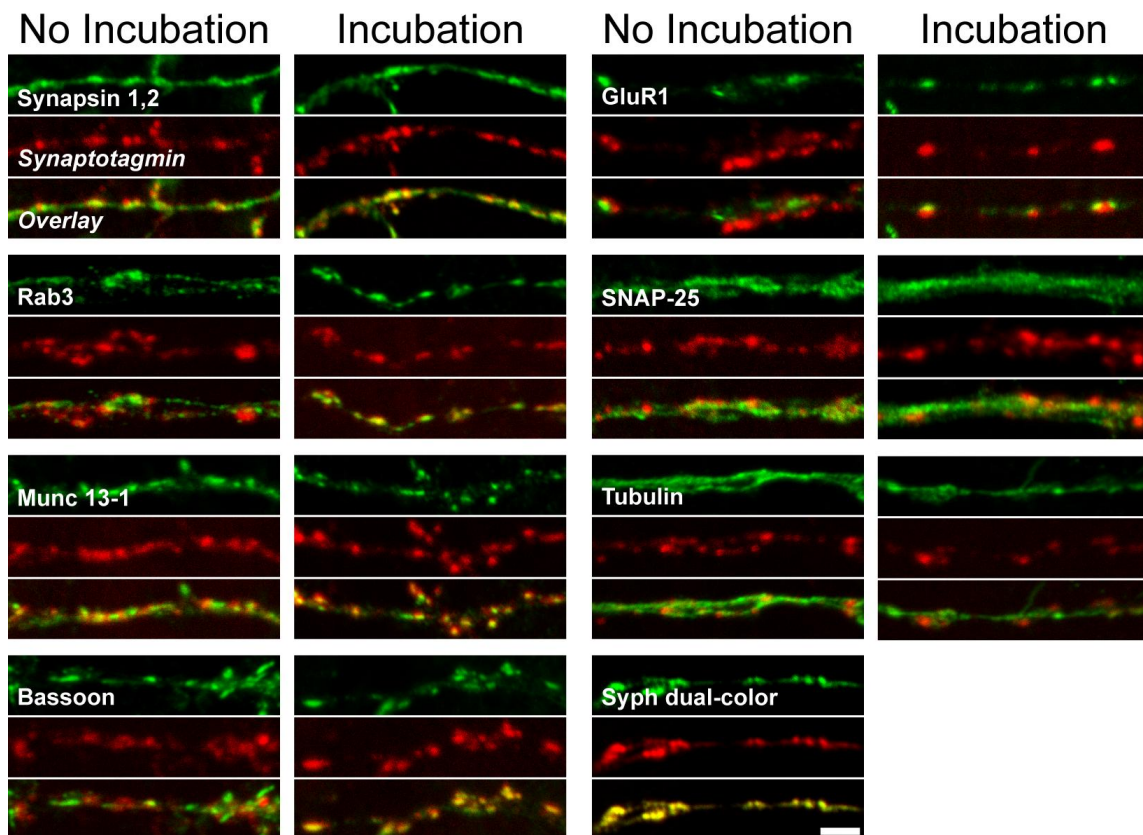
Figure A 2: Cluster integration after incubation. Colocalization of synaptotagmin live-labeled vesicles with immunostained synapse specific proteins (AZ markers: Munc 13-1, bassoon, postsynaptic glutamate receptors (GluR1); synaptic vesicle markers: synapsin 1,2, rab3) as well as with SNAP-25 (plasma membrane marker) and tubulin (cytoskeleton). Live-labeled vesicles with anit-synaptotagmin antibodies (red) were fixed either after 20 minutes at RT after labeling (No Incubation, left corresponding panel) or after 2 hours of incubation at 37°C (Incubation, right corresponding panel) and then immunostained (with permeabilization) against the specific marker proteins. Scale bar: 2.5 μm.

4. Specificity of Synaptotagmin Antibodies Labeled with Atto647N

Monoclonal synaptotagmin antibodies (clone 604.2; Synaptic Systems) were fluorescently labeled with Atto647N in our laboratory by conventional NHS-ester methods. The antibodies were purified from ascites fluids by Protein-G-Sepharose binding. A low pH (2.2) eluted the antibodies from the Sepharose, which were then coupled to the NHS-ester of Atto647N in presence of 100 mM $NaHCO_3$. The reaction was quenched with hydroxylamine. Free Atto647N dye was separated from antibody-bound dye via a Sephadex G25 size-exclusion column.

The antibodies lost their specificity, as a substantial fraction of the antibodies were denatured by the low pH treatment, and since the epitope-binding pockets were not protected during labeling. These antibodies were termed "non-specific". "Specific" Atto647N-coupled synaptotagmin antibodies (same clone, 604.2) became purchasable during this work from Synaptic Systems (Göttingen, Germany) (Figure A 3).
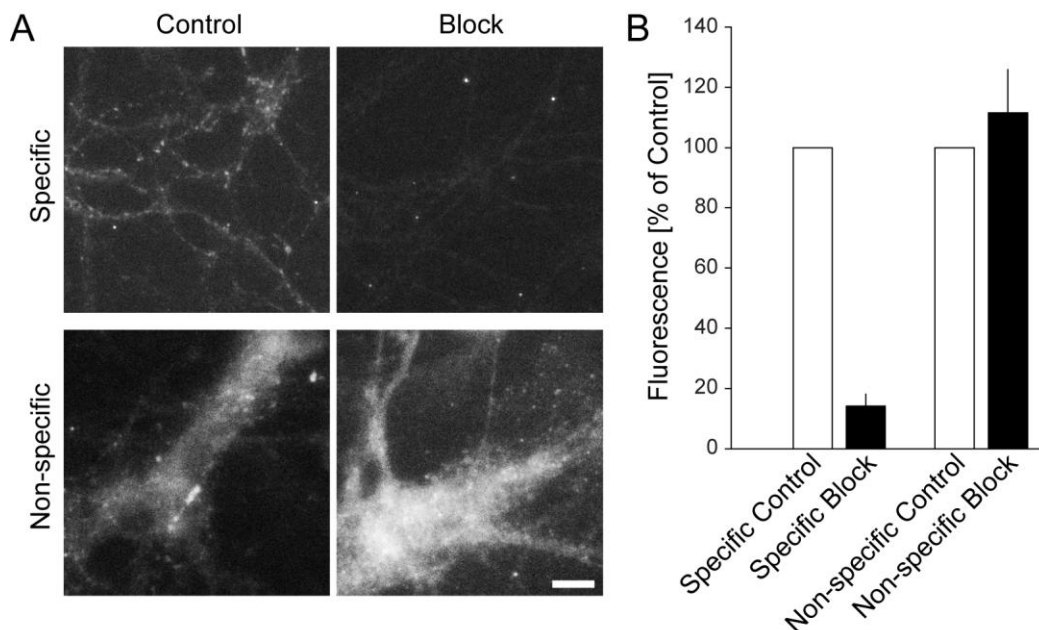
Figure A 3: (A) Hippocampal cultures were incubated with the Atto647N-coupled synaptotagmin antibodies for 15 minutes either without (left panels, control) or with a previous incubation with unlabeled synaptotagmin antibodies (right panels, block). The labeling with the specific antibody disappeared due to epitope masking by the unlabeled antibodies, while the non-specific labeling was unaffected. Scale bar 10 μm. (B) Quantification of the staining. White bars: control staining. Black bars: staining after blocking the epitopes with unlabeled antibodies. Note that the specific labeling is almost eliminated, while the non-specific labeling persists. Means ± s.e.m. are shown from 3 independent experiments, with at least 10 cells analyzed per experiment. Fluorescence intensity was analyzed by manually selecting regions of interest, calculating the mean

intensity, and subtracting the mean background intensity in neighboring manually selected "empty" regions of interest.

5. P2X-Receptor Inhibition with Suramin

I demonstrated during this work that FM dyes permeate non-selective through channels located at the apex of cochlear IHCs, most likely through the mechanotransduction channels as proposed by two independent groups (Gale et al., 2001; Meyers et al., 2003). Moreover, Meyers and colleagues found that FM1-43 penetrates cells expressing other non-selective ion channels, like the capsaicin receptor TRPV1 or the ATP-gated P2X receptor (Meyers et al., 2003). Interestingly, the non-selective P2X receptor is specifically expressed at the apex of mammalian cochlear IHCs (Järlebark et al., 2000; Järlebark et al., 2002). As a consequence of the receptor localization FM dye could permeate through these channels in parallel to the mechanotransduction channels. In an attempt to inhibit P2X receptor-mediated styryl dye entry into chick cochlear hair cells, Crumling and colleagues used the pharmacological, non-competitive P2X receptor antagonist suramin (100 μM) (Crumling et al., 2009). They observed a block of around 85% of styryl dye signal in hair cells compared to untreated cells, and thus concluded that FM dyes can enter through these channels.

The inhibition of apical located channels would possibly allow the application of FM dyes for vesicle recycling studies *in vivo*. To test for this I repeated the suramin experiments of Crumling and colleagues on cochlear IHCs of the mouse. After 5 minutes of pre-incubation in 100 μM suramin (Sigma-Aldrich) in standard HBSS the organ of Corti was incubated for 1 minute in 5 μM FM1-43 dissolved in standard suramin-containing HBSS (100 μM). After washing with normal suramin containing HBSS the IHCs were imaged using confocal optics (with the same setup as for normal FM1-43 imaging; see Methods). Interestingly, I got similar results as shown for the chick cochlear hair cells, namely that almost no FM fluorescence appeared inside the IHCs with normal imaging (Figure A 4).
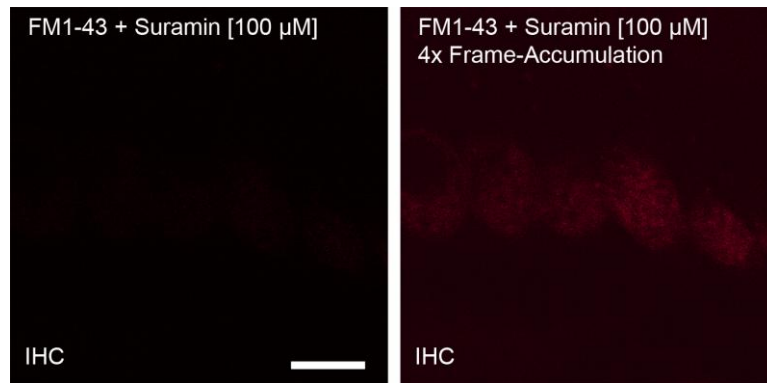
Figure A 4: Effect of the P2X receptor antagonist suramin on FM1-43 entry into cochlear IHCs. FM1-43 fluorescence is almost non-detectable in normal scanning mode (left image; microscope setup adjusted as for FM1-43 imaging of untreated IHC). Little fluorescence is detectable when imaging with multiple frame-accumulation (4x, right image). Scale bar: 10 μm.

However, a careful comparison to control images (Figure 3.17 and Figure 3.18) revealed that also no FM fluorescence signal of neighboring cells or of the stereocilia was observable. A closer view on the FM1-43-suramin dilution revealed that suramin changed the color of FM1-43 from orange in normal HBSS to pink in suramin-containing buffer (Figure A 5A).
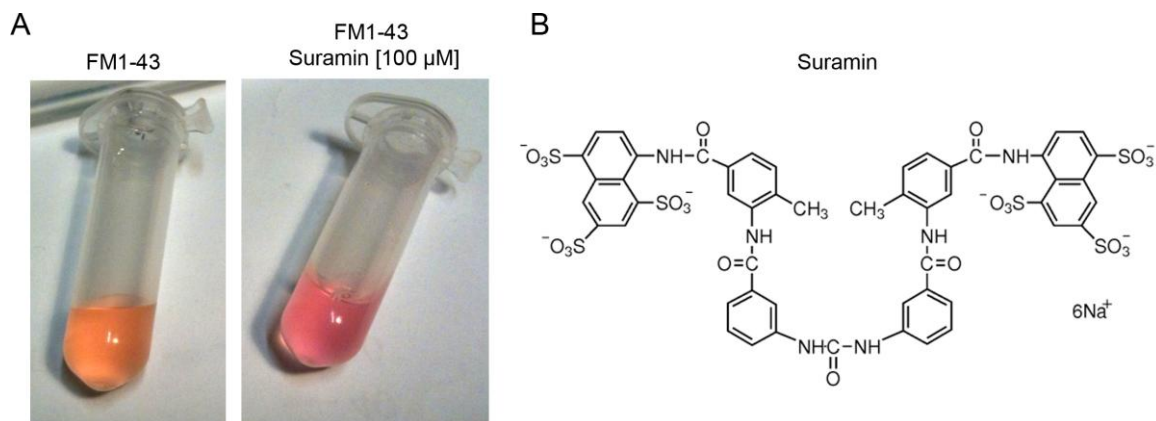
Figure A 5: Interaction of FM1-43 with suramin. (A) FM1-43 has an orange-colored appearance in standard HBSS buffer (left). Suramin changed the FM1-43 color to pink (right). (B) The molecular structure of suramin exhibits six sulfonate groups, which make this component a highly negatively charged molecule (the molecular structure of suramin was downloaded from the homepage of Sigma-Aldrich http://www.sigmaaldrich.com/structureimages/17/mfcd00210217.gif (downloaded 05.02.2011, 2:07 pm)).

The color change likely occurred from the interaction of the highly negative charged sulfonate groups of suramin with the positive charged head group of the FM1-43 molecules

(Figure 2.2).

Spectrophotometer experiments were aimed at analyzing the emission and excitation spectra of FM1-43 in presence or absence of suramin. 1.8 ml of a 2 μm FM1-43 dilution (in H_2O) were added to a quartz cuvette (10 mm width) under constant stirring. 200 μl of a 1 mM suramin stock (final concentration 100 μM) or 200 μl H_2O (control) were added. A spectrum measurement of dye excitation was performed by measuring dye fluorescence at 570 nm (±2.5 nm bandwidth; (Henkel et al., 1996a)) over a broad range of excitation wavelength between 300 and 550 nm (2 nm increments; integration time 1 second). Dye emission was measured over a broad range of wavelength between 480 and 700 nm (2 nm increments; integration time 1 second) at a constant excitation wavelength of 460 nm (±2.5 nm bandwidth).

Interestingly, suramin addition caused a shift in the peak excitation wavelength from approximately 460 nm to around 530 nm (Figure A 6 A). Despite the shift in the excitation peak, the emission wavelength of FM1-43 surprisingly showed no significant alteration of its spectrum after suramin addition (Figure A 6 B), which demonstrates the direct interaction of the two molecules.
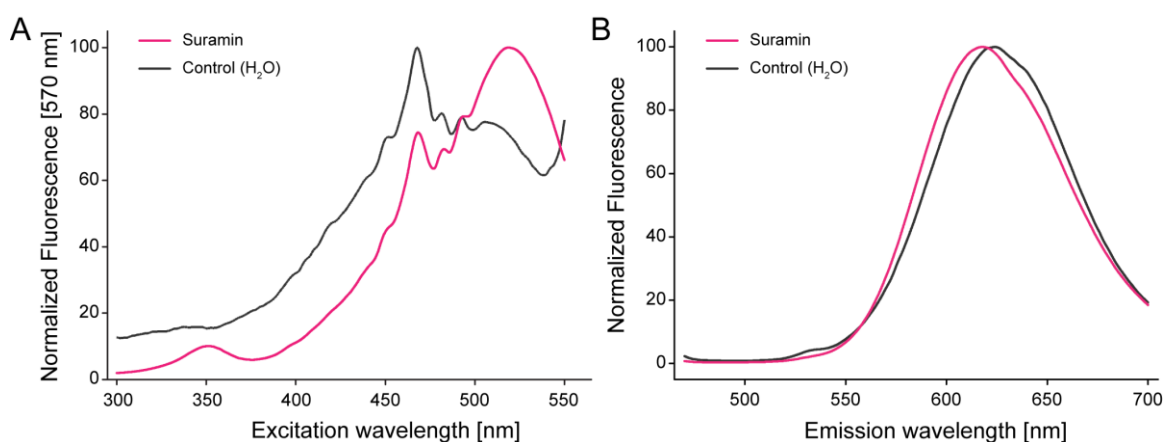
Figure A 6: Normalized excitation and emission spectra of FM1-43 in H_2O and suramin. Spectrum measurement of FM1-43 excitation under control (in ddH_2O) conditions or in 100 μM suramin (dissolved in ddH_2O). (A) Emission was measured at 570 nm while the excitation wavelength was stepwise changed (increments of 2 nm from 300 to 550 nm). Suramin shifted the peak excitation to a higher wavelength. (B) Dye emission was measured from 470 to 700 nm (increments of 2 nm) at a constant excitation wavelength of 460 nm.

In the next step I used cultured PC12 cells to check whether a direct suramin-dependent change in FM1-43 fluorescence can be observed. To test for this 200 μl FM1-43 (10 μM in PBS) was added to the cells and imaged. Next, to control for a change in fluorescence of membrane bound FM dye an equal concentration of FM1-43 in PBS was added and imaged.

Finally, 200 µl PBS with FM1-43 (10 µM) and suramin (100 µM) was added and several images were captured to document possible changes.

FM1-43 stained the outer leaflet of the plasma membrane of the PC12 cells (Figure A 7). As expected, no change in fluorescence was detected for the control. Interestingly, the addition of FM-suramin resulted in an immediate disappearance of FM fluorescence at the periphery of the cell cluster. Within a few seconds the FM fluorescence faded away inside the cluster (Figure A 7, FM1-43/Suramin #1-#4).
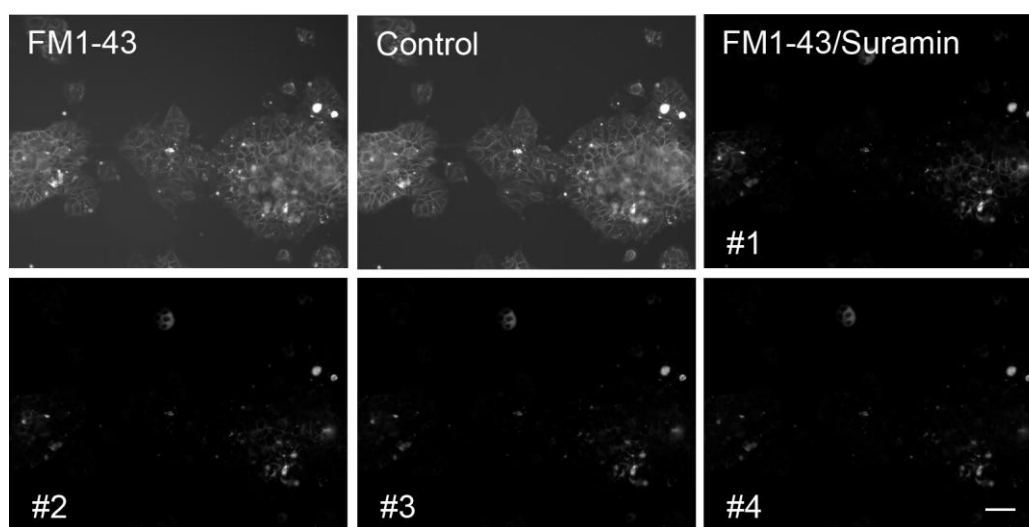
Figure A 7: Suramin effect on FM1-43 membrane staining. FM1-43 alone bound to the plasma membrane of the PC12 cells, clearly visualizing the cell cluster (upper left panel). The application of FM1-43 with suramin (100 µM) resulted in FM fluorescence decrease starting at the periphery of the cell cluster witch reached after a few seconds the center of the cluster (FM1-43/Suramin #1-#4). The application of only FM1-43 revealed no change in membrane bound FM fluorescence (control). Scale bar: 40 µm.

I conclude therefore that FM1-43 interacts on an ionical basis with the sulfonate groups of suramin and consequently FM1-43 is taken of the membrane and becomes almost non-fluorescent (as styryl dyes are only fluorescent when inserted into membranes). Suramin-bound FM dye still has a 4-5 fold higher quantum yield compared to the unbound aqueous form, as observed from non-normalized spectrophotometer measurements (Figure A 8), indicating that suramin has "membrane simulative" properties for styryl dyes. However, with the quantum yield increasing by 700-fold in membranes, it is clear that sequestration by suramin reduces dramatically overall FM fluorescence when applied in cellular experiments.
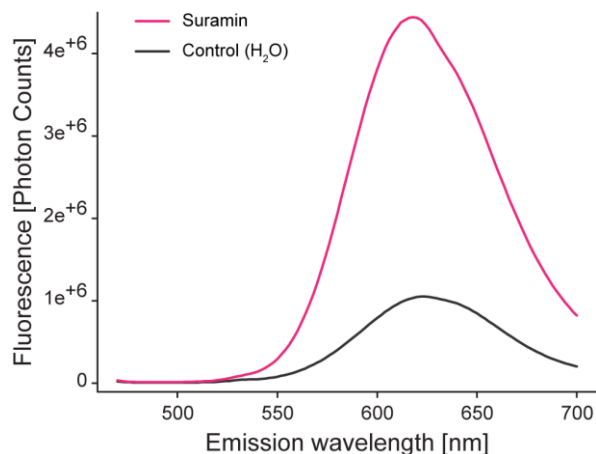
Figure A 8: Non-normalized FM1-43 fluorescence spectra. Dye emission was measured from 470 to 700 nm (increments of 2 nm) at a constant excitation wavelength of 460 nm. Suramin-bound FM1-43 showed higher photon flux than in an aqueous environment.

Taken together, suramin application on hair cells does not inhibit FM dye permeation through the non-selective P2X receptor channels, moreover, suramin interacts directly with the styryl dye, which severely inhibits its native interaction with the plasma membrane and results in the observed block of styryl dye uptake.

6. Immunostaining of Inner Hair Cells with Anti-Otoferlin Antibodies

The correct functionality of the anti-otoferlin antibodies was tested with immunostainings before trying to label otoferlin *in vivo*.

Protocol: The organ of Corti was fixed (4% PFA) for 60 minutes (30 minutes on ice then at RT) and afterwards incubated in 100 mM ammoniumchloride for 30 minutes. After TX-100 permeabilization (3 times 10 minutes) affinity purified polyclonal rabbit otoferlin antibodies (Synaptic Systems, concentration 0.6 mg/ml) were diluted 1:200 in PBS containing 1.5% BSA and 0.5% and applied on the organ of Corti for 90 minutes at RT in a humidified chamber. After washing with PBS (with 0.5% TX-100) secondary antibodies (Cy3-tagged goat anti-rabbit) were applied in the same manner as the primaries for 60 minutes. The organ was washed with PBS high salt and with normal PBS before finally embedding it in Dako mounting medium. Imaging was performed using confocal optics. Figure A 9 below shows the IHC specific staining of otoferlin.
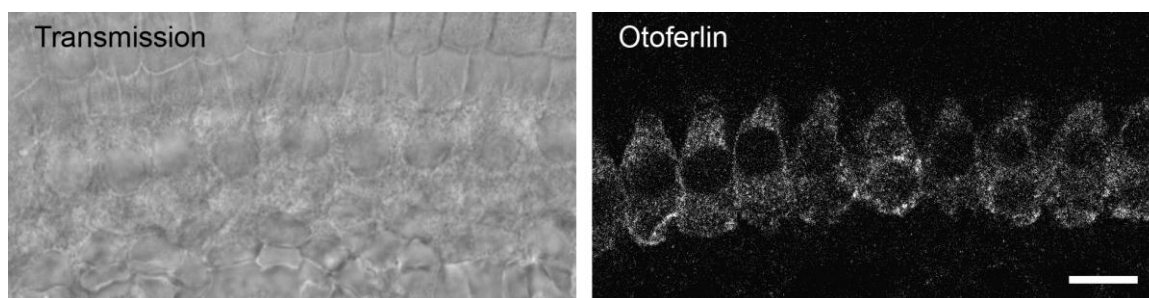
Figure A 9: Immunostaining of IHCs with anti-otoferlin antibodies. Left transmission image, right confocal fluorescence image. Imaging was performed with a Leica TCS SP5 confocal microscope (Leica Microsystems), using a 63x, 1.4 numerical aperture HCX PL APO CS oil objective. The secondary Cy3 dye was excited at 543 nm with a Helium-Neon laser and fluorescence was detected with PMTs in the spectral range of 555-665 nm. Scale bar: 10 μm

Bibliography

Abbe E (1873) Beitrage zur Theorie des Mikroskops und der mikroskopischen Wahrnehmung. Arch f Mikroskop Anat 9:413-420.

Aguado F, Majó G, Ruiz-Montasell B, Canals JM, Casanova A, Marsal J, Blasi J (1996) Expression of synaptosomal-associated protein SNAP-25 in endocrine anterior pituitary cells. Eur J Cell Biol 69:351-359.

Alvarez De Toledo G, Fernández-Chacón R, Fernández JM (1993) Release of secretory products during transient vesicle fusion. Nature 363:554-558.

Aravanis AM, Pyle JL, Tsien RW (2003) Single synaptic vesicles fusing transiently and successively without loss of identity. Nature 423:643-647.

Artalejo CR, Elhamdani A, Palfrey HC (1998) Secretion: dense-core vesicles can kiss-and-run too. Curr Biol 8:R62-65.

Baumert M, Maycox PR, Navone F, De Camilli P, Jahn R (1989) Synaptobrevin: an integral membrane protein of 18,000 daltons present in small synaptic vesicles of rat brain. EMBO J 8:379-384.

Benfenati F, Greengard P, Brunner J, Bähler M (1989) Electrostatic and hydrophobic interactions of synapsin I and synapsin I fragments with phospholipid bilayers. J Cell Biol 108:1851-1862.

Bennett MK, Calakos N, Scheller RH (1992a) Syntaxin: a synaptic protein implicated in docking of synaptic vesicles at presynaptic active zones. Science 257:255-259.

Bennett MK, Calakos N, Kreiner T, Scheller RH (1992b) Synaptic vesicle membrane proteins interact to form a multimeric complex. J Cell Biol 116:761-775.

Bennett MVL, Zukin RS (2004) Electrical coupling and neuronal synchronization in the Mammalian brain. Neuron 41:495-511.

Betz A, Okamoto M, Benseler F, Brose N (1997) Direct interaction of the rat unc-13 homologue Munc13-1 with the N terminus of syntaxin. J Biol Chem 272:2520-2526.

Betz A, Thakur P, Junge HJ, Ashery U, Rhee JS, Scheuss V, Rosenmund C, Rettig J, Brose N (2001) Functional interaction of the active zone proteins Munc13-1 and RIM1 in synaptic vesicle priming. Neuron 30:183-196.

Betz WJ, Bewick GS (1992) Optical analysis of synaptic vesicle recycling at the frog neuromuscular junction. Science 255:200-203.

Betz WJ, Mao F, Bewick GS (1992) Activity-dependent fluorescent staining and destaining of living vertebrate motor nerve terminals. J Neurosci 12:363-375.

Beutner D, Voets T, Neher E, Moser T (2001) Calcium dependence of exocytosis and endocytosis at the cochlear inner hair cell afferent synapse. Neuron 29:681-690.

Bewersdorf J, Schmidt R, Hell SW (2006) Comparison of I5M and 4Pi-microscopy. Journal of microscopy 222:105-117.

Birks R, Huxley HE, Katz B (1960) The fine structure of the neuromuscular junction of the frog. J Physiol (Lond) 150:134-144.

Block MR, Glick BS, Wilcox CA, Wieland FT, Rothman JE (1988) Purification of an N-ethylmaleimide-sensitive protein catalyzing vesicular transport. Proc Natl Acad Sci USA 85:7852-7856.

Bloom O, Evergren E, Tomilin N, Kjaerulff O, Löw P, Brodin L, Pieribone VA, Greengard P, Shupliakov O (2003) Colocalization of synapsin and actin during synaptic vesicle recycling. J Cell Biol 161:737-747.

Bonanomi D, Benfenati F, Valtorta F (2006) Protein sorting in the synaptic vesicle life cycle. Prog Neurobiol 80:177-217.

Bonifacino JS, Glick BS (2004) The mechanisms of vesicle budding and fusion. Cell 116:153-166.

Boucrot E, Saffarian S, Zhang R, Kirchhausen T (2010) Roles of AP-2 in clathrin-mediated endocytosis. PLoS ONE 5:e10597.

Brose N, Petrenko AG, Südhof TC, Jahn R (1992) Synaptotagmin: a calcium sensor on the synaptic vesicle surface. Science 256:1021-1025.

Brose N, Hofmann K, Hata Y, Südhof TC (1995) Mammalian homologues of Caenorhabditis elegans unc-13 gene define novel family of C2-domain proteins. J Biol Chem 270:25273-25280.

Bruns D, Jahn R (1995) Real-time measurement of transmitter release from single synaptic vesicles. Nature 377:62-65.

Cajal SRY (1894) La fine structure des centres nerveaux. Proceedings of the Royal Society of London 55:24.

Ceccarelli B, Hurlbut WP (1980) Ca2+-dependent recycling of synaptic vesicles at the frog neuromuscular junction. J Cell Biol 87:297-303.

Ceccarelli B, Hurlbut WP, Mauro A (1973) Turnover of transmitter and synaptic vesicles at the frog neuromuscular junction. J Cell Biol 57:499-524.

Chapman ER, Hanson PI, An S, Jahn R (1995) Ca2+ regulates the interaction between synaptotagmin and syntaxin 1. J Biol Chem 270:23667-23671.

Chen X, Barg S, Almers W (2008) Release of the styryl dyes from single synaptic vesicles in hippocampal neurons. J Neurosci 28:1894-1903.

Chi P, Greengard P, Ryan TA (2001) Synapsin dispersion and reclustering during synaptic activity. Nat Neurosci 4:1187-1193.

Clayton EL, Evans GJO, Cousin MA (2007) Activity-dependent control of bulk endocytosis by protein dephosphorylation in central nerve terminals. J Physiol (Lond) 585:687-691.

Cochilla AJ, Angleson JK, Betz WJ (1999) Monitoring secretory membrane with FM1-43 fluorescence. Annu Rev Neurosci 22:1-10.

Coppola T, Magnin-Luthi S, Perret-Menoud V, Gattesco S, Schiavo G, Regazzi R (2001) Direct interaction of the Rab3 effector RIM with Ca2+ channels, SNAP-25, and synaptotagmin. J Biol Chem 276:32756-32762.

Corey DP, Hudspeth AJ (1979) Ionic basis of the receptor potential in a vertebrate hair cell. Nature 281:675-677.

Crocker J, Grier D (1996) Methods of digital video microscopy for colloidal studies. Journal of Colloid and Interface Science.

Crumling MA, Tong M, Aschenbach KL, Liu LQ, Pipitone CM, Duncan RK (2009) P2X antagonists inhibit styryl dye entry into hair cells. Neuroscience 161:1144-1153.

Darcy KJ, Staras K, Collinson LM, Goda Y (2006) Constitutive sharing of recycling synaptic vesicles between presynaptic boutons. Nat Neurosci 9:315-321.

David C, McPherson PS, Mundigl O, De Camilli P (1996) A role of amphiphysin in synaptic vesicle endocytosis suggested by its binding to dynamin in nerve terminals. Proc Natl Acad Sci USA 93:331-335.

De Camilli P, Cameron R, Greengard P (1983a) Synapsin I (protein I), a nerve terminal-specific phosphoprotein. I. Its general distribution in synapses of the central and peripheral nervous system demonstrated by immunofluorescence in frozen and plastic sections. J Cell Biol 96:1337-1354.

De Camilli P, Harris SM, Huttner WB, Greengard P (1983b) Synapsin I (Protein I), a nerve terminal-specific phosphoprotein. II. Its specific association with synaptic vesicles demonstrated by immunocytochemistry in agarose-embedded synaptosomes. J Cell Biol 96:1355-1373.

De Robertis ED, Bennett HS (1954) A submicroscopic vesicular component of Schwann cells and nerve satellite cells. Exp Cell Res 6:543-545.

Denker A, Rizzoli SO (2010) Synaptic vesicle pools: an update. Front Syn Neurosci 2:1-12.

Denker A, Kröhnert K, Rizzoli SO (2009) Revisiting synaptic vesicle pool localization in the Drosophila neuromuscular junction. J Physiol (Lond) 587:2919-2926.

Dick O, tom Dieck S, Altrock WD, Ammermüller J, Weiler R, Garner CC, Gundelfinger ED, Brandstätter JH (2003) The presynaptic active zone protein bassoon is essential for photoreceptor ribbon synapse formation in the retina. Neuron 37:775-786.

Ding JB, Takasaki KT, Sabatini BL (2009) Supraresolution imaging in brain slices using stimulated-emission depletion two-photon laser scanning microscopy. Neuron 63:429-437.

Doherty GJ, McMahon HT (2009) Mechanisms of endocytosis. Annu Rev Biochem 78:857-902.

Donnert G, Keller J, Wurm CA, Rizzoli SO, Westphal V, Schönle A, Jahn R, Jakobs S, Eggeling C, Hell SW (2007) Two-color far-field fluorescence nanoscopy. Biophysical Journal 92:L67-69.

Dresbach T, Qualmann B, Kessels MM, Garner CC, Gundelfinger ED (2001) The presynaptic cytomatrix of brain synapses. Cellular and molecular life sciences : CMLS 58:94-116.

Dulubova I, Lou X, Lu J, Huryeva I, Alam A, Schneggenburger R, Südhof TC, Rizo J (2005) A Munc13/RIM/Rab3 tripartite complex: from priming to plasticity? EMBO J 24:2839-2850.

Fasshauer D, Sutton RB, Brunger AT, Jahn R (1998) Conserved structural features of the synaptic fusion complex: SNARE proteins reclassified as Q- and R-SNAREs. Proc Natl Acad Sci USA 95:15781-15786.

Ferguson SM, Brasnjo G, Hayashi M, Wölfel M, Collesi C, Giovedi S, Raimondi A, Gong L-W, Ariel P, Paradise S, O'toole E, Flavell R, Cremona O, Miesenböck G, Ryan TA, De Camilli P (2007) A selective activity-dependent requirement for dynamin 1 in synaptic vesicle endocytosis. Science 316:570-574.

Fernandez I, Araç D, Ubach J, Gerber SH, Shin O, Gao Y, Anderson RG, Südhof TC, Rizo J (2001) Three-dimensional structure of the synaptotagmin 1 C2B-domain: synaptotagmin 1 as a phospholipid binding machine. Neuron 32:1057-1069.

Fernandez-Alfonso T, Ryan TA (2008) A heterogeneous "resting" pool of synaptic vesicles that is dynamically interchanged across boutons in mammalian CNS synapses. Brain Cell Bio 36:87-100.

Fernández-Alfonso T, Kwan R, Ryan TA (2006) Synaptic vesicles interchange their membrane proteins with a large surface reservoir during recycling. Neuron 51:179-186.

Fernández-Busnadiego R, Zuber B, Maurer UE, Cyrklaff M, Baumeister W, Lucic V (2010) Quantitative analysis of the native presynaptic cytomatrix by cryoelectron tomography. J Cell Biol 188:145-156.

Fernández-Chacón R, Königstorfer A, Gerber SH, García J, Matos MF, Stevens CF, Brose N, Rizo J, Rosenmund C, Südhof TC (2001) Synaptotagmin I functions as a calcium regulator of release probability. Nature 410:41-49.

Fesce R, Grohovaz F, Valtorta F, Meldolesi J (1994) Neurotransmitter release: fusion or 'kiss-and-run'? Trends Cell Biol 4:1-4.

Fletcher TL, Cameron P, De Camilli P, Banker G (1991) The distribution of synapsin I and synaptophysin in hippocampal neurons developing in culture. J Neurosci 11:1617-1626.

Forster MS, Sherrington CSS (1897) A text book of physiology: Macmillan.

Francis HW, Rivas A, Lehar M, Ryugo DK (2004) Two types of afferent terminals innervate cochlear inner hair cells in C57BL/6J mice. Brain Res 1016:182-194.

Frank T, Rutherford MA, Strenzke N, Neef A, Pangršič T, Khimich D, Fetjova A, Gundelfinger ED, Liberman MC, Harke B, Bryan KE, Lee A, Egner A, Riedel D, Moser T (2010) Bassoon and the synaptic ribbon organize ca(2+) channels and vesicles to add release sites and promote refilling. Neuron 68:724-738.

Gaffield MA, Betz WJ (2006) Imaging synaptic vesicle exocytosis and endocytosis with FM dyes. Nat Protoc 1:2916-2921.

Gaffield MA, Betz WJ (2007) Synaptic Vesicle Mobility in Mouse Motor Nerve Terminals with and without Synapsin. Journal of Neuroscience 27:13691-13700.

Gaffield MA, Rizzoli SO, Betz WJ (2006) Mobility of synaptic vesicles in different pools in resting and stimulated frog motor nerve terminals. Neuron 51:317-325.

Gale J, Marcotti W, Kennedy H, Kros C, Richardson G (2001) FM1-43 dye behaves as a permeant blocker of the hair-cell mechanotransducer channel. Journal of Neuroscience 21:7013.

Gandhi SP, Stevens CF (2003) Three modes of synaptic vesicular recycling revealed by single-vesicle imaging. Nature 423:607-613.

Gennaro JF, Nastuk WL, Rutherford DT (1978) Reversible depletion of synaptic vesicles induced by application of high external potassium to the frog neuromuscular junction. J Physiol (Lond) 280:237-247.

Geppert M, Archer BT, Südhof TC (1991) Synaptotagmin II. A novel differentially distributed form of synaptotagmin. J Biol Chem 266:13548-13552.

Gitler D, Takagishi Y, Feng J, Ren Y, Rodriguiz RM, Wetsel WC, Greengard P, Augustine GJ (2004) Different presynaptic roles of synapsins at excitatory and inhibitory synapses. J Neurosci 24:11368-11380.

Glowatzki E, Ruppersberg JP, Zenner HP, Rüsch A (1997) Mechanically and ATP-induced currents of mouse outer hair cells are independent and differentially blocked by d-tubocurarine. Neuropharmacology 36:1269-1275.

Golgi C (1906) The neuron doctrine - theory and facts. Nobel Lecture.

Grabenbauer M, Geerts WJC, Fernadez-Rodriguez J, Hoenger A, Koster AJ, Nilsson T (2005) Correlative microscopy and electron tomography of GFP through photooxidation. Nat Meth 2:857-862.

Gracheva EO, Hadwiger G, Nonet ML, Richmond JE (2008) Direct interactions between C. elegans RAB-3 and Rim provide a mechanism to target vesicles to the presynaptic density. Neurosci Lett 444:137-142.

Granseth B, Odermatt B, Royle SJ, Lagnado L (2006) Clathrin-mediated endocytosis is the dominant mechanism of vesicle retrieval at hippocampal synapses. Neuron 51:773-786.

Griesinger CB, Richards CD, Ashmore JF (2002) Fm1-43 reveals membrane recycling in adult inner hair cells of the mammalian cochlea. J Neurosci 22:3939-3952.

Griesinger CB, Richards CD, Ashmore JF (2004) Apical endocytosis in outer hair cells of the mammalian cochlea. Eur J Neurosci 20:41-50.

Griesinger CB, Richards CD, Ashmore JF (2005) Fast vesicle replenishment allows indefatigable signalling at the first auditory synapse. Nature 435:212-215.

Guatimosim C, Hull C, Von Gersdorff H, Prado MAM (2002) Okadaic acid disrupts synaptic vesicle trafficking in a ribbon-type synapse. J Neurochem 82:1047-1057.

Hama K, Saito K (1977) Fine structure of the afferent synapse of the hair cells in the saccular macula of the goldfish, with special reference to the anastomosing tubules. J Neurocytol 6:361-373.

Hanse E, Gustafsson B (2001) Vesicle release probability and pre-primed pool at glutamatergic synapses in area CA1 of the rat neonatal hippocampus. J Physiol (Lond) 531:481-493.

Hanson PI, Heuser JE, Jahn R (1997) Neurotransmitter release - four years of SNARE complexes. Curr Opin Neurobiol 7:310-315.

Harata N, Ryan TA, Smith SJ, Buchanan J, Tsien RW (2001) Visualizing recycling synaptic vesicles in hippocampal neurons by FM 1-43 photoconversion. Proc Natl Acad Sci USA 98:12748-12753.

Harata NC, Choi S, Pyle JL, Aravanis AM, Tsien RW (2006) Frequency-dependent kinetics and prevalence of kiss-and-run and reuse at hippocampal synapses studied with novel quenching methods. Neuron 49:243-256.

Hata Y, Slaughter CA, Südhof TC (1993) Synaptic vesicle fusion complex contains unc-18 homologue bound to syntaxin. Nature 366:347-351.

Heidelberger R (2001) ATP is required at an early step in compensatory endocytosis in synaptic terminals. J Neurosci 21:6467-6474.

Hein B, Willig KI, Hell SW (2008) Stimulated emission depletion (STED) nanoscopy of a fluorescent protein-labeled organelle inside a living cell. Proc Natl Acad Sci USA 105:14271-14276.

Hell SW (2007) Far-field optical nanoscopy. Science 316:1153-1158.

Hell SW (2009) Microscopy and its focal switch. Nat Meth 6:24-32.

Hell SW, Stelzer EHK (1992) Properties of a 4Pi confocal fluorescence microscope. Journal of the Optical Society of America A.

Hell SW, Wichmann J (1994) Breaking the diffraction resolution limit by stimulated emission: stimulated-emission-stimulated-emission-depletion fluorescence microscopy. Optics Letters.

Henkel AW, Betz WJ (1995) Monitoring of black widow spider venom (BWSV) induced exo- and endocytosis in living frog motor nerve terminals with FM1-43. Neuropharmacology 34:1397-1406.

Henkel AW, Lübke J, Betz WJ (1996a) FM1-43 dye ultrastructural localization in and release from frog motor nerve terminals. Proc Natl Acad Sci USA 93:1918-1923.

Henkel AW, Simpson LL, Ridge RM, Betz WJ (1996b) Synaptic vesicle movements monitored by fluorescence recovery after photobleaching in nerve terminals stained with FM1-43. J Neurosci 16:3960-3967.

Heuser JE, Reese TS (1973) Evidence for recycling of synaptic vesicle membrane during transmitter release at the frog neuromuscular junction. J Cell Biol 57:315-344.

Hilfiker S, Pieribone VA, Czernik AJ, Kao HT, Augustine GJ, Greengard P (1999) Synapsins as regulators of neurotransmitter release. Philos Trans R Soc Lond, B, Biol Sci 354:269-279.

Hirokawa N, Sobue K, Kanda K, Harada A, Yorifuji H (1989) The cytoskeletal architecture of the presynaptic terminal and molecular structure of synapsin 1. J Cell Biol 108:111-126.

Holt M, Cooke A, Wu MM, Lagnado L (2003) Bulk membrane retrieval in the synaptic terminal of retinal bipolar cells. J Neurosci 23:1329-1339.

Holt M, Cooke A, Neef A, Lagnado L (2004) High mobility of vesicles supports continuous exocytosis at a ribbon synapse. Curr Biol 14:173-183.

Holtzman E, Teichberg S, Abrahams SJ, Citkowitz E, Crain SM, Kawai N, Peterson ER (1973) Notes on synaptic vesicles and related structures, endoplasmic reticulum, lysosomes and peroxisomes in nervous tissue and the adrenal medulla. J Histochem Cytochem 21:349-385.

Höning S, Kreimer G, Robenek H, Jockusch BM (1994) Receptor-mediated endocytosis is sensitive to antibodies against the uncoating ATPase (hsc70). Journal of Cell Science 107 (Pt 5):1185-1196.

Hoopmann P, Punge A, Barysch SV, Westphal V, Bückers J, Opazo F, Bethani I, Lauterbach MA, Hell SW, Rizzoli SO (2010) Endosomal sorting of readily releasable synaptic vesicles. Proc Natl Acad Sci USA 107:19055-19060.

Huttner WB, Schiebler W, Greengard P, De Camilli P (1983) Synapsin I (protein I), a nerve terminal-specific phosphoprotein. III. Its association with synaptic vesicles studied in a highly purified synaptic vesicle preparation. J Cell Biol 96:1374-1388.

Jahn R, Lang T, Südhof TC (2003) Membrane fusion. Cell 112:519-533.

Jahn R, Schiebler W, Ouimet C, Greengard P (1985) A 38,000-dalton membrane protein (p38) present in synaptic vesicles. Proc Natl Acad Sci USA 82:4137-4141.

Järlebark LE, Housley GD, Thorne PR (2000) Immunohistochemical localization of adenosine 5'-triphosphate-gated ion channel P2X(2) receptor subunits in adult and developing rat cochlea. J Comp Neurol 421:289-301.

Järlebark LE, Housley GD, Raybould NP, Vlajkovic S, Thorne PR (2002) ATP-gated ion channels assembled from P2X2 receptor subunits in the mouse cochlea. Neuroreport 13:1979-1984.

Johnson SL, Franz C, Kuhn S, Furness DN, Rüttiger L, Münkner S, Rivolta MN, Seward EP, Herschman HR, Engel J, Knipper M, Marcotti W (2010) Synaptotagmin IV determines the linear Ca2+ dependence of vesicle fusion at auditory ribbon synapses. Nat Neurosci 13:45-52.

Jordan R, Lemke E, Klingauf J (2005) Visualization of synaptic vesicle movement in intact synaptic boutons using fluorescence fluctuation spectroscopy. Biophysical Journal 89:2091-2102.

Kaech S, Banker G (2006) Culturing hippocampal neurons. Nat Protoc 1:2406-2415.

Kahle W, Frotscher M (2005) Taschenatlas der Anatomie: Nervensystem und Sinnesorgane: Georg Thieme Verlag.

Kamin D, Rizzoli SO (2009) Die Mobilität der Synaptischen Vesikel. Neuroforum 15:84-92.

Kamin D, Lauterbach MA, Westphal V, Keller J, Schönle A, Hell SW, Rizzoli SO (2010) High- and low-mobility stages in the synaptic vesicle cycle. Biophysical Journal 99:675-684.

Kandel ER, Schwartz JH, Jessel TM (2000) Principles of Neural Science, 4th edition: The McGraw-Hill Companies, Inc.

Katz B (1969) The Release of Neural Transmitter Substances: Liverpool Univ. Press.

Khimich D, Nouvian R, Pujol R, Tom Dieck S, Egner A, Gundelfinger ED, Moser T (2005) Hair cell synaptic ribbons are essential for synchronous auditory signalling. Nature 434:889-894.

Kirchhausen T, Harrison SC, Heuser J (1986) Configuration of clathrin trimers: evidence from electron microscopy. J Ultrastruct Mol Struct Res 94:199-208.

Klingauf J, Kavalali ET, Tsien RW (1998) Kinetics and regulation of fast endocytosis at hippocampal synapses. Nature 394:581-585.

Koenig JH, Ikeda K (1989) Disappearance and reformation of synaptic vesicle membrane upon transmitter release observed under reversible blockage of membrane retrieval. J Neurosci 9:3844-3860.

Kraszewski K, Daniell L, Mundigl O, De Camilli P (1996) Mobility of synaptic vesicles in nerve endings monitored by recovery from photobleaching of synaptic vesicle-associated fluorescence. J Neurosci 16:5905-5913.

Kraszewski K, Mundigl O, Daniell L, Verderio C, Matteoli M, De Camilli P (1995) Synaptic vesicle dynamics in living cultured hippocampal neurons visualized with CY3-conjugated antibodies directed against the lumenal domain of synaptotagmin. J Neurosci 15:4328-4342.

Krueger SR, Kolar A, Fitzsimonds RM (2003) The presynaptic release apparatus is functional in the absence of dendritic contact and highly mobile within isolated axons. Neuron 40:945-957.

Kuromi H, Kidokoro Y (2005) Exocytosis and endocytosis of synaptic vesicles and functional roles of vesicle pools: lessons from the Drosophila neuromuscular junction. The Neuroscientist 11:138-147.

Lagnado L, Gomis A, Job C (1996) Continuous vesicle cycling in the synaptic terminal of retinal bipolar cells. Neuron 17:957-967.

Lauterbach MA, Keller J, Schönle A, Kamin D, Westphal V, Rizzoli SO, Hell SW (2010) Comparing video-rate STED nanoscopy and confocal microscopy of living neurons. Journal of biophotonics.

Lemke EA, Klingauf J (2005) Single synaptic vesicle tracking in individual hippocampal boutons at rest and during synaptic activity. J Neurosci 25:11034-11044.

Lenzi D, Von Gersdorff H (2001) Structure suggests function: the case for synaptic ribbons as exocytotic nanomachines. Bioessays 23:831-840.

Lenzi D, Crum J, Ellisman MH, Roberts WM (2002) Depolarization redistributes synaptic membrane and creates a gradient of vesicles on the synaptic body at a ribbon synapse. Neuron 36:649-659.

Lenzi D, Runyeon JW, Crum J, Ellisman MH, Roberts WM (1999) Synaptic vesicle populations in saccular hair cells reconstructed by electron tomography. J Neurosci 19:119-132.

Leveque C, Hoshino T, David P, Shoji-Kasai Y, Leys K, Omori A, Lang B, el Far O, Sato K, Martin-Moutot N (1992) The synaptic vesicle protein synaptotagmin associates with calcium channels and is a putative Lambert-Eaton myasthenic syndrome antigen. Proc Natl Acad Sci USA 89:3625-3629.

Li C, Ullrich B, Zhang JZ, Anderson RG, Brose N, Südhof TC (1995) Ca(2+)-dependent and -independent activities of neural and non-neural synaptotagmins. Nature 375:594-599.

Li Z, Murthy VN (2001) Visualizing postendocytic traffic of synaptic vesicles at hippocampal synapses. Neuron 31:593-605.

Mandell JW, Townes-Anderson E, Czernik AJ, Cameron R, Greengard P, De Camilli P (1990) Synapsins in the vertebrate retina: absence from ribbon synapses and heterogeneous distribution among conventional synapses. Neuron 5:19-33.

Matteoli M, Takei K, Perin MS, Südhof TC, De Camilli P (1992) Exo-endocytotic recycling of synaptic vesicles in developing processes of cultured hippocampal neurons. J Cell Biol 117:849-861.

McMahon HT, Wigge P, Smith C (1997) Clathrin interacts specifically with amphiphysin and is displaced by dynamin. FEBS Lett 413:319-322.

Meunier FA, Nguyen TH, Colasante C, Luo F, Sullivan RKP, Lavidis NA, Molgó J, Meriney SD, Schiavo G (2010) Sustained synaptic-vesicle recycling by bulk endocytosis

contributes to the maintenance of high-rate neurotransmitter release stimulated by glycerotoxin. Journal of Cell Science.

Meyers JR, MacDonald RB, Duggan A, Lenzi D, Standaert DG, Corwin JT, Corey DP (2003) Lighting up the senses: FM1-43 loading of sensory cells through nonselective ion channels. J Neurosci 23:4054-4065.

Miesenböck G, De Angelis DA, Rothman JE (1998) Visualizing secretion and synaptic transmission with pH-sensitive green fluorescent proteins. Nature 394:192-195.

Miller TM, Heuser JE (1984) Endocytosis of synaptic vesicle membrane at the frog neuromuscular junction. J Cell Biol 98:685-698.

Mundigl O, Matteoli M, Daniell L, Thomas-Reetz A, Metcalf A, Jahn R, De Camilli P (1993) Synaptic vesicle proteins and early endosomes in cultured hippocampal neurons: differential effects of Brefeldin A in axon and dendrites. J Cell Biol 122:1207-1221.

Murthy VN, Stevens CF (1998) Synaptic vesicles retain their identity through the endocytic cycle. Nature 392:497-501.

Nishikawa S, Sasaki F (1996) Internalization of styryl dye FM1-43 in the hair cells of lateral line organs in Xenopus larvae. J Histochem Cytochem 44:733-741.

Nouvian R, Beutner D, Parsons TD, Moser T (2006) Structure and function of the hair cell ribbon synapse. J Membr Biol 209:153-165.

Opazo F, Punge A, Bückers J, Hoopmann P, Kastrup L, Hell SW, Rizzoli SO (2010) Limited Intermixing of Synaptic Vesicle Components upon Vesicle Recycling. Traffic (Copenhagen, Denmark).

Oyler GA, Higgins GA, Hart RA, Battenberg E, Billingsley M, Bloom FE, Wilson MC (1989) The identification of a novel synaptosomal-associated protein, SNAP-25, differentially expressed by neuronal subpopulations. J Cell Biol 109:3039-3052.

Paillart C, Li J, Matthews G, Sterling P (2003) Endocytosis and vesicle recycling at a ribbon synapse. J Neurosci 23:4092-4099.

Palade G (1975) Intracellular aspects of the process of protein synthesis. Science 189:347-358.

Parsons TD, Sterling P (2003) Synaptic ribbon. Conveyor belt or safety belt? Neuron 37:379-382.

Pearse BM (1976) Clathrin: a unique protein associated with intracellular transfer of membrane by coated vesicles. Proc Natl Acad Sci USA 73:1255-1259.

Pieribone VA, Shupliakov O, Brodin L, Hilfiker-Rothenfluh S, Czernik AJ, Greengard P (1995) Distinct pools of synaptic vesicles in neurotransmitter release. Nature 375:493-497.

Pobbati AV, Stein A, Fasshauer D (2006) N- to C-terminal SNARE complex assembly promotes rapid membrane fusion. Science 313:673-676.

Punge A, Rizzoli SO, Jahn R, Wildanger JD, Meyer L, Schönle A, Kastrup L, Hell SW (2008) 3D reconstruction of high-resolution STED microscope images. Microsc Res Tech 71:644-650.

Purves D, Augustine G, Fitzpatrick D, Hall W, LaMantia A, McNamara J, Williams S (2001) Neuroscience, 2nd edition: Sinauer Associates, Inc.

Pyle JL, Kavalali ET, Piedras-Rentería ES, Tsien RW (2000) Rapid reuse of readily releasable pool vesicles at hippocampal synapses. Neuron 28:221-231.

Rappoport JZ, Taha BW, Simon SM (2003) Movement of plasma-membrane-associated clathrin spots along the microtubule cytoskeleton. Traffic (Copenhagen, Denmark) 4:460-467.

Rea R, Li J, Dharia A, Levitan ES, Sterling P, Kramer RH (2004) Streamlined synaptic vesicle cycle in cone photoreceptor terminals. Neuron 41:755-766.

Richards DA, Guatimosim C, Betz WJ (2000) Two endocytic recycling routes selectively fill two vesicle pools in frog motor nerve terminals. Neuron 27:551-559.

Rizo J, Rosenmund C (2008) Synaptic vesicle fusion. Nat Struct Mol Biol 15:665-674.

Rizzoli SO, Betz WJ (2004) The structural organization of the readily releasable pool of synaptic vesicles. Science 303:2037-2039.

Rizzoli SO, Betz WJ (2005) Synaptic vesicle pools. Nat Rev Neurosci 6:57-69.

Rizzoli SO, Bethani I, Zwilling D, Wenzel D, Siddiqui TJ, Brandhorst D, Jahn R (2006) Evidence for Early Endosome-like Fusion of Recently Endocytosed Synaptic Vesicles. Traffic 7:1163-1176.

Roux I, Safieddine S, Nouvian R, Grati Mh, Simmler M-C, Bahloul A, Perfettini I, Le Gall M, Rostaing P, Hamard G, Triller A, Avan P, Moser T, Petit C (2006) Otoferlin, defective in a human deafness form, is essential for exocytosis at the auditory ribbon synapse. Cell 127:277-289.

Ryan TA, Li L, Chin LS, Greengard P, Smith SJ (1996) Synaptic vesicle recycling in synapsin I knock-out mice. J Cell Biol 134:1219-1227.

Ryan TA, Reuter H, Wendland B, Schweizer FE, Tsien RW, Smith SJ (1993) The kinetics of synaptic vesicle recycling measured at single presynaptic boutons. Neuron 11:713-724.

Safieddine S, Wenthold RJ (1999) SNARE complex at the ribbon synapses of cochlear hair cells: analysis of synaptic vesicle- and synaptic membrane-associated proteins. Eur J Neurosci 11:803-812.

Sankaranarayanan S, Atluri PP, Ryan TA (2003) Actin has a molecular scaffolding, not propulsive, role in presynaptic function. Nat Neurosci 6:127-135.

Sankaranarayanan S, De Angelis D, Rothman JE, Ryan TA (2000) The use of pHluorins for optical measurements of presynaptic activity. Biophysical Journal 79:2199-2208.

Santos MS, Li H, Voglmaier SM (2009) Synaptic vesicle protein trafficking at the glutamate synapse. Neuroscience 158:189-203.

Sara Y, Virmani T, Deák F, Liu X, Kavalali ET (2005) An isolated pool of vesicles recycles at rest and drives spontaneous neurotransmission. Neuron 45:563-573.

Schikorski T, Stevens CF (1997) Quantitative ultrastructural analysis of hippocampal excitatory synapses. J Neurosci 17:5858-5867.

Schikorski T, Stevens CF (2001) Morphological correlates of functionally defined synaptic vesicle populations. Nat Neurosci 4:391-395.

Schmidt R, Wurm CA, Jakobs S, Engelhardt J, Egner A, Hell SW (2008) Spherical nanosized focal spot unravels the interior of cells. Nat Meth 5:539-544.

Schmitz F, Königstorfer A, Südhof TC (2000) RIBEYE, a component of synaptic ribbons: a protein's journey through evolution provides insight into synaptic ribbon function. Neuron 28:857-872.

Schug N, Braig C, Zimmermann U, Engel J, Winter H, Ruth P, Blin N, Pfister M, Kalbacher H, Knipper M (2006) Differential expression of otoferlin in brain, vestibular system, immature and mature cochlea of the rat. Eur J Neurosci 24:3372-3380.

Seiler C, Nicolson T (1999) Defective calmodulin-dependent rapid apical endocytosis in zebrafish sensory hair cell mutants. J Neurobiol 41:424-434.

Shapira M, Zhai RG, Dresbach T, Bresler T, Torres VI, Gundelfinger ED, Ziv NE, Garner CC (2003) Unitary assembly of presynaptic active zones from Piccolo-Bassoon transport vesicles. Neuron 38:237-252.

Shepherd GM, Harris KM (1998) Three-dimensional structure and composition of CA3-->CA1 axons in rat hippocampal slices: implications for presynaptic connectivity and compartmentalization. J Neurosci 18:8300-8310.

Shtrahman M, Yeung C, Nauen DW, Bi G-q, Wu X-l (2005) Probing vesicle dynamics in single hippocampal synapses. Biophysical Journal 89:3615-3627.

Siegel JH, Brownell WE (1986) Synaptic and Golgi membrane recycling in cochlear hair cells. J Neurocytol 15:311-328.

Siksou L, Rostaing P, Lechaire J-P, Boudier T, Ohtsuka T, Fejtova A, Kao H-T, Greengard P, Gundelfinger ED, Triller A, Marty S (2007) Three-Dimensional Architecture of Presynaptic Terminal Cytomatrix. Journal of Neuroscience 27:6868-6877.

Söllner T, Bennett MK, Whiteheart SW, Scheller RH, Rothman JE (1993a) A protein assembly-disassembly pathway in vitro that may correspond to sequential steps of synaptic vesicle docking, activation, and fusion. Cell 75:409-418.

Söllner T, Whiteheart SW, Brunner M, Erdjument-Bromage H, Geromanos S, Tempst P, Rothman JE (1993b) SNAP receptors implicated in vesicle targeting and fusion. Nature 362:318-324.

Sorra KE, Mishra A, Kirov SA, Harris KM (2006) Dense core vesicles resemble active-zone transport vesicles and are diminished following synaptogenesis in mature hippocampal slices. Neuroscience 141:2097-2106.

Spicer SS, Thomopoulos GN, Schulte BA (1999) Novel membranous structures in apical and basal compartments of inner hair cells. J Comp Neurol 409:424-437.

Staras K (2010) Sharing vesicles between central presynaptic terminals: implications for synaptic function. Front Syna Neurosci:1-6.

Staras K, Branco T, Burden JJ, Pozo K, Darcy K, Marra V, Ratnayaka A, Goda Y (2010) A vesicle superpool spans multiple presynaptic terminals in hippocampal neurons. Neuron 66:37-44.

Sudhof TC (2004) The Synaptic Vesicle Cycle. Annu Rev Neurosci 27:509-547.

Sutton RB, Fasshauer D, Jahn R, Brunger AT (1998) Crystal structure of a SNARE complex involved in synaptic exocytosis at 2.4 A resolution. Nature 395:347-353.

Takamori S et al. (2006) Molecular anatomy of a trafficking organelle. Cell 127:831-846.

Takei K, McPherson PS, Schmid SL, De Camilli P (1995) Tubular membrane invaginations coated by dynamin rings are induced by GTP-gamma S in nerve terminals. Nature 374:186-190.

Takei K, Mundigl O, Daniell L, De Camilli P (1996) The synaptic vesicle cycle: a single vesicle budding step involving clathrin and dynamin. J Cell Biol 133:1237-1250.

Teng H, Wilkinson RS (2000) Clathrin-mediated endocytosis near active zones in snake motor boutons. J Neurosci 20:7986-7993.

tom Dieck S, Altrock WD, Kessels MM, Qualmann B, Regus H, Brauner D, Fejtová A, Bracko O, Gundelfinger ED, Brandstätter JH (2005) Molecular dissection of the photoreceptor ribbon synapse: physical interaction of Bassoon and RIBEYE is essential for the assembly of the ribbon complex. J Cell Biol 168:825-836.

tom Dieck S, Sanmartí-Vila L, Langnaese K, Richter K, Kindler S, Soyke A, Wex H, Smalla KH, Kämpf U, Fränzer JT, Stumm M, Garner CC, Gundelfinger ED (1998) Bassoon, a novel zinc-finger CAG/glutamine-repeat protein selectively localized at the active zone of presynaptic nerve terminals. J Cell Biol 142:499-509.

Torri Tarelli F, Bossi M, Fesce R, Greengard P, Valtorta F (1992) Synapsin I partially dissociates from synaptic vesicles during exocytosis induced by electrical stimulation. Neuron 9:1143-1153.

Tsuriel S, Fisher A, Wittenmayer N, Dresbach T, Garner CC, Ziv NE (2009) Exchange and Redistribution Dynamics of the Cytoskeleton of the Active Zone Molecule Bassoon. Journal of Neuroscience 29:351-358.

Tsuriel S, Geva R, Zamorano P, Dresbach T, Boeckers T, Gundelfinger ED, Garner CC, Ziv NE (2006) Local Sharing as a Predominant Determinant of Synaptic Matrix Molecular Dynamics. Plos Biol 4:e271.

Ubach J, Zhang X, Shao X, Südhof TC, Rizo J (1998) Ca2+ binding to synaptotagmin: how many Ca2+ ions bind to the tip of a C2-domain? EMBO J 17:3921-3930.

Vicidomini G, Boccacci P, Diaspro A, Bertero M (2009) Application of the split-gradient method to 3D image deconvolution in fluorescence microscopy. Journal of microscopy 234:47-61.

Voglmaier SM, Kam K, Yang H, Fortin DL, Hua Z, Nicoll RA, Edwards RH (2006) Distinct endocytic pathways control the rate and extent of synaptic vesicle protein recycling. Neuron 51:71-84.

Watanabe S, Punge A, Hollopeter G, Willig KI, Hobson RJ, Davis MW, Hell SW, Jorgensen EM (2010) Protein localization in electron micrographs using fluorescence nanoscopy. Nat Meth.

Westphal V, Rizzoli SO, Lauterbach MA, Kamin D, Jahn R, Hell SW (2008) Video-rate far-field optical nanoscopy dissects synaptic vesicle movement. Science 320:246-249.

Wienisch M, Klingauf J (2006) Vesicular proteins exocytosed and subsequently retrieved by compensatory endocytosis are nonidentical. Nat Neurosci 9:1019-1027.

Wildanger D, Medda R, Kastrup L, Hell SW (2009) A compact STED microscope providing 3D nanoscale resolution. Journal of microscopy 236:35-43.

Wilhelm BG, Groemer TW, Rizzoli SO (2010) The same synaptic vesicles drive active and spontaneous release. Nat Neurosci.

Willig KI, Rizzoli SO, Westphal V, Jahn R, Hell SW (2006) STED microscopy reveals that synaptotagmin remains clustered after synaptic vesicle exocytosis. Nature 440:935-939.

Yeung C, Shtrahman M, Wu X-l (2007) Stick-and-diffuse and caged diffusion: a comparison of two models of synaptic vesicle dynamics. Biophysical Journal 92:2271-2280.

Zefirov AL, Abdrakhmanov MM, Grigor'ev PN (2006a) Effects of high-potassium solutions and caffeine on synaptic vesicle exoendocytosis processes in the frog neuromuscular junction. Neurosci Behav Physiol 36:781-788.

Zefirov AL, Abdrakhmanov MM, Mukhamedyarov MA, Grigoryev PN (2006b) The role of extracellular calcium in exo- and endocytosis of synaptic vesicles at the frog motor nerve terminals. Neuroscience 143:905-910.

Zenisek D, Steyer JA, Feldman ME, Almers W (2002) A membrane marker leaves synaptic vesicles in milliseconds after exocytosis in retinal bipolar cells. Neuron 35:1085-1097.

Zhang Q, Li Y, Tsien RW (2009) The Dynamic Control of Kiss-And-Run and Vesicular Reuse Probed with Single Nanoparticles. Science 323:1448-1453.

Acknowledgements

First of all, I want to thank my supervisor Dr. Silvio O. Rizzoli for his outstanding support and his endless patience in explaining me fundamental science and being a scientist. I am deeply grateful that you shared your ideas and knowledge with me, not only of scientific topics. I will never forget this. Thank you Silvio!

I thank Prof. Moser and Dr. Eimer for being part of my thesis committee and for their comments and ideas not only during the committee meetings.

I thank Dr. Marcel Lauterbach and Dr. Volker Westphal from the department of "NanoBiophotonics" (MPI-BPC) for their excellent collaboration with STED imaging.

I thank all the people in the Rizzoli lab for their help and support. Thank you for interesting discussions and funny lab activities (in- and outside of the lab). You all give the lab its unique atmosphere.

I am extremely grateful to my family, and especially to my parents – you gave me all your love and support one can think of and never gave me up throughout my life. Danke!

Finally, I want to thank my wonderful wife Stefanie who supported me with all her love and warmness. You were there whenever I needed you. Thank you for your honest trust and continuous belief in me. You truly inspire me! …to the moon and back!

Curriculum Vitae

Personal information

Name:	Dirk Kamin
Date of birth:	August, 31st 1981
Place of birth:	Meppen, Germany
Adress:	Kurze-Geismar-Str. 45, 37073 Göttingen, Germany
E-mail:	d.kamin@eni-g.de

Education

01/2008 – 03/2011	PhD with Dr. Silvio O. Rizzoli, STED Microscopy of Synaptic Function, European Neuroscience Institute Göttingen
	Thesis: "Synaptic vesicle recycling investigated by high-resolution microscopy in a conventional and a sensory synapse
12/2006 – 09/2007	Diploma thesis in the Department of Neurobiology
	University of Osnabrück, Prof. Dr. Roland Brandt
	Thesis: "Analysis of Potential Interaction of the A-Kinase-Anchoring Protein Gravin with Myosin in Nerve Cells"
02/2006 – 04/2006	Lab course
	Max-Planck-Institute for Neurological Research, Cologne
	"In-vivo-NMR", Prof. Dr. Matthias Hoehn
	Topic: "Labeling of C17.2 Neuronal Progenitor Cells with Gd-DTPA for NMR-Analysis"
10/2001 – 09/2007	Biology studies ("Diplom Biology")
	University of Osnabrück (Vordiplom 04/2005)
	Major subjects: neurobiology, biochemistry, developmental biology and animal physiology
06/2001	High School Diploma (Abitur) at the Windthorst-Gymnasium-Meppen

Teaching

2009	Supervisor of Labrotation: Hema Chug, International MSc/PhD Program "Molecular Biology"
06/ and 10/2010	Tutor of GGNB Methods Courses: "High-Resolution Microscopy in Synapses"

Honors and Awards

09/2010	2nd Prize Winner for Student Talk 6th International PhD Student Symposium "Horizons in Molecular Biology", Göttingen, Germany
11/2010	GGNB Grant (Tavel Stipend)

Conferences

10/2008	"New Frontiers in Neurophotonics" – 1st Franco-Canadian Symposium, University of Bordeaux, France (poster)
09/2009	"Horizons in Molecular Biology" – 6th International PhD Student Symposium, Göttingen, Germany (invited talk)
11/2009	"2nd European Synapse Meeting", Göttingen, Germany (poster)
11/2010	"Neuroscience 2010" – SfN's 40th annual meeting, San Diego, CA, USA (invited talk)